Department of Mathematics   PhD Thesis

2014

Analysis on Viscous Incompressible Thermal Flow on a Ventilated Enclosure by Finite Element Method

Ahammad, Main Uddin

University of Rajshahi

Analysis on Viscous Incompressible Thermal Flow on a Ventilated Enclosure by Finite Element Method

By

Main Uddin Ahammad
Roll No. 11302
Registration No. 0006, Session: 2011-12

DOCTOR OF PHILOSOPHY
IN
MATHEMATICS

Department of Mathematics
Rajshahi University, Rajshahi-6205
September- 2014

Candidate's Declaration

I am hereby declaring that no portion of the work considered in this thesis has been submitted in support of an application for another degree or qualification of this or any other University or Institute of learning either in home or abroad.

_____

Main Uddin Ahammad

September 2014

Certificate of Research

This is to certify that the work presented in this thesis is carried out by the author under the supervision of Dr. Md. Lutfor Rahman, Professor, Department of Mathematics, Rajshahi University, Rajshahi-6205 and Dr. Md. Mustafizur Rahman, Professor, Department of Mathematics, Bangladesh University of Engineering and Technology, Dhaka-1000.

Dr. Md. Lutfor Rahman
(Supervisor)

Dr. Md. Mustafizur Rahman
(Co-supervisor)

Dedicated to my Parents

Acknowledgement

Abstract

Heat transfer in enclosure in which the influence of free (natural) and forced convection (mixed convection) are of comparable magnitude occurs frequently in engineering situations. The applications include the heat transfer improvement in heat exchanger devices, design of solar collectors, thermal design of building, air conditioning, cooling of electronic circuit boards, lubrication technologies, chemical processing equipment etc. Convection in ventilated enclosures containing obstruction has gained recent research significance as a means of heat transfer enhancement. The mathematical model of the present problem is governed by the couple equations of conservation of mass, momentum and energy. Discretization of the governing equations is achieved using a finite element scheme based on the Galerkin weighted residuals method. Then Newton–Raphson iterative algorithm is used to obtain the solutions of the obtained algebraic equations. Comparisons with previously established on particular cases of the problem are performed and the results show excellent agreement.

Firstly, for mixed convection flow the effect of inlet and outlet position of a square ventilated enclosure with a centered heat generating solid body has been investigated. The bottom wall of the enclosure is kept at a uniform constant temperature, while the rest three walls of the enclosure are assumed adiabatic. A transverse uniform magnetic field is imposed in the horizontal direction normal to the right vertical wall. An external flow enters the cavity through an inlet opening whereas it exits via another outlet opening.

After that, the effect of pertinent parameters in the considered flow problem in this thesis was analyzed for three different types of internal cavity solid body (heat generating, heat conducting, adiabatic) for a selected *BT* (bottom inlet and top outlet) configuration.

Obtained results from the present study are presented in the form of streamlines, isotherms, average Nusselt number along the bottom heated surface and average fluid temperature in the cavity for each of four configurations as well as three different confined blocks for the pertinent parameters namely Reynolds number, Prandtl

number, Hartmann number, solid-fluid thermal conductivity ratio, solid block diameter at the three values of Richardson number, varying from 0.1 to 10.

The computational findings of this thesis reveals that both the flow and the thermal fields strongly depend on the parameters Reynolds number Re, Prandtl number Pr, Hartmann number Ha at the three convective regimes ($Ri = 0.1, 1, 10$). The centered solid body of the enclosure influences the steamlines pattern slightly for the smaller dimension of the block D whereas it has a considerable disparity in temperature distribution inside the enclosure. It is also observed that the solid-fluid thermal conductivity ratio K have insignificant effect on the flow fields and have significant effect on the thermal fields at the three convective regimes.

List of Published Papers

i. Ahammad, M. U., Rahman, M. M., Rahman, M. L., "Effect of inlet and outlet position in a ventilated cavity with a heat generating square block", Engineering e-Transaction, Vol. 7, No. 2, pp. 107–115, 2012.

ii. Ahammad, M. U., Rahman, M. M., Rahman, M. L., "Mixed convection flow and heat transfer behavior inside a vented enclosure in the presence of heat generating obstacle", International Journal of Innovation and Applied Studies, Vol. 3, No.4, pp. 967-978, 2013.

iii. Ahammad, M. U., Rahman, M. M., Rahman, M. L., Mollah, S. H., "Interior solid block study on combined convection flow through square enclosure with a hot bottom surface", ARPN Journal of Science and Technology, Vol. 4, No. 3, pp. 167-174, 2014.

iv. Ahammad, M. U., Rahman, M. M., Rahman, M. L., "A study on the governing parameters of MHD mixed convection problem in a ventilated cavity containing a centered square block", International Journal of Scientific & Technology Research, Vol.3, No. 5, pp. 269-277, 2014.

v. Ahammad, M. U., Rahman, M. M., Rahman, M. L., "Numerical investigation of heat transfer enhancement about a thermally isolated body: outcome of Hartmann and Reynolds numbers", International Journal of Innovation and Scientific Research, Vol. 4, No. 1, pp. 61-69, 2014.

Chapter 1

Introduction

The fundamental manners of a mechanism for heat transfer enhancement in enclosures by combined free and forced convection have been the subject of investigations for many years. Magneto hydrodynamic (MHD) flow has become essential in the context of many engineering applications such as magneto hydrodynamic generators, pumps, metallurgical processing, and cooling of fusion reactors. The effects of viscous incompressible thermal flow in enclosures or channels have been studied by many investigators due to its popularity in research field. The cavities including solid bodies are the topics of special attention in recent times due to their extensive applications in heat exchangers, cooling of electronic equipment, solar heat collector, ventilation of buildings, air conditioning and furnaces etc. Many researchers have investigated the flow of electrically conducting fluid in presence of magnetic field for its importance from the technical point of view. Numerical solutions are obtained for the mathematical models that are used to predict flow and thermal behavior are governed by coupled non-linear partial differential equations.

In order to realize the present work, the introductory chapter is designed as follows. The problems that will be presented in this thesis are basically heat transfer problems in enclosures and thus a concise description on heat transfer through convection is given in section 1.1. In addition flows and heat transfer within an enclosure are narrated in section 1.2 for understanding the fluid flow and heat transfer characteristics of mixed convection in a vented cavity. In section 1.3 some fluid properties relevant to the recent work have been included. For showing the previous research work related to the current subject by many authors, a literature review is presented shortly in section 1.4. And lastly an overview of the present investigation is included in section 1.5.

1.1 Heat Transfer through Convection

Convective heat transfer, often referred to simply as convection, is a system of heat transport that occurs for the reason of bulk motion of fluids. The term 'convection' generally refers to the observable movement of fluids that indicates liquids and gases. The fluid motion enhances convection heat transfer (the higher the velocity the greater the heat transfer rate). Convection heat transfer is complicated due to its involving fluid motion as well as heat conduction. In convection, heat is the entity of interest being advected and diffused. On the contrary, conductive heat transfer is the transfer of energy by vibrations at a molecular level through solid-solid or solid-fluid, and radiative heat transfer means the transfer of energy through electromagnetic waves. However the heated fluid itself is actually moving in case of convection and such flow of heated fluid is called convection current. Convection is related directly to heat and temperature and in some way linked to another phenomenon, thermal energy. Frequently what we term heat is actually thermal energy or kinetic energy formed by molecules in motion relative to one another. Heat is transferred by convection is found in the case of naturally occurring fluid flow, specifically wind, oceanic currents, and movements within the earth's mantle causes tectonic plates to move. In order to provide preferred temperature changes; convection is also used in heating of dwellings, industrial processes, cooling of electronic equipments, etc. A heat source (e.g. Bunsen burner) can be considered a good model for convection; if it is placed at any side of a glass full of a liquid; one can feel the different levels of heat in the glass. In general, convection is classified as natural (or free) and forced convection depending on how the fluid motion is initiated, though another mechanism also exists which is referred as mixed convection. However the distinction between free and forced convection is needed for convective heat transfer. Convection heat transfer rate is found to be proportional to the temperature difference that is conveniently expressed by Newton's law of cooling as

$$Q_{conv} = hA_S \left(T_S - T_\infty \right)$$

Natural Convection

Natural convection is a process in which the fluid motion is set up by buoyancy effects due to density differences within the fluid caused by the temperature

variations and thus the fluid be at rest in the absence of temperature variations in such convection. Free convection velocities are comparatively gentle and the resultant wall heat flux will usually be less than in forced motion. A phenomenon for natural convection can be described as; at heating the density change in the boundary layer will cause the fluid to rise and be replaced by cooler fluid that also will be heated and rise. In free convection heavier (more dense) components will fall and lighter (less dense) components will rise that leads to bulk fluid movement. Therefore natural convection can only occur in a gravitational field. A well-known example of natural convection is the rise of smoke from a fire; one can be noticed that in a pot of boiling water the hot and less-dense water on the bottom layer moves upwards in plumes, and the cool and more-dense water near the top of the pot likewise sinks.

Note that when the differences in buoyancy within a fluid occur for reasons other than temperature variations, the fluid motion is called gravitational convection. However, all types of buoyant convection which also includes natural convection do not arise in microgravity environments. All have need of the existence of an environment which experiences g-force (proper acceleration).

Forced Convection

The fluid is forced to flow over the surface in forced convection, by external means such as a fan, pump or the wind. For the reason of faster velocity of the currents, forced convection is commonly more efficient than natural convection. However in forced convection, the buoyancy has little effect on the flow direction and naturally forced convection is used to increase the rate of heat exchange. Various types of mixing also utilize forced convection to distribute one substance within another while it also occurs as a by-product to other processes, such as the action of a propeller in a fluid or aerodynamic heating. Some familiar examples of forced convection can be mentioned as fluid radiator systems, and also heating and cooling of parts of the body by blood circulation. In microgravity, the flow which happens in all directions along with diffusion is the only means by which fires are able to draw in fresh oxygen to maintain themselves. Some types of ovens and even refrigerators or air conditioners can be treated as examples of forced-convection apparatuses. For instance, a convection oven works by forced convection, as a fan which quickly circulates hot

air forces heat into food more rapidly than would naturally happen due to simple heating without the fan. Note that, it is possible to transfer heat only from a high-temperature reservoir to a low-temperature one, and thus these cooling machines work by removing hot air. An air conditioner pulls heat from a room or building and releases it to the outside while the refrigerator pulls heat from its compartment and expels it to the surrounding room. However, forced convection does not necessarily involve man-made machines: the human heart is a pump, and blood carries excess heat generated by the body to the skin. Heat transfer coefficients encountered in forced convection are typically much higher than those encountered in free convection due to the higher fluid velocities associated with forced convection.

Mixed Convection

A convection situation that involves both natural and forced convection is commonly referred as mixed convection or combined convection. In mixed convection flows, neither the natural convection nor the forced convection effects are dominant and thus both modes are of comparable magnitudes. The fluid motion is the result of the interaction between an external forced flow and an internal buoyancy flow for a mixed convection problem. Therefore, combined natural and forced convection occurs if the effect of buoyancy forces on a forced flow or the effect of forced flow on a buoyant flow is significant. For a certain fluid, it is observed that the parameter Gr/Re^2 represents the significance of natural convection relative to forced convection. This is not unexpected as the convection heat transfer coefficient is a strong function of the Reynolds number Re in forced convection and the Grashof number Gr in free convection. Both of the natural and forced convection must be measured in heat transfer calculations when the Gr and Re^2 are of the same order of magnitude.

1.2 Flows and Heat Transfer within an Enclosure

Two types of convection are involved in vented enclosure, one that the internal buoyancy-induced natural convection and the other external mechanical-driven forced convection. Thus it is essential to realize the fluid flow and heat transfer structures of mixed convection in a vented cavity. In the mixed convection, the interaction between the external forced flow provided by the inlet and the buoyancy

driven flows induced by the heat source leads to the possibility of complex flows in a ventilated cavity. For the traditional ventilation system, the fresh cold air is supplied from the top ceiling and the polluted hot air is exhausted from the bottom of the sidewall. In this way, the ventilation system can achieve the goal of maintaining a healthy indoor air environment at a low cost of the external forced convection whereby to save energy and also to reduce the noise. Note that in conventional ventilation scheme, natural convection becomes a burden of the external forced convection, so, the forced convection should be increased to eliminate the negative effect of the natural convection. Due to the wide applications of buoyancy-driven natural convection in confined enclosures have been received more and more research attention; some of these are multi-layered walls, double-pane windows and other air gaps in unventilated spaces. In addition, an appropriate flow patterns in confined enclosures can greatly enhance the efficiency of utilization of building systems. Moreover, convection in enclosures having blocks has attained current research significance as a means of heat transfer enhancement.

1.3 Some Fluid Properties

Viscosity

The viscosity of a fluid which is a strong function of temperature is a measure of its resistance to deformation. A friction force develops between two adjacent fluid layers while they move relative to each other and the slower layer tries to slow down the faster layer. This type of internal resistance to flow is quantified by the fluid property viscosity. All fluid flows involve viscous effects to some degree and therefore no fluid with zero viscosity. As temperature increases, the viscosities of liquids decrease whereas the viscosities of gases increase with temperature.

Viscous Flow

Such flows are called viscous whose flow patterns are dominated by the viscous properties of the fluid. This arises in fluids where the velocity gradients are comparatively large. Within pipes the flows close to the walls of the pipes can be treated as viscous flows.

Non-viscous Flow

The flows are defined as non-viscous or inviscid flows if the viscous properties are not dominant. These types of flows are common in the centre region of flowing pipes and in gas flows.

Newton's Law of Viscosity

If the shearing stress, τ, increases by increasing the force P, the rate of shearing strain also increases in direct proportion to that; $\tau \, \alpha \, \dfrac{du}{dy}$ i.e., $\tau = \mu \dfrac{du}{dy}$, where μ is the dynamic viscosity of the fluid. This principle is known as the Newton's law of viscosity.

Newtonian Fluid

Newtonian fluids are those fluids for which the constant of proportionality i.e. the co-efficient of viscosity (μ) does not change with the rate of deformation. In other words, fluids that follow the Newton's law of viscosity are known as Newtonian fluids. Water, air and mercury are some examples of Newtonian fluids.

Non-Newtonian Fluid

Non-Newtonian fluids are those fluids for which the constant of proportionality i.e. the co-efficient of viscosity (μ) changes with the rate of deformation. In other words, fluids that do not follow the Newton's law of viscosity are known as Non-Newtonian fluids. Blood, liquid plastic and polymer solutions are Non-Newtonian fluids.

Compressibility

Compressibility is a property of fluid that measures the change in density and consequently, the change in the volume of a fluid during motion under the action of external forces. The compressibility is expressed in terms of Mach number (M) which is defined by $M = \dfrac{\text{speed of fluid}}{\text{speed of sound}} = \dfrac{u}{\alpha_0}$

Compressible Flow

A compressible flow is one in which the density vary in the different portion of the fluids. Thus the volume of every portion of fluid differs in compressible flow over the course of its motion.

Incompressible Flow

A flow is said to be incompressible if the density remains nearly constant throughout. Therefore, for incompressible flow the volume of every portion of fluid remains unchanged over the course of its motion. The densities of liquids are basically constant and accordingly the flow of liquids is naturally referred to as incompressible.

1.4 Literature Review

A number of experimental and numerical studies have been carried out by different researchers in order to assess the thermal behavior and the flow pattern of convection induced flows in geometrical configurations which frequently come into sight in various engineering designs and science. Literature review on the subject shows that many authors have been studied the natural and mixed convective flows in cavities, channels by considering with and without obstacle using analytical, experimental and numerical methods. The succeeding survey demonstrates some of that works.

Natural Convection in Enclosure/Channel with and without Obstacle

Natural convection is a physical phenomenon occurring frequently in natural process such as in the atmosphere, lakes, oceans etc. It also becomes relevant in engineering areas where the flow and heat transfer conditions are strongly affected by buoyancy forces. Some applications are solar collectors, energy storage systems, ventilation of rooms and design of electronic equipment etc. The study of the natural convection in enclosures and channels has been an active research topic in recent years because of the multiple applications in which it is involved. Furthermore, convection in enclosures having blocks has gained modern research significance due to the enhancement of heat transfer. Many experimental and numerical studies have been carried out on the natural convection in the cavity.

The effect on the steady-state natural convection heat transfer enhancement of a centrally-placed adiabatic block within a differentially heated square cavity with a fixed temperature drop between the vertical walls have been carried out by Bhave et al. (2006). Bilgen and Yamane (2004) studied the conjugate heat transfer by free convection and conduction in two-dimensional rectangular enclosures with openings. They examined the effects of the different geometrical parameters and the thickness of the insulation layer on the fluid flow and heat transfer characteristics. Later, Bilgen (2005) performed heat transfer by free convection in differentially heated square cavities with horizontal thin fin and it was focused that normalized Nusselt number is an increasing function of Rayleigh number whereas decreasing function of fin length and relative conductivity ratio. A steady laminar natural convection within a square cavity filled with a fixed amount of conducting solid material consisting of either circular or square obstacles were computed by Braga and Lemos (2005). The authors' pointed out that the average Nusselt number for cylindrical rods is lesser slightly than those for square rods. Das and Reddy (2006) investigated natural convection problem inside an inclined square cavity with an internal conducting block. A study on free convection heat transfer in a rectangular enclosure with a transverse magnetic field was found in Garandet et al. (1992). House et al. (1990) analyzed natural convection in a vertical square cavity with heat conducting body which is kept on center of the cavity. They carried out the effect of the heat conducting body on heat transfer process in the cavity and observed that the heat transfer across the enclosure improved by a body with thermal conductivity ratio less than unity. Jami et al. (2007) studied the laminar natural convective flow in an enclosure with a heat-generating cylindrical body. Natural convection heat transfer from two horizontal heated cylinders confined to a rectangular enclosure with conducting walls was found in the work of Lacroix and Joyeux (1995). In their work it is presented that wall heat conduction decreases the average temperature differences across the cavity and reduces natural convection heat transfer around the cylinders. Merrikh and Lage (2005) studied natural convection in an enclosure with disconnected and conducting solid blocks. Laminar, steady conjugate natural convection around a centered finned pipe of a square enclosure with uniform internal heat generation has been investigated by Nakhi and Chamkha (2007). Oreper and

Szekely (1983) discussed the outcome of an externally enforced magnetic field on buoyancy driven flow in a rectangular cavity. The reality that revealed in their work is the presence of a magnetic field can suppress natural convection currents and the strength of the magnetic field is one of the important factors in determining the crystal quality. Oztop and Dagtekin (2004) studied free convection heat transfer in a square cavity containing a heated plate built-in vertically and horizontally. They focused that mean Nusselt numbers at both vertical and horizontal location enlarged with the increasing value of Rayleigh number. Oztop and Bilgen (2006) studied a differentially heated, partitioned, square cavity filled with a heat generating fluid. The horizontal walls and the vertical walls were considered adiabatic and isothermal in that order. In addition, an isothermal cold partitioned was attached to the bottom wall. In their essays the external and internal Rayleigh numbers (Ra_E and Ra_I) were taken ranging from 10^3 to 10^6. The flow field was modified noticeably with partial dividers and heat transfer was generally decreased particularly when the ratio of internal and external Rayleigh numbers was between 10^1 and 10^2. Rudraiah et al. (1995) computed the effect of a magnetic field on natural convection in a rectangular enclosure. Natural convection in a square cavity having a heat generating body was investigated by Shuja et al. (2000). They have taken air and water as working fluid inside the cavity whereas steel substrate is considered as the heat generating body. It was concluded that the heat transfer from the solid body surfaces enhanced where the surfaces facing the inlet and the exit of the cavity. They also presented that the solid body losses more heat in the air than in water. Tasnim and Collins (2005) studied laminar natural convection heat transfer in a square cavity with an adiabatic arc shaped baffle. The problem of laminar natural convection in enclosures surrounded by a solid wall with its outer boundary at constant temperature while the opposing side has a constant heat flux was analyzed by Yedder and Bilgen (1997).

Mixed Convection in Enclosure/Channel with and without Obstacle

Mixed convective flow in which neither the free convection nor the forced convection effects are dominant has gained its extensive applications in many natural and technological processes. Analysis of mixed convection plays an important role in many natural and technological processes such as furnaces, lubrication technologies,

the design of solar collectors, thermal design of buildings, air conditioning, cooling of electronic devices etc. The existing literature in this area has focused considerable attention on mixed convection in vented cavities or channels. In recent times, many researchers have studied heat transfer with obstacles, partitions and fins; a brief review of the relevant literature has been presented here. Combined natural and forced convection in a vented square enclosure with isothermal vertical surface was studied by Angirasa (2000). Amir Hossein Zarei et al. (2013) presented heat transfer manners of combined free and forced convection flow in lid driven cavity containing hot obstacle subjected to nano-fluid with variable properties. In their research the results indicate that the average Nusselt number for all range of solid volume fraction increases with decrease in the Richardson number. Chamkha (2002) analyzed an unsteady laminar mixed convection flow and heat transfer problem of an electrically conducting and heat generating or absorbing fluid in a vertical lid-driven cavity considering the effect of a magnetic field. Mixed convection heat transfer in a semi porous open cavity has been investigated by Carlos et al. (2008). Their study shows how free convection effects may develop the forced convection inside the open cavity. Gau and Sharif (2004) investigated the problem of combined free and forced convection heat transfer in a two-dimensional rectangular cavity with constant heat flux. The cavity was partially heated bottom wall while the isothermal sidewalls are moving in the vertical direction. Gowda et al. (1997) performed an analysis of heat transfer and fluid flow over a row of in-line cylinders kept between two parallel plates. A considerable effect of buoyancy and the blockage on the flow and heat transfer over the cylinders are noticed in their work. The effects of viscous dissipation on unsteady combined convective heat transfer to water near its density maximum in a rectangular cavity with isothermal wall was studied by Hossain and Gorla (2006). Analysis of combined free and forced convection in a partially divided rectangular enclosure for wide range of Reynolds and Grashof numbers were found in the works of How and Hsu (1998), Hsu et al. (1997). They have concluded that average Nusselt number and the dimensionless surface temperature are influenced by the location and height of the divider. Later on, Hsu and How (1999) discussed mixed convection flow and heat transfer in a square enclosure with heat conducting body and a finite-size heat source. In this work it was shown that both the heat

transfer coefficient and the dimensionless temperature in the center of the body strongly depend on the systems configurations. Combined natural and forced convection heat transfer was performed by Hsu and Wang (2000), in where the heat source was embedded on a board mounted vertically on the bottom wall at the center of the enclosure. Joshi and Sukhatme (2010) analysed combined natural and forced convection heat transfer from a horizontal circular cylinder to a transverse flow. In their study the numerical work is performed for the boundary conditions of constant surface temperature and constant wall heat flux. Kalam et al. (2014) analyzed the combined convection in an open cavity by finite element method under constant heat flux boundary conditions with magnetic field. They showed that increasing of Hartmann number decreases the heat transfer inside the cavity. Khanafer et al. (2002) studied mixed convection heat transfer in two-dimensional open-ended enclosure. Mixed convection flow of an electrically conducting and heat-generating/ absorbing fluid in a vertical channel consisting of two parallel plates in the presence of transverse magnetic field has been analyzed by Mahmud et al. (2003). Manca et al. (2003) studied numerically the effect of heated wall position on a laminar mixed convection in a channel with an open cavity. Three different heating modes such as assisting flow, opposing flow and heating from below are considered in their article. Mixed convection heat transfer in vertical elliptic ducts containing an upward flowing laminar fluid rotating about a parallel axis has been investigated by Olumuyiwa (2007). The author found that the mean Nusselt number is highest at duct eccentricity, e = 0 for a given Prandtl number. The fluid flow behavior of combined convection in lid-driven cavity containing a circular body was investigated by Oztop et al. (2009). A simulation of combined free and forced convective cooling of heat dissipating electronic components positioned in rectangular enclosure that was cooled by an external through flow of air has been investigated by Papanicolaou and Jaluria (1990, 1992, 1993 and 1994). Rahman et al. (2008b) performed combined convection in a vented square cavity containing a heat conducting horizontal solid circular cylinder. Pop et al. (2010) studied the heat generation effect by an exothermic reaction on the fully developed mixed convection flow in a vertical channel. Raji and Hasnaoui (1998a, 1998b) have been used finite difference procedure to analyze mixed convection flow in a rectangular cavity heated from the

side with a constant heat flux. They submitted a laminar cold jet from the bottom of its heated wall while the fluid leaves the cavity through the top or the bottom of the opposite vertical wall. Further, Raji and Hasnaoui (2000) studied the mixed convection in ventilated cavities with opposing and assisting flows where the upper and the left walls were arranged with equal heat fluxes. A two-dimensional finite-volume based numerical approach is adopted by Sudipta and Dipankar (2014) to solve the hydro-magnetic mixed convection in a horizontal lid-driven square cavity with a circular solid object. The object is located centrally within the enclosure. The results indicate a major influence of the prevailing convection method and the applied magnetic field on the flow as well as the thermal field, while the effect of Joule heating is found to be of very small significance. Saleh et al. (2013) performed flow reversal of fully developed mixed convection in a vertical channel with chemical reaction. Combined free and forced convection in a square cavity due to heat generating rectangular body was presented by Shuja et al. (2000) and examined the effect of exit port locations on the heat transfer characteristics in the cavity. They concluded that the normalized irreversibility increases with the increases of the exit port location number. Singh and Sharif (2003) reported mixed convective cooling of a rectangular cavity with inlet and exit openings on differentially heated side walls. Xianglong et al. (2014) studied combined natural convection and radiation heat transfer of various absorbing-emitting-scattering media in a square cavity.

Analytical Study

Mixed convection flow of couple stress fluid between two circular cylinders with Hall and ion-slip effects performed analytically by Srinivasacharya and Kaladhar (2012). Gaikwad and Kamble (2011) presented an analytical study of mixed convection through vertical channel in presence of porous media. Yang et al. (2009) performed both analytical and numerical calculations to study the buoyancy effect on the reversed flow structure and heat transfer processes in a finite vertical duct with a height to spacing ratio of 12. One of the walls is kept heated uniformly and the opposite wall is considered adiabatic. They developed simple analytical models to predict the penetration depth of the reversed flow for both assisted and opposed convection.

Experimental Study

Gau et al. (2000) carried out an experimental investigation on combined free and forced convection in a horizontal rectangular channel which was heated from a side. Mixed convection in a channel with an open cavity has been investigated experimentally by Manca et al. (2006). Prakash and Ravikumar (2013) investigated thermal comfort in a room with windows at adjacent walls along with additional vents. The authors studied indoor airflow behavior under various locations of the roof vent and best location was identified. Radhakrishnan et al. (2007) presented the results of experimental and numerical investigation of combined free and forced convection from a heat generating element in a ventilated cavity. From this study it can be concluded that a combined experimental and numerical investigation will significantly reduce the effort required to optimize the thermal performance in such kind of problems. Tahseen (2011) presented an experimental study for mixed convection through a circular tube filled with porous media and fixed horizontally and inclined. Xu et al. (2006) investigated experimentally the thermal flow around a square obstruction on a vertical wall in a differentially heated cavity.

Numerical Study

Deng and Tang (2002) conducted numerically mass and heat transport for conjugate natural convection/ heat conduction by streamlines and heat lines. In order to explore the transient heat transfer and flow nature of free convection of three different fluids in a vertical square enclosure having a heat-generating conducting body was numerically investigated by Ha et al. (1999). Kumar and Dalal (2006) performed natural convection about a tilled heated square cylinder placed in an enclosure in the range of Rayleigh number from $10^3 \leq 10^6$. It was noted that the uniform wall heat flux heating is quantitatively different from the uniform wall temperature heating. Lee and Ha (2005) used an accurate and efficient Chebyshev spectral collocation approach to examine natural convection in a horizontal layer of fluid with a conducting body in the interior. After that a numerical simulation of natural convection in a horizontal enclosure with a heat-generating conducting body was conducted by the same authors Lee and Ha (2006). Mansour and Alireza (2012) performed numerically the convective heat transfer of CuO nanofluids flowing

through a straight tube with uniform heat flux. A finite element analysis of conjugate free convection in a square enclosure with a conducting vertical wall was presented by Misra and Sarkar (1997). Oh et al. (1997) carried out numerical study of heat transfer and flow of natural convection in an enclosure with a heat generating conducting body. The effects of Rayleigh numbers Ra and temperature difference ratio on streamlines, isotherms and the average Nusselt numbers on the hot and cold walls are considered in their work. By the use of control volume finite element method, mixed convection in an air-cooled cavity with differentially heated vertical sidewalls has been analyzed by Omri and Nasrallah (1999). A numerical study of mixed convection in a square cavity with a heat conducting square cylinder at different locations was performed by Rahman et al. (2008a). Rahman et al. (2009) investigated combined natural and forced convection in a rectangular cavity containing a heat conducting horizontal circular cylinder by means of finite element method. Numerical simulation of natural convection heat transfer and fluid flow around a heated cylinder kept in a square enclosure with different thermal boundary conditions was presented by Roychowdhury et al. (2002). Sasaguchi et al. (1998) studied numerically the effect of the position of a cylinder in a rectangular cavity on the transient cooling of water around the cylinder. Shuja et al. (2009) analyzed numerically the flow over heat generating bodies in an open-ends cavity to show the effects of blocks' orientations and aspect ratios on the heat transfer rates, which finds applications in electronics cooling and industrial processing. Saeidi and Khodadadi (2006) analyzed numerically forced convection in a square cavity with inlet and outlet ports. Tasnim and Collins (2004) investigated buoyancy induced flow and heat transfer inside a square cavity with a thin baffle on the hot wall. They presented how heat transfer performance depends on baffle height, length and Rayleigh number and noted that adding baffle on the hot wall increases the rate of heat transfer. Laminar fluid flow and heat transfer in a channel with a built-in heated square cylinder was performed numerically by Turki et al. (2003). Yucel and Turkoglu (1998) performed free convection heat transfer in vertical cavities with conducting fins attached to the cold wall numerically.

1.5 Overview of the Present Study

It is apparent from the literature review that a little study on viscous incompressible thermal flow in mixed convection heat transfer in vented cavities heated bottom surface with inner obstacle has been performed. Such kinds of problems are very important for numerous engineering applications and hence the investigations of these types of study are necessary to ensure efficient performance of heat transfer equipments. As far it is known to the author, nobody has carried out the mixed convection problem in a square vented enclosure having heat generating, heat conducting and adiabatic solid obstacle, even though these are largely used. From this point of view the topics of the present study is chosen.

Present Work

The present study is a numerical analysis on the vented enclosures with centered solid block for the purpose of actual heat transfer performance. In the current research, three different types of inner obstacle inside the square cavities are considered, where the bottom wall is heated and the remaining three walls of the cavity are adiabatic in each of the three cases. Fresh and cold air enters into the cavity through inlet at uniform velocity u_i and ambient temperature T_i whereas it exits via outlet at the convective boundary condition (CBC). A uniform transverse magnetic field of strength B_0 is applied in the opposite to flow direction. It is expected to expose that the heat transfers in such chosen arrangements are dissimilar from those performed in the above mentioned literature which motivates the designer in choosing the best physical condition that is appropriate for his model.

Main Objective of the Thesis

In particular the aim of this thesis is to analyze numerically fluid flow and heat transfer behaviors inside vented enclosure containing three types of centered body as stated in above. The effects of non-dimensional governing parameters such as Hartmann number, Prandtl number, Reynolds number, Richardson number, solid-fluid thermal conductivity ratio and physical parameter such as obstacle diameter have been carried out in this work. Moreover, the effect of inlet and outlet port locations is studied for the case of heat generating obstacle. The outcomes will be

displayed in terms of streamlines, isotherms, as well as the average Nusselt number at the hot bottom wall and average fluid temperature inside the enclosure for different values of the considered parameters. The precise objectives of the current study are as follows:

- To develop a mathematical model concerning the mixed convection flow about a center lined obstacle (heat generating, heat conducting and adiabatic) kept in a square ventilated enclosure and thus to solve that model by means of finite element method.

- To execute the validity of the present finite element model by examining the effect of combined convection flow and heat transfer in a square vented cavity with selected solid bodies located in the center of the cavity.

- To get the optimum location of the inlet and outlet port for which most advantageous heat transfer performance can be achieved in vented enclosure.

- To find out the effects of Hartmann number, Prandtl number, Reynolds number, Richardson number, solid-fluid thermal conductivity ratio and diameter of the centered solid block.

Plan of the Work

This thesis is exposed in seven chapters. In chapter 1, an introductory talk is presented which includes heat transfer behavior, some relevant fluid properties, literature review described categorically and the main objective of the present research. Chapter 2 gives an idea of computational system. Also a finite element formulation is carried out for the problem of two-dimensional viscous incompressible steady-state thermal flow. To find out the maximum cooling efficiency among the four cavity configurations; the effect of inlet and outlet port is studied in chapter 3.

A detailed parametric study on MHD mixed convection flow and heat transfer in vented cavities with heat generating centered obstacle is conducted in chapter 4. Further, the effects of pertinent parameters are investigated for the case of heat conducting and adiabatic obstacle in chapters 5 and 6 respectively.

Last of all, in chapter 7 the essay is concluded by revealing the major outcomes of the study with comparison in heat transfer rate between three different types of centered solid body and probable further works is proposed.

Chapter 2

Computational Details

Finite element method has been used to analyze viscous incompressible thermal flows numerically in our present investigation. Physical phenomena of such problems can be expressed by mathematical model which may be consists of ordinary or partial differential equations and this types of problems is solved either experimentally or numerically. In the current study fluid motion is governed by the coupling of energy equations and the Navier-Stokes equations and thus the problem is somewhat complicated. The governing equations involve a set of coupled nonlinear partial differential equations that is difficult to solve; particularly for complex geometries with boundary conditions. Firstly we have to use a discretization scheme to obtain a numerical approximate solution. After discretization a system of algebraic equations is yielded and a computer program is then applied to solve these equations. The reason of preferring numerical system, a brief description of solution process together with finite element formulation is presented in this chapter.

2.1 Advantages of Numerical Investigation

The numerical method which always works with iteration is mainly to solve complex problem, physically or geometrically. In numerical analysis, numerical integration constitutes a broad family of algorithms for calculating an approximate value of a definite integral, and by extension, the term is also sometimes used to describe the numerical solution of differential equations.

Consider a situation when the governing equations are a function of several parameters. For each combination of parameters a numerical solution is required. Suppose you have a mathematical model and you want to find a solution to the set of equations in order to understand its behavior. Then you turn to numerical methods of solving the equations. For a differential equation that describes behavior over time, the numerical method starts with the initial values of the variables, and then uses the equations to figure out the changes in these variables over a very brief time period. Its only an approximation, but it can be a very good approximation under certain circumstances.

Especially the numerical method FEM is an excellent tool to solve complicated geometrical shapes with a boundary and load condition that is difficult to describe with analytical expressions available in the industry. Famous Navier-stoke equation has not been solved till now analytically but can be easily solved by Numerical Schemes.

However the advantages of numerical methods are also conditional. The numerical solution method selected must have the important properties of consistency, stability, convergence, conservation, boundedness, reliability and most importantly accuracy. It should be understood that numerical solutions of fluid flow and heat transfer problems are only approximate solutions. The systematic errors due to modeling, discretization and iteration must be minimum (set as a condition). Mathematical model involving partial differential equations in two-dimensional thermodynamics problems are required to be solved simultaneously with some boundary conditions. The analytical methods are not of much help in solving the practical problems and thus, there no alternatives except the numerical methods for the solution of the problems of practical interest.

However, if analytical solution is not possible or very difficult/complicated etc., then numerical method has an advantage of being the only method, provided the results are somewhere close to those inferred from properties of analytical/experimental results.

2.2 Different Steps of Numerical Solution Methods

In general numerical methods are formed with some sequential steps. Ferziger and Perić (1997) presented a number of components of numerical solution methods in their study; some major steps only are discussed here.

2.2.1 Mathematical Model

For any numerical method, the initial step is the mathematical model which is a description of a system using mathematical concepts and language. A mathematical model usually reveals a structure by a set of variables and a set of equations with boundary conditions. The procedure of developing a mathematical model is known as mathematical modeling. Mathematical models are widely used in the natural

sciences and engineering disciplines. Such a model may help to clarify a system and to study the effects of different parameters, and thus to guess about behavior.

2.2.2 Discretization Method

Numerical discretization is the first step to solve a mathematical model numerically. One has to choose an appropriate discretization method, i.e. a method of approximating the differential equations by a system of algebraic equations for the variable at some set of distinct positions in space and time. After using successive linearization of the non-linear equations, the obtained linear systems are usually solved by iterative techniques. Finally the selection of solver depends on the nature of grid and the number of nodes concerning in each equation.

Various spatial discretization schemes are finite volume (FV) method, finite element (FE) method, boundary element (BE) method and boundary volume (BV) method. Galerkin weighted residual based finite element method (FEM) is used in the present numerical calculation and a details of this method is available in the literatures of Chung (2002) and Dechaumphai (1999).

2.2.3 Numerical Grid Generation

The array of discrete points throughout the flow field is basically called a grid and grid generation is the mode of determining such a grid. Numerical grid generation plays a crucial role in any computational simulation problem when the geometry of the underlying region is complicated or when the solution has a complex structure. The capability to perform successful numerical procedures for the approximation of computational fluid dynamics (CFD) problems depends on the geometric modeling and grid generation phases which is very recognized. A proper grid generation can remove difficulties from this computational phase and help to prevent girding from becoming a hazardous bottleneck in complex simulations with consuming a noteworthy simulation time. For this reason, different research projects have concentrated on the development of numerical methods for the generation of structured and unstructured grids.

Finite element method can be used for unstructured grids as the governing equations in this technique are found in integral form and numerical integration can be

performed directly on such domain where no coordinate transformation is necessary. In finite element method, the mesh generation is the process to subdivide a domain into a set of sub-domains which are known as finite elements. Figure 2.1 shows a domain, Λ where Λ^e is the sub-domain which may be of the form square, triangle, rectangle, trapezium etc. with boundary, Γ^e. Anderson (1995) and Chung (2002) presented a detailed discussion on this topic. A two-dimensional domain as shown in Fig. 2.1 is considered for present working area with triangular sub-domain in our study.
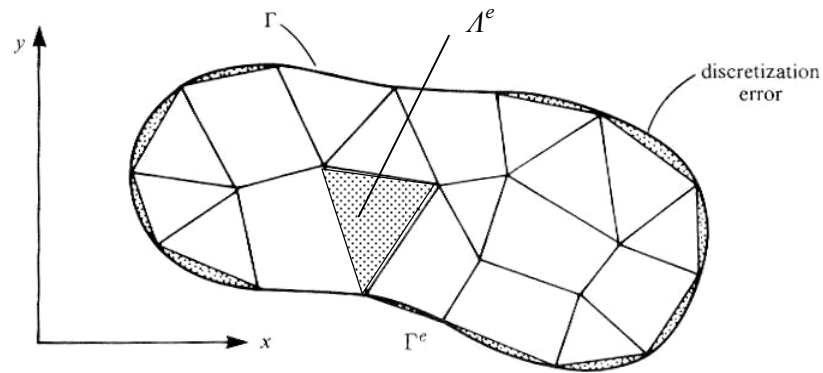
Figure 2.1: A typical FE discretization of a domain, Reddy & Gartling (1994)

2.2.4 Finite Approximations

One has to choose the appropriate approximations that will be used in the discretization process after the selection of grid type. In a finite difference method, approximations for the derivatives at the grid points have to be selected whereas one has to select the methods of approximating surface and volume integrals in a finite volume method. But the approximating functions and weighting functions should be chosen in a finite element method.

2.2.5 Algorithm

The computational system was forwarded by means of the iterative Newton-Raphson algorithm; the discrete forms of the continuity, momentum and energy equations are solved to obtain the desired value of the velocity and the temperature. To estimate
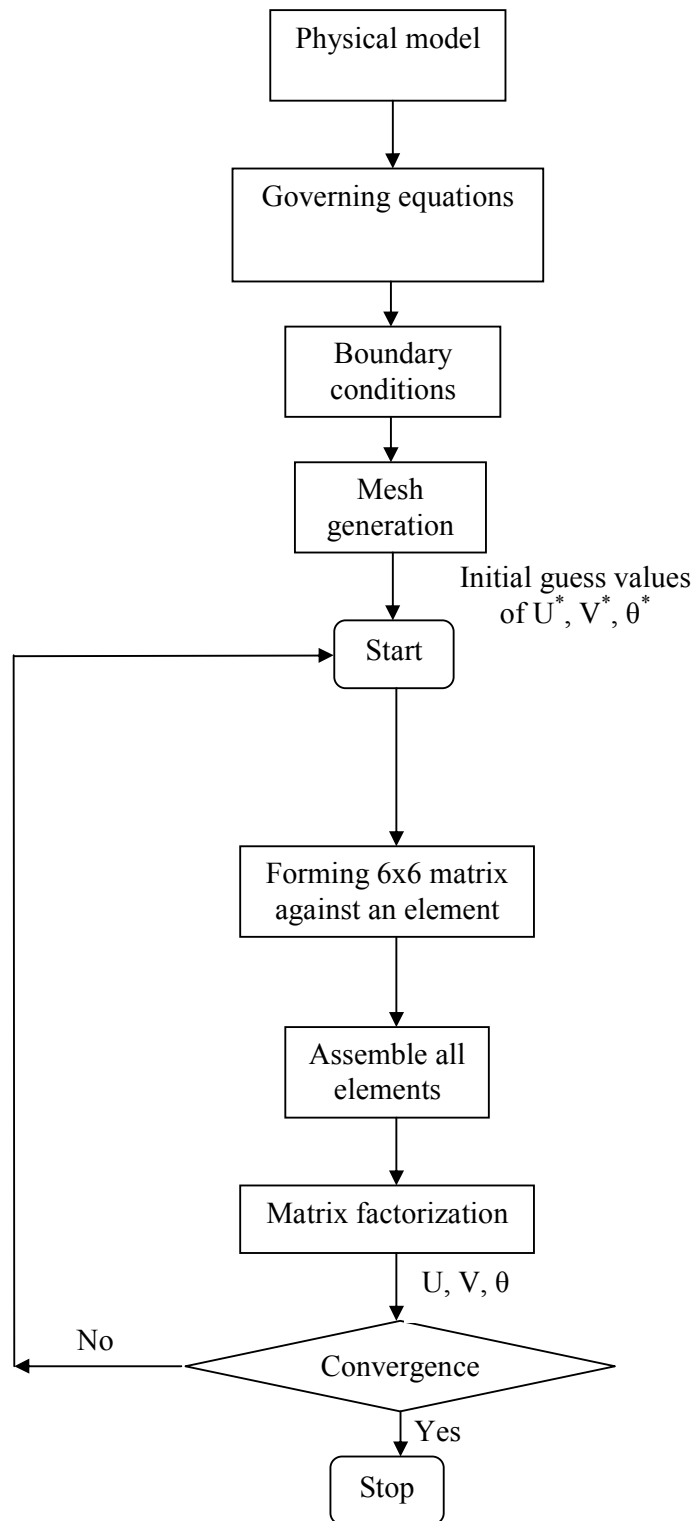
Physical model

$\downarrow$

Governing equations

$\downarrow$

Boundary conditions

$\downarrow$

Mesh generation

Initial guess values
of U^*, V^*, θ^*

Start

$\downarrow$

Forming 6x6 matrix against an element

$\downarrow$

Assemble all elements

$\downarrow$

Matrix factorization

U, V, θ

$\downarrow$

No ← Convergence

Yes $\downarrow$

Stop

Figure 2.2: Flow chart of the computational procedure

21

the initial values of the pertinent variables is essential for further steps. Then the numerical solutions of the variables are found while the convergent criterion is satisfied after performing some successive steps. The algorithm that used in this problem is exposed by the above flow diagram.

2.2.6 Solution of System of Equations

A system of linear algebraic equations has been solved by the UMFPACK with MATLAB interface. UMFPACK is a set of routines for solving asymmetric sparse linear systems $Ax = b$, using the Asymmetric MultiFrontal method and direct sparse LU factorization. Five primary UMFPACK routines are required to factorize A or $Ax = b$:

1. Pre-orders the columns of A to reduce fill-in and performs a symbolic analysis.
2. Numerically scales and then factorizes a sparse matrix.
3. Solves a sparse linear system using the numeric factorization.
4. Frees the Symbolic object.
5. Frees the Numeric object.

Additional routines are:

1. Passing a different column ordering
2. Changing default parameters
3. Manipulating sparse matrices
4. Getting LU factors
5. Solving the LU factors
6. Computing determinant

UMFPACK factorizes PAQ, PRAQ, or $PR^{-1}AQ$ into the product LU, where L and U are lower and upper triangular, respectively, P and Q are permutation matrices, and R is a diagonal matrix of row scaling factors (or $R = I$ if row-scaling is not used). Both P and Q are chosen to reduce fill-in (new non zeros in L and U that are not present in A). The permutation P has the dual role of reducing fill-in and maintaining numerical accuracy (via relaxed partial pivoting and row interchanges). The sparse matrix A can be square or rectangular, singular or non-singular, and real or complex (or any combination). Only square matrices A can be used to solve $Ax = b$ or related

systems. Rectangular matrices can only be factorized. UMFPACK first finds a column pre-ordering that reduces fill-in, without regard to numerical values. It scales and analyzes the matrix, and then automatically selects one of three strategies for pre-ordering the rows and columns: asymmetric, 2-by-2 and symmetric. These strategies are described below.

One notable attribute of the UMFPACK is that whenever a matrix is factored, the factorization is stored as a part of the original matrix so that further operations on the matrix can reuse this factorization. Whenever a factorization or decomposition is calculated, it is preserved as a list (element) in the factor slot of the original object. In this way a sequence of operations, such as determining the condition number of a matrix and then solving a linear system based on the matrix, do not require multiple factorizations of the intermediate results.

Conceptually, the simplest representation of a sparse matrix is as a triplet of an integer vector **i** giving the row numbers, an integer vector **j** giving the column numbers, and a numeric vector **x** giving the non-zero values in the matrix. The triplet representation is row-oriented if elements in the same row were adjacent and column-oriented if elements in the same column were adjacent. The compressed sparse row (csr) or compressed sparse column (csc) representation is similar to row-oriented triplet or column-oriented triplet respectively. These compressed representations remove the redundant row or column in indices and provide faster access to a given location in the matrix.

2.3 Finite Element Method

The finite element method (FEM) is one of the powerful computational methods of numerical analysis for finding the approximate solution of ordinary and partial differential equations that arise in the various fields of science and engineering. The finite element was initially developed on a physical basis for the analysis of problems in structural mechanics. However it was soon recognized that the method can be applied equally to the solution of many other classes of problems such as fluid flow, heat flow, computational fluid dynamics, electric and magnetic field etc. Although its application is still under intensive research in the field of fluid mechanics, particularly to convective viscous flows. It has its superiority over other methods

because of its ability to solve problems concerning domain with irregular geometry and heterogeneous composition.

The basic concept of the finite element method is to generate systematically piecewise approximation functions needed in the solution of partial differential equations by the Galerkin weighted residual method. That is we approximate a solution to a complicated problem by subdividing the region of interest into simple geometric shapes, called finite elements, as shown in Fig. 2.1 and representing the solution within each sub-domain by relatively simple function. The ideas from interpolation theory are used frequently to construct the approximation functions, which satisfy the governing equations and boundary conditions of a problem. The necessary approximating functions in finite elements are determined in terms of nodal values of a physical domain.

The major steps involved in finite element analysis of a typical problem are:

1. Discretization (or representation) of the given domain into a collection of finite elements (mesh generation).

2. Derivation of approximation function.

3. Derivation of element equations for all typical elements of the mesh.

4. Assembly of element equations to obtain the equation of whole problem.

5. Imposition of the boundary conditions of the problem.

6. Solution of the assembled equations.

7. Post-processing the results.

2.3.1 Finite Element Formulation

The differential equations for the two-dimensional steady-state thermal flow are,

$$u_{,x} + v_{,y} = 0 \tag{1}$$

$$\rho\left(u\, u_{,x} + v\, u_{,y}\right) = \sigma_{x,x} + \tau_{xy,y} \tag{2}$$

$$\rho\left(u\, v_{,x} + v\, v_{,y}\right) = \tau_{xy,x} + \sigma_{y,y} - \rho g\left[1 - \beta\left(T - T_0\right)\right] \tag{3}$$

$$\rho c \left(u \, T_{,x} + v \, T_{,y} \right) = \left(k \, T_{,x} \right)_{,x} + \left(k \, T_{,y} \right)_{,y} \tag{4}$$

Where, u and v are the velocity components in the x and y direction, respectively; T is the fluid temperature, T_0 is the reference temperature for which buoyant temperature vanishes, ρ is the fluid density, g is the gravitational constant, β is the volumetric coefficient of thermal expansion, c is the fluid specific heat, and k is the fluid thermal conductivity. The stress components are defined by,

$$\sigma_x = -p + 2\mu \, u_{,x} \tag{5}$$

$$\sigma_y = -p + 2\mu \, v_{,y} \tag{6}$$

$$\tau_{xy} = \mu \left(u_{,y} + v_{,x} \right) \tag{7}$$

Where, p is the total pressure and μ is the fluid dynamic viscosity.

The partial equations, Eqs (1-4), are to be solved together with appropriate boundary conditions of,

(1) Specifying velocity components $\left(u_i, \, v_i \right)$ and fluid temperature $\left(T_i \right)$ along inflow boundary $\left(S_i \right)$.

$$u = u_i \left(x, y \right)$$

$$v = v_i \left(x, y \right)$$

$$T = T_i \left(x, y \right)$$

(2) Specifying surface tractions $\left(P_x, \, P_y \right)$ along outflow boundary $\left(S_0 \right)$.

$$P_x = \sigma_x l + \tau_{xy} m$$

$$P_y = \tau_{xy} l + \sigma_y m$$

Where, l and m are direction cosines of the unit vector normal to the boundary.

(3) Specifying velocity components $\left(u_w, \, v_w \right)$ and fluid temperature $\left(T_w \right)$ or heat flux $\left(q_w \right)$ that flows into or out from domain along wall boundary $\left(S_w \right)$.

$$u = u_w \left(x, y \right)$$

$$v = v_w \left(x, y \right)$$

$$T = T_w \left(x, y \right) \quad \text{or} \quad q = q_w \left(x, y \right)$$

$$u(x,y) = N_\alpha \, u_\alpha$$

$$v(x,y) = N_\alpha \, v_\alpha$$

$$T(x,y) = N_\alpha \, T_\alpha$$

$$p(x,y) = H_\lambda \, p_\lambda$$

Where $\alpha = 1, 2, \ldots \ldots , 6$; $\lambda = 1, 2, 3$; N_α are the element interpolation functions for the velocity components and the temperature, and H_λ are the element interpolation functions for the pressure.

Equations (2), (3) (4) and (1) respectively are as follows

$$\int_A N_\alpha \, \rho \left(u \, u_{,x} + v \, u_{,y} \right) dA = \int_A N_\alpha \left(\sigma_{x,x} + \tau_{xy,y} \right) dA \qquad\qquad 8(a)$$

$$\int_A N_\alpha \, \rho \left(u \, v_{,x} + v \, v_{,y} \right) dA = \int_A N_\alpha \left(\tau_{xy,x} + \sigma_{y,y} \right) dA - \int_A N_\alpha \, \rho g \, [1 - \beta \, (T - T_0)] \, dA \qquad 8(b)$$

$$\int_A N_\alpha \rho c \left(u \, T_{,x} + v \, T_{,y} \right) dA = \int_A N_\alpha \left[(k \, T_{,x})_{,x} + (k \, T_{,y})_{,y} \right] dA \qquad\qquad 8(c)$$

$$\int_A H_\lambda \left(u_{,x} + v_{,y} \right) dA = 0 \qquad\qquad 8(d)$$

Where, A is the element area.

Gauss's theorem is then applied to equations $8(a)$-$8(c)$ to generate the boundary integral terms associated with the surface tractions and heat flux. Then equations $8(a)$-$8(d)$ become,

According to Gausss's theorem

$$\int_A \nabla.F dA = \int_C F.n dS \text{ , we have}$$

$$\int_A \nabla.N_\alpha \nabla u \, dA = \int_A N_\alpha \nabla u.n dS, \text{ where } F = N_\alpha \nabla u \qquad\qquad (*)$$

Using the vector identity

$$\nabla.(\phi F) = \phi \nabla.F + \nabla \phi.F,$$

$i.e., \nabla.(N_\alpha \nabla u) = N_\alpha \nabla.\nabla u + \nabla N_\alpha.\nabla u$ in (*) we have

$$\left[\varphi = N_\alpha, \ F = \nabla u \right]$$

$$\int_A N_\alpha \nabla.\nabla u \, dA + \int_A \nabla N_\alpha.\nabla u \, dA = \int_C N_\alpha \nabla u.n \, dS$$

$$\Rightarrow \int_A N_\alpha \nabla.\nabla u \, dA = \int_C N_\alpha \nabla u.n \, dS - \int_A \nabla N_\alpha.\nabla u \, dA$$

Equation 8(a) can be written in the form

$$\int_A N_\alpha \, \rho\left(u \, u_{,x} + v \, u_{,y}\right) dA = \int_A N_\alpha \left(\sigma_{x,x} + \tau_{xy,y}\right) dA$$

$$\int_A N_\alpha \, \rho\left(u \, u_{,x} + v \, u_{,y}\right) dA = \int_A N_\alpha \sigma_{x,x} \, dA + \int_A N_\alpha \tau_{xy,y} \, dA$$

$$\int_A N_\alpha \, \rho\left(u \, u_{,x} + v \, u_{,y}\right) dA = \int_A N_\alpha \sigma_{x,x} \, \partial x \partial y + \int_A N_\alpha \tau_{xy,y} \, \partial y \partial x$$

$$\int_A N_\alpha \, \rho\left(u \, u_{,x} + v \, u_{,y}\right) dA = \int\left[\int N_\alpha \sigma_{x,x} \partial x\right] \partial y + \int\left[\int N_\alpha \tau_{xy,y} \partial y\right] \partial x$$

$$\int_A N_\alpha \, \rho\left(u \, u_{,x} + v \, u_{,y}\right) dA = \int\left[N_\alpha \int \sigma_{x,x} \partial x - \int\left\{\frac{\partial}{\partial x} N_\alpha \int \sigma_{x,x} \partial x\right\} \partial x\right] \partial y + \int\left[N_\alpha \int \tau_{xy,y} \partial y - \int\left\{\frac{\partial}{\partial y} N_\alpha \int \tau_{xy,y} \partial y\right\} \partial y\right] \partial x$$

$$\int_A N_\alpha \, \rho\left(u \, u_{,x} + v \, u_{,y}\right) dA = \int\left[N_\alpha \, \sigma_x - \int N_{\alpha,x} \sigma_x \partial x\right] \partial y + \int\left[N_\alpha \tau_{xy} - \int N_{\alpha,y} \tau_{xy} \partial y\right] \partial x$$

$$\int_A N_\alpha \, \rho\left(u \, u_{,x} + v \, u_{,y}\right) dA = \int N_\alpha \, \sigma_x \partial y - \int_A N_{\alpha,x} \sigma_x \, dA + \int N_\alpha \tau_{xy} \partial x - \int_A N_{\alpha,y} \tau_{xy} \, dA$$

$$\int_A N_\alpha \, \rho\left(u \, u_{,x} + v \, u_{,y}\right) dA = \int N_\alpha \, \sigma_x \partial y + \int N_\alpha \tau_{xy} \partial x - \int_A \left(N_{\alpha,x} \sigma_x + \int N_{\alpha,y} \tau_{xy}\right) dA$$

$$\int_A N_\alpha \, \rho\left(u \, u_{,x} + v \, u_{,y}\right) dA + \int_A \left(N_{\alpha,x} \sigma_x + \int N_{\alpha,y} \tau_{xy}\right) dA = \int_{S_0} N_\alpha \sigma_x l \, dS_0 + \int_{S_0} N_\alpha \tau_{xy} m \, dS_0$$

$$\int_A N_\alpha \, \rho\left(u \, u_{,x} + v \, u_{,y}\right) dA + \int_A \left(N_{\alpha,x} \sigma_x + \int N_{\alpha,y} \tau_{xy}\right) dA = \int_{S_0} N_\alpha (\sigma_x l + \tau_{xy} m) \, dS_0$$

$$\int_A N_\alpha \, \rho\left(u \, u_{,x} + v \, u_{,y}\right) dA + \int_A \left(N_{\alpha,x} \sigma_x + \int N_{\alpha,y} \tau_{xy}\right) dA = \int_{S_0} N_\alpha P_x \, dS_0 \text{ (taking } \partial y = l \, dS_0, \partial x = m \, dS_0) \qquad 9(a)$$

Equation 8(b) can be written in the form

$$\int_A N_\alpha \, \rho\left(u \, v_{,x} + v \, v_{,y}\right) dA = \int_A N_\alpha \left(\tau_{xy,x} + \sigma_{y,y}\right) dA - \int_A N_\alpha \, \rho g \, [1-\beta(T-T_0)] \, dA$$

$$\int_A N_\alpha \, \rho\left(u \, v_{,x} + v \, v_{,y}\right) dA = \int_A N_\alpha \tau_{xy,x} \, dA + \int_A N_\alpha \sigma_{y,y} \, dA - \int_A N_\alpha \, \rho g \, [1-\beta(T-T_0)] \, dA$$

$$\int_A N_\alpha \, \rho\left(u \, v_{,x} + v \, v_{,y}\right) dA = \int_A N_\alpha \tau_{xy,x} \, \partial x \partial y + \int_A N_\alpha \sigma_{y,y} \, \partial y \partial x - \int_A N_\alpha \, \rho g \, [1-\beta(T-T_0)] \, dA$$

$$\int_A N_\alpha \, \rho\left(u \, v_{,x} + v \, v_{,y}\right) dA = \int\left[\int N_\alpha \tau_{xy,x} \partial x\right] \partial y + \int\left[\int N_\alpha \sigma_{y,y} \partial y\right] \partial x - \int_A N_\alpha \, \rho g \, [1-\beta(T-T_0)] \, dA$$

$$\int_A N_\alpha\, \rho\left(u\, v_{,x} + v\, v_{,y}\right) dA = \int\left[N_\alpha \int \tau_{xy,x} \partial x - \int\left\{\frac{\partial}{\partial x} N_\alpha \int \tau_{xy,x} \partial x\right\} \partial x\right]\partial y + \int\left[N_\alpha \int \sigma_{y,y}\partial y - \int\left\{\frac{\partial}{\partial y} N_\alpha \int \sigma_{y,y}\partial y\right\}\partial y\right]\partial x$$
$$-\int_A N_\alpha\, \rho g\, [1-\beta(T-T_0)]\, dA$$

$$\int_A N_\alpha\, \rho\left(u\, v_{,x} + v\, v_{,y}\right) dA = \int\left[N_\alpha \tau_{xy} - \int N_{\alpha,x}\tau_{xy}\partial x\right]\partial y + \int\left[N_\alpha\, \sigma_y - \int N_{\alpha,y}\sigma_y \partial y\right]\partial x$$
$$-\int_A N_\alpha\, \rho g\, [1-\beta(T-T_0)]\, dA$$

$$\int_A N_\alpha\, \rho\left(u\, v_{,x} + v\, v_{,y}\right) dA = \int N_\alpha \tau_{xy}\partial y - \int_A N_{\alpha,x}\tau_{xy} dA + \int N_\alpha\, \sigma_y \partial x - \int_A N_{\alpha,y}\sigma_y dA$$
$$-\int_A N_\alpha\, \rho g\, [1-\beta(T-T_0)]\, dA$$

$$\int_A N_\alpha\, \rho\left(u\, v_{,x} + v\, v_{,y}\right) dA = \int N_\alpha \tau_{xy}\partial y + \int N_\alpha\, \sigma_y \partial x - \int_A \left(N_{\alpha,x}\tau_{xy} + N_{\alpha,y}\sigma_y\right) dA$$
$$-\int_A N_\alpha\, \rho g\, [1-\beta(T-T_0)]\, dA$$

$$\int_A N_\alpha\, \rho\left(u\, v_{,x} + v\, v_{,y}\right) dA + \int_A \left(N_{\alpha,x}\tau_{xy} + N_{\alpha,y}\sigma_y\right) dA = \int_{S_0} N_\alpha \tau_{xy} l\, dS_0 + \int_{S_0} N_\alpha \sigma_y m\, dS_0$$
$$-\int_A N_\alpha\, \rho g\, [1-\beta(T-T_0)]\, dA$$

$$\int_A N_\alpha\, \rho\left(u\, v_{,x} + v\, v_{,y}\right) dA + \int_A \left(N_{\alpha,x}\tau_{xy} + N_{\alpha,y}\sigma_y\right) dA = \int_{S_0} N_\alpha\left(\tau_{xy} l + \sigma_y\, m\right) dS_0$$
$$-\int_A N_\alpha\, \rho g\, [1-\beta(T-T_0)]\, dA$$

$$\int_A N_\alpha\, \rho\left(u\, v_{,x} + v\, v_{,y}\right) dA + \int_A \left(N_{\alpha,x}\tau_{xy} + N_{\alpha,y}\sigma_y\right) dA = \int_{S_0} N_\alpha P_y\, dS_0$$

9(b)

$$-\int_A N_\alpha\, \rho g\, [1-\beta(T-T_0)]\, dA \quad \text{(taking } \partial y = l\, dS_0, \partial x = m\, dS_0)$$

Equation 8(c) can be written in the form

$$\int_A N_\alpha \rho c\left(u\, T_{,x} + v\, T_{,y}\right) dA = \int_A N_\alpha\left[(k\, T_{,x})_{,x} + (k\, T_{,y})_{,y}\right] dA$$

$$\int_A N_\alpha\, \rho c\left(u\, T_{,x} + v\, T_{,y}\right) dA = k\int_A N_\alpha\left[(T_{,x})_{,x} + (T_{,y})_{,y}\right] dA$$

$$\int_A N_\alpha\, \rho c\left(u\, T_{,x} + v\, T_{,y}\right) dA = k\int_c N_\alpha \nabla T.n\, ds - k\int_A \nabla N_\alpha.\nabla T\, dA$$

$$\int_A N_\alpha\, \rho c\left(u\, T_{,x} + v\, T_{,y}\right) dA + k\int_A \nabla N_\alpha.\nabla T\, dA = \int_{S_w} N_\alpha\, q_s\, dS_w$$

$$\int_A N_\alpha\, \rho c\left(u\, T_{,x} + v\, T_{,y}\right) dA + k\int_A \left(N_{\alpha,x}T_{,x} + N_{\alpha,y}T_{,y}\right) dA = \int_{S_w} N_\alpha\, q_s\, dS_w$$

$$\int_A N_\alpha\, \rho c\left(u\, T_{,x} + v\, T_{,y}\right) dA + \int_A N_{\alpha,x}\left(kT_{,x}\right) dA + \int_A N_{\alpha,y}\left(kT_{,y}\right) dA = \int_{S_w} N_\alpha\, q_s\, dS_w$$

9(c)

$$[k\nabla T.n = q_S]$$

Equation 8(d) can be written in the form

$$\int_A H_\lambda \left(u_{,x} + v_{,y} \right) dA = 0$$

$$\int_A H_\lambda N_{\beta,x} u_\beta \, dA + \int_A H_\lambda N_{\beta,y} v_\beta \, dA = 0$$

$$\frac{1}{\rho} \int_A H_\mu N_{\beta,x} u_\beta \, dA + \frac{1}{\rho} \int_A H_\mu N_{\beta,y} v_\beta \, dA = 0 \qquad\qquad 9(d)$$

Substituting the element velocity component distributions, the temperature distribution, and the pressure distribution, and the stress components from equation (5)-(7), the finite element equations can be written as,

$$u(x,y) = N_\beta u_\beta \qquad \frac{\partial u}{\partial x} = \frac{\partial N_\gamma}{\partial x} u_\gamma, \quad \frac{\partial u}{\partial y} = \frac{\partial N_\gamma}{\partial y} u_\gamma$$

$$v(x,y) = N_\beta v_\beta \qquad \frac{\partial v}{\partial x} = \frac{\partial N_\gamma}{\partial x} v_\gamma, \quad \frac{\partial v}{\partial y} = \frac{\partial N_\gamma}{\partial y} v_\gamma$$

$$T(x,y) = N_\beta T_\beta \qquad \frac{\partial T}{\partial x} = \frac{\partial N_\gamma}{\partial x} T_\gamma, \quad \frac{\partial T}{\partial y} = \frac{\partial N_\gamma}{\partial y} T_\gamma$$

$$p(x,y) = H_\lambda p_\lambda \qquad \frac{\partial p}{\partial x} = \frac{\partial H_\delta}{\partial x} p_\delta, \quad \frac{\partial p}{\partial y} = \frac{\partial H_\delta}{\partial y} p_\delta$$

From equation 9(a),

$$\int_A N_\alpha \, \rho \left(u\, u_{,x} + v\, u_{,y} \right) dA + \int_A \left(N_{\alpha,x} \sigma_x + N_{\alpha,y} \tau_{xy} \right) dA = \int_{S_0} N_\alpha P_x ds_0$$

$$\int_A N_\alpha \, \rho \left(u\, u_{,x} + v\, u_{,y} \right) dA + \int_A N_{\alpha,x} \left(-p + 2\mu u_{,x} \right) dA + \int_A N_{\alpha,y} \left\{ \mu \left(u_{,y} + v_{,x} \right) \right\} dA = \int_{S_0} N_\alpha P_x ds_0$$

$$\int_A N_\alpha \, \rho \left(u\, u_{,x} + v\, u_{,y} \right) dA - \int_A p N_{\alpha,x} dA + 2\mu \int_A N_{\alpha,x} u_{,x} dA + \mu \int_A N_{\alpha,y} u_{,y} dA + \mu \int_A N_{\alpha,y} v_{,x} dA = \int_{S_0} N_\alpha P_x ds_0$$

$$\rho \int_A N_\alpha \left(N_\beta u_\beta N_{\gamma,x} u_\gamma + N_\beta v_\beta N_{\gamma,y} u_\gamma \right) dA - \int_A N_{\alpha,x} H_\lambda p_\lambda \, dA + 2\mu \int_A N_{\alpha,x} N_{\beta,x} u_\beta dA$$

$$+ \mu \int_A N_{\alpha,y} N_{\beta,y} u_\beta dA + \mu \int_A N_{\alpha,y} N_{\beta,x} v_\beta dA = \int_{S_0} N_\alpha P_x ds_0$$

$$\int_A N_\alpha N_\beta N_{\gamma,x} u_\beta u_\gamma dA + \int_A N_\alpha N_\beta N_{\gamma,y} v_\beta u_\gamma dA - \frac{1}{\rho} \int_A N_{\alpha,x} H_\lambda p_\lambda \, dA + 2\upsilon \int_A N_{\alpha,x} N_{\beta,x} u_\beta dA$$

$$+ \upsilon \int_A N_{\alpha,y} N_{\beta,y} u_\beta dA + \upsilon \int_A N_{\alpha,y} N_{\beta,x} v_\beta dA = \frac{1}{\rho} \int_{S_0} N_\alpha P_x ds_0$$

Equation 9(b) gives

$$\int_A N_\alpha \, \rho \left(u\, v_{,x} + v\, v_{,y} \right) dA + \int_A \left(N_{\alpha,x} \tau_{xy} + N_{\alpha,y} \sigma_y \right) dA = \int_{S_0} N_\alpha P_y ds_0 - \int_A N_\alpha \, \rho g \, [1 - \beta(T - T_0)] \, dA$$

$$\int_A N_\alpha \, \rho \left(u\, v_{,x} + v\, v_{,y} \right) dA + \int_A N_{\alpha,x} \left\{ \mu \left(u_{,y} + v_{,x} \right) \right\} dA + \int_A N_{\alpha,y} \left(-p + 2\mu v_{,y} \right) dA = \int_{S_0} N_\alpha P_y ds_0 - \int_A N_\alpha \, \rho g \, [1 - \beta(T - T_0)] \, dA$$

$$\int_A N_\alpha \, \rho \left(u\, v_{,x} + v\, v_{,y} \right) dA + \mu \int_A N_{\alpha,x} u_{,y} dA + \mu \int_A N_{\alpha,x} v_{,x} dA - \int_A p N_{\alpha,y} dA + 2\mu \int_A N_{\alpha,y} v_{,y} dA = \int_{S_0} N_\alpha P_y ds_0$$

$$- \int_A N_\alpha \, \rho g \, [1 - \beta(T - T_0)] \, dA$$

$$\int_A N_\alpha \, \rho \left(u \, v_{,x} + v \, v_{,y} \right) dA + \mu \int_A N_{\alpha,x} u_{,y} dA + \mu \int_A N_{\alpha,x} v_{,x} dA - \int_A p N_{\alpha,y} dA + 2\mu \int_A N_{\alpha,y} v_{,y} dA = \int_{S_0} N_\alpha P_y dS_0$$

$$- \rho g \int_A N_\alpha dA + \rho g \beta \int_A N_\alpha T dA - \rho g \beta T_0 \int_A N_\alpha dA$$

$$\rho \int_A N_\alpha \left(N_\beta u_\beta N_{\gamma,x} v_\gamma + N_\beta v_\beta N_{\gamma,y} v_\gamma \right) dA + \mu \int_A N_{\alpha,x} N_{\beta,y} u_\beta dA + \mu \int_A N_{\alpha,x} N_{\beta,x} v_\beta dA - \int_A N_{\alpha,y} H_\lambda P_\lambda \, dA$$

$$+ 2\mu \int_A N_{\alpha,y} N_{\beta,y} v_\beta dA = \int_{S_0} N_\alpha P_y dS_0 - \rho g \int_A N_\alpha dA + \rho g \beta \int_A N_\alpha N_\beta T_\beta dA - \rho g \beta T_0 \int_A N_\alpha dA$$

$$\int_A N_\alpha N_\beta N_{\gamma,x} u_\beta v_\gamma dA + \int_A N_\alpha N_\beta N_{\gamma,y} v_\beta v_\gamma dA - \frac{1}{\rho} \int_A N_{\alpha,y} H_\lambda P_\lambda \, dA - g\beta \int_A N_\alpha N_\beta T_\beta dA + \upsilon \int_A N_{\alpha,x} N_{\beta,y} u_\beta dA$$

$$+ \upsilon \int_A N_{\alpha,x} N_{\beta,x} v_\beta dA + 2\upsilon \int_A N_{\alpha,y} N_{\beta,y} v_\beta dA = \frac{1}{\rho} \int_{S_0} N_\alpha P_y dS_0 - g \int_A N_\alpha dA - g\beta T_0 \int_A N_\alpha dA$$

From equation 9(*c*),

$$\int_A N_\alpha \, \rho c \left(u \, T_{,x} + v \, T_{,y} \right) dA + \int_A N_{\alpha,x} \left(kT_{,x} \right) dA + \int_A N_{\alpha,y} \left(kT_{,y} \right) dA = \int_{S_w} N_\alpha \, q_s \, dS_w$$

$$\rho c \int_A N_\alpha \left(N_\beta u_\beta N_{\gamma,x} T_\gamma + N_\beta v_\beta N_{\gamma,y} T_\gamma \right) dA + k \int_A N_{\alpha,x} N_{\beta,x} T_\beta dA + k \int_A N_{\alpha,y} N_{\beta,y} T_\beta dA = \int_{S_w} N_\alpha \, q_s \, dS_w$$

$$\int_A N_\alpha N_\beta N_{\gamma,x} u_\beta T_\gamma dA + \int_A N_\alpha N_\beta N_{\gamma,y} v_\beta T_\gamma dA + \frac{k}{\rho c} \int_A N_{\alpha,x} N_{\beta,x} T_\beta dA + \frac{k}{\rho c} \int_A N_{\alpha,y} N_{\beta,y} T_\beta dA$$

$$= \frac{k}{\rho c} \int_{S_w} N_\alpha \, q_s \, dS_w$$

Finally equation 9(*d*) reduces to

$$\frac{1}{\rho} \int_A H_\mu N_{\beta,x} u_\beta dA + \frac{1}{\rho} \int_A H_\mu N_{\beta,y} v_\beta dA = 0$$

Finally the finite element equations can be written as,

$$K_{\alpha\beta\gamma}{}^x u_\beta u_\gamma + K_{\alpha\beta\gamma}{}^y v_\beta u_\gamma - L_{\lambda\alpha}{}^x p_\lambda + S_{\alpha\beta}{}^{xx} u_\beta + S_{\alpha y \beta}{}^x v_\beta = Q_\alpha^u$$

$$K_{\alpha\beta\gamma}{}^x u_\beta v_\gamma + K_{\alpha\beta\gamma}{}^y v_\beta v_\gamma - L_{\lambda\alpha}{}^y p_\lambda + S_{\alpha x \beta}{}^y u_\beta + S_{\alpha\beta}{}^{yy} v_\beta - K_{\alpha\beta} T_\beta$$

$$= Q_\alpha^v - C_\alpha - D_\alpha$$

$$K_{\alpha\beta\gamma}{}^x u_\beta T_\gamma + K_{\alpha\beta\gamma}{}^y v_\beta T_\gamma + M_{\alpha x \beta}{}^x T_\beta + M_{\alpha y \beta}{}^y T_\beta = Q_\alpha^T$$

$$L_{\mu\beta}{}^x u_\beta + L_{\mu\beta}{}^y v_\beta = 0$$

Where the coefficients in element matrices are in the form of the integrals over the element area and along the element edges S_0 and S_w as

$$K_{\alpha\beta\gamma}{}^x = \int_A N_\alpha N_\beta N_{\gamma,x} dA$$

$$K_{\alpha\beta\gamma^y} = \int_A N_\alpha N_\beta N_{\gamma,y} dA$$

$$L_{\lambda\alpha^x} = \frac{1}{\rho} \int_A H_\gamma N_{\alpha,x} dA$$

$$L_{\lambda\alpha^y} = \frac{1}{\rho} \int_A H_\gamma N_{\alpha,y} dA$$

$$S_{\alpha\beta^{xx}} = 2\upsilon \int_A N_{\alpha,x} N_{\beta,x} dA + \upsilon \int_A N_{\alpha,y} N_{\beta,y} dA$$

$$S_{\alpha\beta^{yy}} = 2\upsilon \int_A N_{\alpha,y} N_{\beta,y} dA + \upsilon \int_A N_{\alpha,x} N_{\beta,x} dA$$

$$S_{\alpha^x\beta^y} = \upsilon \int_A N_{\alpha,x} N_{\beta,y} dA$$

$$S_{\alpha^y\beta^x} = \upsilon \int_A N_{\alpha,y} N_{\beta,x} dA$$

$$M_{\alpha^x\beta^x} = \frac{k}{\rho c} \int_A N_{\alpha,x} N_{\beta,x} dA$$

$$M_{\alpha^y\beta^y} = \frac{k}{\rho c} \int_A N_{\alpha,y} N_{\beta,y} dA$$

$$K_{\alpha\beta} = g\beta \int_A N_\alpha N_\beta dA$$

$$Q_{\alpha^u} = \frac{1}{\rho} \int_{S_0} N_\alpha P_x dS_0$$

$$C_\alpha = g \int_A N_\alpha dA$$

$$D_\alpha = g\beta T_0 \int_A N_\alpha dA$$

$$L_{\mu\beta^x} = \frac{1}{\rho} \int_A H_\mu N_{\beta,x} dA$$

$$L_{\mu\beta^y} = \frac{1}{\rho} \int_A H_\mu N_{\beta,y} dA$$

Here the closed form ready for computer programming has been used for the evaluation of these element matrices. For brevity details of the derivation for these element matrices are omitted herein.

Chapter 3

Effect of Inlet and Outlet Port on Mixed Convection Flow in a Square Vented Enclosure with a Centered Solid Body

The effect of inlet and outlet location on mixed convection flow inside a square vented enclosure with a centered heat generating solid body has been studied in this chapter. Based on inlet and exit position, the four cavity configurations namely *BB*, *BT*, *TB* and *TT* are considered along with an interior solid obstacle. At the beginning, the governing equations of the present problem with appropriate boundary conditions are transformed into non-dimensional forms which are then solved numerically using a finite element method. The dimensionless governing parameters namely, Reynolds number *Re*, Richardson number *Ri*, Prandtl number *Pr*, Hartmann number *Ha*, solid-fluid thermal conductivity ratio *K*, heat generating parameter *Q* and also some physical parameters i.e. the inlet and outlet position of the cavity and the diameter of the inner body are studied here. The outcomes of the current research are presented in terms of streamlines and isotherms to visualize the flow and heat transfer behavior. Moreover, the average Nusselt number at the heated bottom wall, average temperature of the fluid in the cavity are presented graphically in this thesis. Numerical values of the average Nusselt number at the heated surface for the four configurations have been also presented in tabular form.

The aim of the research is to optimize the relative positions of inlet and exit in order to obtain most effective cooling inside the cavity by maximizing the heat-removal rate from the heated surface of the cavity. It is noticed that highest cooling effectiveness is achieved if the inlet is kept at the bottom of the left wall while the outlet is placed at the top of the right wall.

This chapter is divided in the different sections as stated here. The physical configurations of the current research domain are shown in section 3.1. In section 3.2 the appropriate mathematical formulation for the present problem is presented. Then section 3.3 describes the numerical procedure that has been applied in the current work. The parametric results are explained in section 3.4 whereas section 3.5 reveals a conclusion.

3.1 Physical Configuration

The schematic of the system considered in the present article is displayed in Fig. 3.1. The bottom wall of the enclosure is kept at constant temperature T_h and the remaining walls are considered adiabatic. An inlet port is located at the bottom of the left vertical wall, whereas the exit port situated at the bottom of the opposite side wall (*BB* configuration) and these vary in location either top or bottom position as illustrated in Fig. 3.1. The size of each port is equal to $w = 0.1L$, where L is the length of the cavity. A heat generating solid square block of thermal conductivity k_s is placed at the center of the cavity that generates uniform heat flux (q). A transverse magnetic field of strength B_0 is applied along the normal of the right vertical wall. It is supposed that the incoming flow is at a uniform velocity, u_i and at the ambient
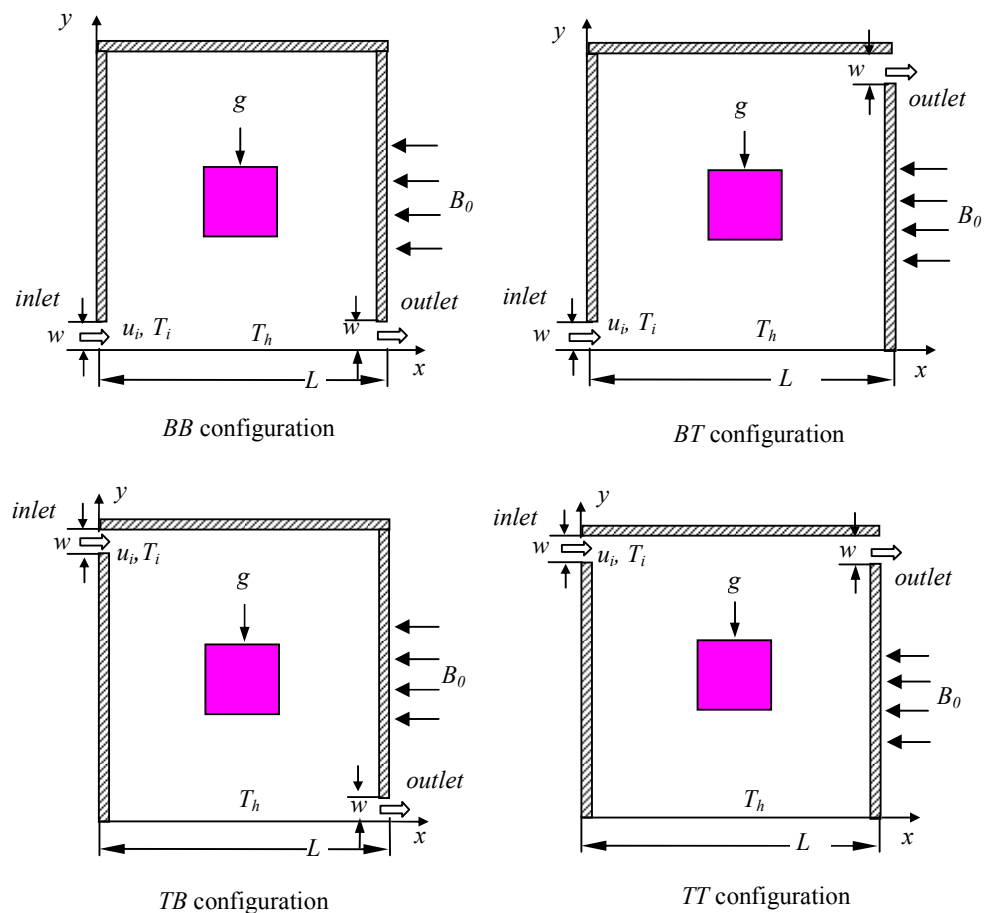
Figure 3.1: Four schematic diagrams of ventilated enclosure with a square solid body.

temperature, T_i. The outgoing flow is assumed to have zero diffusion flux for all variables i.e.; convective boundary condition (CBC). All solid boundaries are assumed to be rigid no-slip walls.

3.2 Mathematical Formulation

The several steps of the mathematical formulation for the above physical configurations are shown here.

3.2.1 Governing Equations

In the present problem the assumptions are made as the flow within the cavity is two-dimensional, steady, laminar, and incompressible with constant fluid properties. There is no viscous dissipation, the radiation effects are neglected and the Boussinesq approximation is considered. The governing equations for the problem can be described as below:

Continuity Equation

$$\frac{\partial u}{\partial x} + \frac{\partial v}{\partial y} = 0 \tag{3.1}$$

Momentum Equations

$$u\frac{\partial u}{\partial x} + v\frac{\partial u}{\partial y} = -\frac{1}{\rho}\frac{\partial p}{\partial x} + \upsilon\left(\frac{\partial^2 u}{\partial x^2} + \frac{\partial^2 u}{\partial y^2}\right) \tag{3.2}$$

$$u\frac{\partial v}{\partial x} + v\frac{\partial v}{\partial y} = -\frac{1}{\rho}\frac{\partial p}{\partial y} + \upsilon\left(\frac{\partial^2 v}{\partial x^2} + \frac{\partial^2 v}{\partial y^2}\right) + g\beta(T - T_i) - \sigma\frac{B_0^2 v}{\rho} \tag{3.3}$$

Energy Equations

$$u\frac{\partial T}{\partial x} + v\frac{\partial T}{\partial y} = \frac{k_f}{\rho c_p}\left(\frac{\partial^2 T}{\partial x^2} + \frac{\partial^2 T}{\partial y^2}\right) \tag{3.4}$$

For solid square block

$$\frac{k_s}{\rho c_p}\left(\frac{\partial^2 T_s}{\partial x^2} + \frac{\partial^2 T_s}{\partial y^2}\right) + q = 0 \tag{3.5}$$

Where, x and y are the distances measured along the horizontal and vertical directions respectively; u and v are the velocity components in the x- and y-direction respectively; T denotes the temperature; ν and α are the kinematics viscosity and the thermal diffusivity respectively; p is the pressure, ρ is the density and q is the uniform constant heat flux.

3.2.2 Boundary Conditions

The boundary conditions for the present problem are specified as follows:

At the inlet: $u = u_i, v = 0, T = T_i$

At the outlet: convective boundary condition (CBC), $p = 0$

At all solid boundaries: $u = 0, v = 0$

At the heated bottom wall: $T = T_h$

At the left, right and top walls: $\dfrac{\partial T}{\partial n} = 0$

At the fluid-solid interface: $\left(\dfrac{\partial T}{\partial n}\right)_{fluid} = \dfrac{k_s}{k_f}\left(\dfrac{\partial T_s}{\partial n}\right)_{solid}$

Where, n is the non-dimensional distances either along x or y direction acting normal to the surface and k_f and k_s are the thermal conductivity of the fluid and the solid block respectively.

3.2.3 Dimensional Analysis

Non-dimensional variables that are used in order to making the governing equations (3.1−3.5) into dimensionless form are stated as follows:

$$X = \frac{x}{L},\ Y = \frac{y}{L},\ U = \frac{u}{u_i},\ V = \frac{v}{u_i},\ P = \frac{p}{\rho\,u_i^{\,2}},\ D = \frac{d}{L},\ \theta = \frac{(T - T_i)}{(T_h - T_i)},$$

$$\theta_s = \frac{(T_s - T_i)}{(T_h - T_i)}$$

Where, X and Y are the coordinates varying along horizontal and vertical directions, respectively, U and V are the velocity components in the X and Y directions,

respectively, θ is the dimensionless temperature and P is the dimensionless pressure. After substitution the dimensionless variables into the equations (3.1−3.5), we get the following dimensionless equations as

Continuity Equation

$$\frac{\partial U}{\partial X} + \frac{\partial V}{\partial Y} = 0 \tag{3.6}$$

Momentum Equations

$$U\frac{\partial U}{\partial X} + V\frac{\partial U}{\partial Y} = -\frac{\partial P}{\partial X} + \frac{1}{Re}\left(\frac{\partial^2 U}{\partial X^2} + \frac{\partial^2 U}{\partial Y^2}\right) \tag{3.7}$$

$$U\frac{\partial V}{\partial X} + V\frac{\partial V}{\partial Y} = -\frac{\partial P}{\partial Y} + \frac{1}{Re}\left(\frac{\partial^2 V}{\partial X^2} + \frac{\partial^2 V}{\partial Y^2}\right) + Ri\,\theta - \frac{Ha^2}{Re}V \tag{3.8}$$

Energy Equations

$$U\frac{\partial \theta}{\partial X} + V\frac{\partial \theta}{\partial Y} = \frac{1}{Re\,Pr}\left(\frac{\partial^2 \theta}{\partial X^2} + \frac{\partial^2 \theta}{\partial Y^2}\right) \tag{3.9}$$

For centered solid body

$$\frac{K}{Re\,Pr}\left(\frac{\partial^2 \theta_s}{\partial X^2} + \frac{\partial^2 \theta_s}{\partial Y^2}\right) + Q = 0 \tag{3.10}$$

The dimensionless parameters that appear in the equations from (3.6) to (3.10) are the Reynolds number Re, Richardson number Ri, Hartmann number Ha, Prandtl number Pr, heat generating parameter Q and solid fluid thermal conductivity ratio K. They are respectively defined as follows:

$$Re = u_i L/\upsilon, \ Ri = Gr/Re^2, \ Ha^2 = \sigma B_0^2 L^2/\upsilon, \ Pr = \upsilon/\alpha, \ Q = qL^2/k_s \Delta T,$$
$$K = k_s/k_f$$

Where, $\Delta T = T_h - T_i$ and $\alpha = k_f/\rho c_p$ are the temperature difference and thermal diffusivity of the fluid respectively.

The dimensionless boundary conditions under consideration can be written as:

At the inlet: $U = 1$, $V = 0$, $\theta = 0$

At the outlet: convective boundary condition (CBC), $P = 0$

At all solid boundaries: $U = 0$, $V = 0$,

At the heated bottom wall: $\theta = 1$

At the left, right and top walls: $\dfrac{\partial \theta}{\partial N} = 0$

At the fluid-solid interface: $\left(\dfrac{\partial \theta}{\partial N}\right)_{fluid} = K\left(\dfrac{\partial \theta_s}{\partial N}\right)_{solid}$

Where, N is assumed as the dimensionless distances either along X or Y direction acting normal to the surface. According to Singh and Sharif (2003), the average Nusselt number at the heated wall of the cavity based on the dimensionless variables may be expressed as $Nu_{av} = -\int_0^1 \dfrac{\partial \theta}{\partial Y} dX$ and the bulk average temperature of the fluid inside the cavity defined as $\theta_{av} = \int \theta \, d\overline{V} / \overline{V}$, where $\overline{V}$ is the cavity volume.

3.3 Numerical Analysis

The governing equations are solved numerically along with the boundary conditions using Galerkin weighted residual based finite element techniques that is discussed below.

3.3.1 Derivation of Finite Element Equations and Solution Techniques

The weighted residuals Zienkiewicz method (1991) is applied to the equations (3.6) – (3.10) and finite element equations are derived from these equations.

$$\int_A N_\alpha \left(\frac{\partial U}{\partial X} + \frac{\partial V}{\partial Y}\right) dA = 0 \tag{3.11}$$

$$\int_A N_\alpha \left(U\frac{\partial U}{\partial X} + V\frac{\partial U}{\partial Y}\right) dA = -\int_A H_\lambda \left(\frac{\partial P}{\partial X}\right) dA + \frac{1}{Re}\int_A N_\alpha \left(\frac{\partial^2 U}{\partial X^2} + \frac{\partial^2 U}{\partial Y^2}\right) dA \tag{3.12}$$

$$\int_A N_\alpha \left(U \frac{\partial V}{\partial X} + V \frac{\partial V}{\partial Y} \right) dA = -\int_A H_\lambda \left(\frac{\partial P}{\partial Y} \right) dA + \frac{1}{Re} \int_A N_\alpha \left(\frac{\partial^2 V}{\partial X^2} + \frac{\partial^2 V}{\partial Y^2} \right) dA$$

$$+ Ri \int_A N_\alpha \theta \, dA - \frac{Ha^2}{Re} \int_A N_\alpha V dA \qquad (3.13)$$

$$\int_A N_\alpha \left(U \frac{\partial \theta}{\partial X} + V \frac{\partial \theta}{\partial Y} \right) dA = \frac{1}{Re\,Pr} \int_A N_\alpha \left(\frac{\partial^2 \theta}{\partial X^2} + \frac{\partial^2 \theta}{\partial Y^2} \right) dA \qquad (3.14)$$

$$\frac{K}{Re.Pr} \int_A N_\alpha \left(\frac{\partial^2 \theta_s}{\partial X^2} + \frac{\partial^2 \theta_s}{\partial Y^2} \right) dA + \int_A N_\alpha Q dA = 0 \qquad (3.15)$$

Where, A indicates the area of the element, N_α (α = 1, 2, … … , 6) are the element interpolation functions for the velocity components and the temperature, while H_λ (λ = 1, 2, 3) stands for the element interpolation functions for the pressure.

To generate the boundary integral terms associated with the surface tractions and heat flux, Gauss's theorem is then applied to equations (3.12)-(3.15) that reduce to the following equations.

$$\int_A N_\alpha \left(U \frac{\partial U}{\partial X} + V \frac{\partial U}{\partial Y} \right) dA + \int_A H_\lambda \left(\frac{\partial P}{\partial X} \right) dA$$

$$+ \frac{1}{Re} \int_A \left(\frac{\partial N_\alpha}{\partial X} \frac{\partial U}{\partial X} + \frac{\partial N_\alpha}{\partial Y} \frac{\partial U}{\partial Y} \right) dA = \int_{S_0} N_\alpha S_x dS_0 \qquad (3.16)$$

$$\int_A N_\alpha \left(U \frac{\partial V}{\partial X} + V \frac{\partial V}{\partial Y} \right) dA + \int_A H_\lambda \left(\frac{\partial P}{\partial Y} \right) dA$$

$$+ \frac{1}{Re} \int_A \left(\frac{\partial N_\alpha}{\partial X} \frac{\partial V}{\partial X} + \frac{\partial N_\alpha}{\partial Y} \frac{\partial V}{\partial Y} \right) dA - Ri \int_A N_\alpha \theta \, dA = \int_{S_0} N_\alpha S_y dS_0 \qquad (3.17)$$

$$\int_A N_\alpha \left(U \frac{\partial \theta}{\partial X} + V \frac{\partial \theta}{\partial Y} \right) dA + \frac{1}{Re.Pr} \int_A \left(\frac{\partial N_\alpha}{\partial X} \frac{\partial \theta}{\partial X} + \frac{\partial N_\alpha}{\partial Y} \frac{\partial \theta}{\partial Y} \right) dA = \int_{S_w} N_\alpha q_{1w} dS_w \qquad (3.18)$$

$$\frac{K}{Re.Pr} \int_A \left(\frac{\partial N_\alpha}{\partial X} \frac{\partial \theta_s}{\partial X} + \frac{\partial N_\alpha}{\partial Y} \frac{\partial \theta_s}{\partial Y} \right) dA = \int_{S_w} N_\alpha q_{2w} dS_w \qquad (3.19)$$

Here (3.16)-(3.17) specifying surface tractions (S_x, S_y) along outflow boundary S_0 and (3.18)-(3.19) specifying velocity components and fluid temperature or heat flux (q_w) that flows into or out from domain along wall boundary S_w.

The fundamental unknowns for the differential equations described above are the velocity components, U, V, the temperature, θ, θ_s and the pressure, P. In order to develop the finite element equations, the six node triangular element is used in this work. All of the six nodes are associated with velocities and temperature; whereas only the corner nodes are associated with pressure. This implies that a lower order polynomial is preferred for pressure which is satisfied through continuity equation. The velocity components, temperature distributions and linear interpolation for the pressure distribution according to their highest order derivatives in the differential equations (3.6)-(3.10) are expressed as

$$U(X,Y) = N_\beta U_\beta \tag{3.20}$$

$$V(X,Y) = N_\beta V_\beta \tag{3.21}$$

$$\theta(X,Y) = N_\beta \theta_\beta \tag{3.22}$$

$$\theta_s(X,Y) = N_\beta \theta_{s\,\beta} \tag{3.23}$$

$$P(X,Y) = H_\lambda P_\lambda \tag{3.24}$$

Where, $\beta = 1, 2, \ldots, 6$ and $\lambda = 1, 2, 3$.

Substituting the element velocity component distributions, the temperature distributions and the pressure distribution respectively from equations (3.20)-(3.24) in equations (3.16)-(3.19); the finite element equations can be written in the form,

$$K_{\alpha\beta^x} U_\beta + K_{\alpha\beta^y} V_\beta = 0 \tag{3.25}$$

$$K_{\alpha\beta\gamma^x} U_\beta U_\gamma + K_{\alpha\beta\gamma^y} V_\beta U_\gamma + M_{\alpha\mu^x} P_\mu + \frac{1}{Re}\left(S_{\alpha\beta^{xx}} + S_{\alpha\beta^{yy}}\right) U_\beta = Q_{\alpha^u} \tag{3.26}$$

$$K_{\alpha\beta\gamma^x} U_\beta V_\gamma + K_{\alpha\beta\gamma^y} V_\beta V_\gamma + M_{\alpha\mu^y} P_\mu +$$
$$\frac{1}{Re}\left(S_{\alpha\beta^{xx}} + S_{\alpha\beta^{yy}}\right) V_\beta - Ri\, K_{\alpha\beta} \theta_\beta = Q_{\alpha^v} \tag{3.27}$$

$$K_{\alpha\beta\gamma^x} U_\beta \theta_\gamma + K_{\alpha\beta\gamma^y} V_\beta \theta_\gamma + \frac{1}{Re.Pr}\left(S_{\alpha\beta^{xx}} + S_{\alpha\beta^{yy}}\right) \theta_\beta = Q_{\alpha^\theta} \tag{3.28}$$

$$\frac{K}{Re.Pr}\left(S_{\alpha\beta^{xx}} + S_{\alpha\beta^{yy}}\right) \theta_{s_\beta} = Q_{\alpha^{\theta_s}} \tag{3.29}$$

The coefficients in element matrices are in the form of the integrals over the element area A and along the element edges S_0 and S_w stated as

$$K_{\alpha\beta^x} = \int_A N_\alpha N_{\beta,x} dA \qquad (3.30a)$$

$$K_{\alpha\beta^y} = \int_A N_\alpha N_{\beta,y} dA \qquad (3.30b)$$

$$K_{\alpha\beta\gamma^x} = \int_A N_\alpha N_\beta N_{\gamma,x} dA \qquad (3.30c)$$

$$K_{\alpha\beta\gamma^y} = \int_A N_\alpha N_\beta N_{\gamma,y} dA \qquad (3.30d)$$

$$K_{\alpha\beta} = \int_A N_\alpha N_\beta dA \qquad (3.30e)$$

$$S_{\alpha\beta^{xx}} = \int_A N_{\alpha,x} N_{\beta,x} dA \qquad (3.30f)$$

$$S_{\alpha\beta^{yy}} = \int_A N_{\alpha,y} N_{\beta,y} dA \qquad (3.30g)$$

$$M_{\alpha\mu^x} = \int_A H_\lambda H_{\mu,x} dA \qquad (3.30h)$$

$$M_{\alpha\mu^y} = \int_A H_\lambda H_{\mu,y} dA \qquad (3.30i)$$

$$Q_{\alpha^u} = \frac{1}{\mathrm{Re}} \int_{S_0} N_\alpha S_x dS_0 \qquad (3.30j)$$

$$Q_{\alpha^v} = \frac{1}{\mathrm{Re}} \int_{S_0} N_\alpha S_y dS_0 \qquad (3.30k)$$

$$Q_{\alpha^\theta} = \frac{1}{\mathrm{Re}} \int_{S_w} N_\alpha q_{1w} dS_w \qquad (3.30l)$$

$$Q_{\alpha^{\theta s}} = \frac{1}{\mathrm{Re}} \int_{S_w} N_\alpha q_{2w} dS_w \qquad (3.30m)$$

There-after these element matrices are computed in closed form ready for numerical simulation and the details of the derivation for these element matrices are skipped herein.

The derived finite element equations (3.25)-(3.29) are nonlinear. These nonlinear algebraic equations are solved by applying the Newton-Raphson iteration technique

by first writing the unbalanced values from the set of the finite element equations (3.25)-(3.29) as,

$$F_{\alpha^p} = K_{\alpha\beta^x} U_\beta + K_{\alpha\beta^y} V_\beta \tag{3.31a}$$

$$F_{\alpha^u} = K_{\alpha\beta\gamma^x} U_\beta U_\gamma + K_{\alpha\beta\gamma^y} V_\beta U_\gamma + M_{\alpha\mu^x} P_\mu$$
$$+ \frac{1}{Re}(S_{\alpha\beta^{xx}} + S_{\alpha\beta^{yy}}) U_\beta - Q_{\alpha^u} \tag{3.31b}$$

$$F_{\alpha^v} = K_{\alpha\beta\gamma^x} U_\beta V_\gamma + K_{\alpha\beta\gamma^y} V_\beta V_\gamma + M_{\alpha\mu^y} P_\mu +$$
$$\frac{1}{Re}(S_{\alpha\beta^{xx}} + S_{\alpha\beta^{yy}}) V_\beta - Ri\, K_{\alpha\beta}\theta_\beta - Q_{\alpha^v} \tag{3.31c}$$

$$F_{\alpha^\theta} = K_{\alpha\beta\gamma^x} U_\beta \theta_\gamma + K_{\alpha\beta\gamma^y} V_\beta \theta_\gamma + \frac{1}{Re.Pr}\left(S_{\alpha\beta^{xx}} + S_{\alpha\beta^{yy}}\right)\theta_\beta - Q_{\alpha^\theta} \tag{3.31d}$$

$$F_{\alpha^{\theta_s}} = \frac{K}{Re.Pr}\left(S_{\alpha\beta^{xx}} + S_{\alpha\beta^{yy}}\right)\theta_{s\,\beta} - Q_{\alpha^{\theta_s}} \tag{3.31e}$$

This set leads to a system of algebraic equations together with the incremental unknowns of the element nodal velocity components, temperatures, and pressure in the form,

$$
\begin{bmatrix}
K_{pu} & K_{pv} & 0 & 0 & 0 \\
K_{uu} & K_{uv} & 0 & K_{up} & 0 \\
K_{\theta u} & K_{\theta v} & K_{\theta\theta} & 0 & 0 \\
K_{vu} & K_{vv} & K_{v\theta} & K_{vp} & 0 \\
0 & 0 & 0 & 0 & K_{\theta_s\theta_s}
\end{bmatrix}
\begin{Bmatrix}
\Delta p \\
\Delta u \\
\Delta\theta \\
\Delta v \\
\Delta\theta_s
\end{Bmatrix}
= -
\begin{Bmatrix}
F_{\alpha^p} \\
F_{\alpha^u} \\
F_{\alpha^\theta} \\
F_{\alpha^v} \\
F_{\alpha^{\theta_s}}
\end{Bmatrix}
\tag{3.32}
$$

Where, $K_{uu} = K_{\alpha\beta\gamma^x} U_\beta + K_{\alpha\beta\gamma^x} U_\gamma + K_{\alpha\beta\gamma^y} V_\beta + \frac{1}{Re}\left(S_{\alpha\beta^{xx}} + S_{\alpha\beta^{yy}}\right)$

$K_{uv} = K_{\alpha\beta\gamma^y} U_\gamma$

$K_{u\theta} = K_{u\theta_s} = 0$, $K_{up} = M_{\alpha\mu^x}$

$K_{vu} = K_{\alpha\beta\gamma^x} V_\gamma$

$$K_{vv} = K_{\alpha\beta\gamma x}U_\beta + K_{\alpha\gamma\beta y}V_\gamma + K_{\alpha\beta\gamma y}V_\gamma + \frac{1}{Re}\left(S_{\alpha\beta xx} + S_{\alpha\beta yy}\right)$$

$$K_{v\theta} = -Ri\,K_{\alpha\beta}, \; K_{vp} = M_{\alpha\mu y}$$

$$K_{v\theta_s} = 0, \; K_{\theta u} = K_{\alpha\beta\gamma x}\theta_\gamma, \; K_{\theta v} = K_{\alpha\beta\gamma y}\theta_\gamma$$

$$K_{\theta\theta} = K_{\alpha\beta\gamma x}U_\beta + K_{\alpha\beta\gamma y}V_\beta + \frac{1}{Re.Pr}(S_{\alpha\beta xx} + S_{\alpha\beta yy})$$

$$K_{\theta p} = K_{\theta\theta_s} = 0, \; K_{\theta_s u} = K_{\theta_s v} = K_{\theta_s \theta} = K_{\theta_s p} = 0$$

$$K_{\theta_s\theta_s} = \frac{K}{Re.Pr}(S_{\alpha\beta xx} + S_{\alpha\beta yy})$$

$$K_{pu} = K_{\alpha\beta x}, \; K_{pv} = K_{\alpha\beta y} \; \text{and} \; K_{p\theta} = K_{pp} = K_{p\theta_s} = 0$$

In the present computation the iteration process is terminated if the percentage of the overall change compared to the previous iteration is lower than the specified value.

The Newton-Raphson iteration technique has been adapted through PDE solver with MATLAB interface for solving the sets of the global non-linear algebraic equations in the matrix form. It is assumed that the solution converges when the relative error for each variable between two consecutive iterations is recorded less than the convergence criterion ε such that $\left|\Psi^{n+1} - \Psi^n\right| < \varepsilon$, where n indicates the number of iteration and $\Psi = U, V, \theta$. In this case the convergence criterion was set to $\varepsilon = 10^{-4}$.

3.3.2 Grid Size Sensitivity Test

At first the grid refinement test is needed for this study so that the difficulty of the computational domain can be avoided. Various types of grid such as: 14313 nodes, 1986 elements; 24388 nodes, 3536 elements; 42913 nodes, 6386 elements; 70329 nodes, 10711 elements and 83304 nodes, 12600 elements have been taken for the grid refinement examination. From Table 3.1 it is observed that the deviations among the results are very minor. On the basis of the outcomes from the table the grid with 42913 nodes and 6386 elements are selected throughout the simulation.

Table 3.1: Grid Sensitivity Check at $Re = 100$, $Ha = 10$, $Ri = 1.0$, $K = 5$, $D = 0.2$ and $Pr = 0.71$

Elements (Nodes)	1986 (14313)	3536 (24388)	6386 (42913)	10711 (70329)	12600 (83304)
Nu_{av}	4.0511	4.1501	4.1510	4.1512	4.1513
θ_{av}	0.1905	0.1901	0.1897	0.1837	0.1831
Time (s)	385.219	493.235	682.985	698.703	927.359
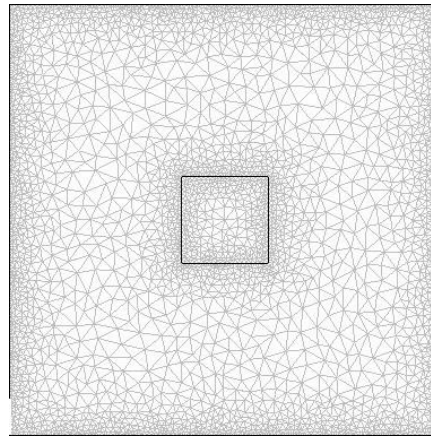
Figure 3.2: Grid used for numerical simulations at the present study

3.3.3 Validation of the Numerical Scheme

The current numerical code is verified based on the problem of mixed convection in a lid-driven enclosure having a circular body performed by Oztop et al. (2009), where the cavity was heated at the left wall, cooled at the right wall and the rest of the other two sides were insulated. The relationship between the outcome of the present code and the results obtained in the literature Oztop et al. (2009) with respect to average Nusselt number (at the hot wall) for $Re=1000$, $Gr=10^5$ are shown in Table 3.2. It follows that the present results expose an excellent agreement with the reported studies. Hence the chosen code can be used to predict the flow field for the present problem.

Table 3.2: Comparison of average Nusselt number at the hot wall of the cavity for $Re = 1000$, $Gr = 10^5$, C ($x = 0.5$, $y = 0.5$) between the present data and that of the Oztop et al. (2009)

Present	Oztop et al. (2009)	Error (%)
9.125	9.13	0.05
10.38	10.37	0.10
11.20	11.10	0.90

3.4 Results and Discussions

The effects of different inlet and outlet port locations of a ventilated square enclosure along with heat generating centered block on MHD mixed convection flow and thermal fields as well as heat transfer rates at hot wall, average fluid temperature in the cavity have been carried out in this study. Here, the Richardson number, Ri is considered as the controlling parameter for the four configurations while the Prandtl number Pr, Hartmann number Ha and the Reynolds number Re are kept fixed at 0.71, 10 and 100 respectively. For each configuration, computations are done for three convective regimes of Richardson number ($Ri = 0.1, 1, 10$). The results of this present study are displayed in terms of streamlines and isotherms. Moreover, the effects of heat transfer at the hot wall of the enclosure are shown in terms of average Nusselt number Nu_{av} and the average fluid temperature θ_{av}.

A detailed analysis for the distribution of streamlines and isotherms is carried out to examine the flow and thermal fields structure of the mixed convection problem for various cavity configurations as *BB, BT, TB* and *TT* and displayed in Fig. 3.3. Fig. 3.3(*a*) presents the effect of inlet and outlet position of ventilated cavity on fluid flow field for Richardson number $Ri = 0.1, 1, 10$ while $Re = 100$, $Ha = 10$ and $Pr = 0.71$ are kept fixed. In the case of dominant forced convection area ($Ri = 0.1$), the effects are exposed in the third row of Fig. 3.3(*a*). For *BB* configuration (entering in the left bottom and leave by the right bottom) it is found that the fluid flow is characterized by the open lines about the whole domain and a counter-clockwise vortex appears at the left side above the inlet. Another anti-clockwise rotating cell is noted at right side of the cavity in the *BB* configuration. The reason is due to the effect of buoyancy driven flow and convective currents (the fresh and colder fluids entering the cavity

cannot come into intimate mixing with the hotter fluids). When the inlet port is situated at the bottom of the left vertical wall and outlet is at the top of the opposite vertical wall, i.e.; for *BT* configuration the left sided recirculation cell reduces in size, right vortex disappears and the main flow is diagonal from the inlet to the exit. For *TB* configuration a small CW rotating vortex is developed at below just inlet and the main streams capture the whole cavity which are elongated from the entrance to the passageway. In *TT* configuration it is followed that the main flow pattern is reverse of *BB* configuration and a CW unicellular vortex is created at left top corner below the inlet at $Ri = 0.1$. Also a very small eddy is found near the right wall.

For the case of pure mixed convection, ($Ri = 1$) the effect of different configuration of the vented cavity on flow fields are illustrated in the second row of Fig. 3.3(*a*). It is seen that the intensity of the vortices in the cavity increases. A very large anti-clockwise circulating cell containing the obstacle is formed above the major flow and another CW vortex is noted at right top corner in the *BB* configuration. For *BT* configuration the major flow shrinks from the left side and a small CW vortex is seen at the left top corner. There is no significant change in *TB* configuration as that was found for the same configuration at $Ri = 0.1$. The left top cornered vortex decreases in size and the small eddy disappears which was seen in the case for $Ri = 0.1$ in *TT* configuration.

The streamlines for the mentioned four cases with $Re = 100$, $Ha = 10$ and $Pr = 0.71$ have been presented in the first row of Fig. 3.3(*a*), whereas the dominant natural convection effect ($Ri = 10$) is considered. The CCW vortex in the cavity gets smaller from the top right corner and the clockwise rotating cell enlarges, consequently squeezes the induced flow path for *BB* configuration, indicating the supremacy of natural convection heat transfer in the cavity. It is followed that in *BT* configuration the upper vortex vanishes and the lower vortex swells so that open lines are minimized. *TB* configuration shows a very large vortex at the surrounding of the centered block. The centered vortex shrinks from the right side; as a result the open flow covers this domain for *TT* configuration. Moreover a small eddy is found at the lower left corner of the cavity.

The isotherms of the above mentioned four configurations are displayed in Fig. 3.3(*b*). The third row of Fig. 3.3(*b*) shows the effect of inlet and outlet position of
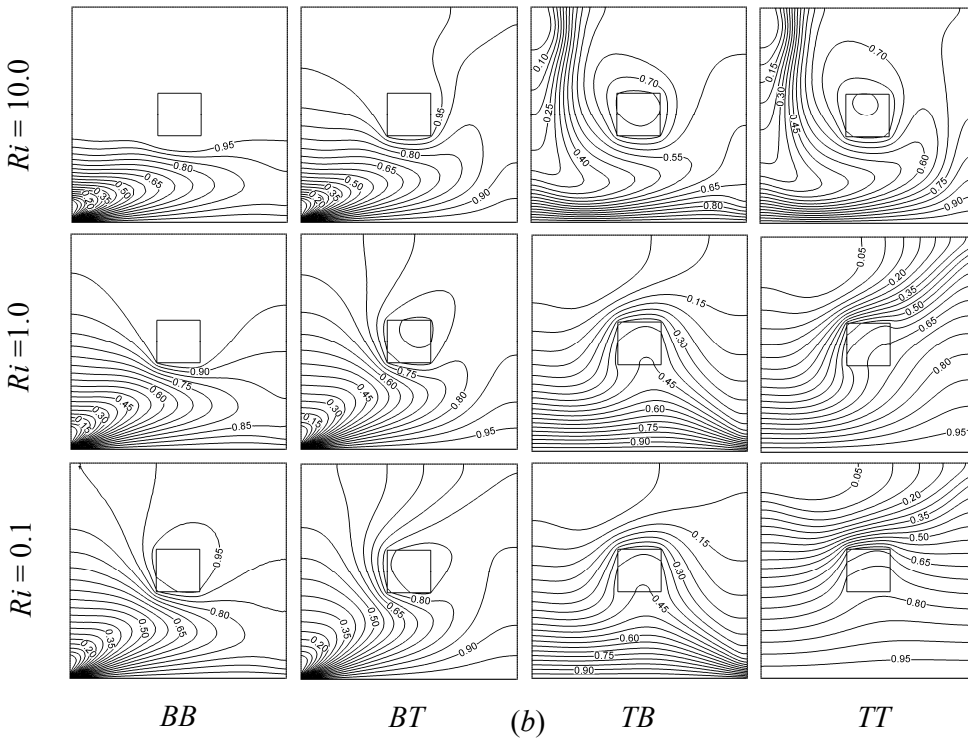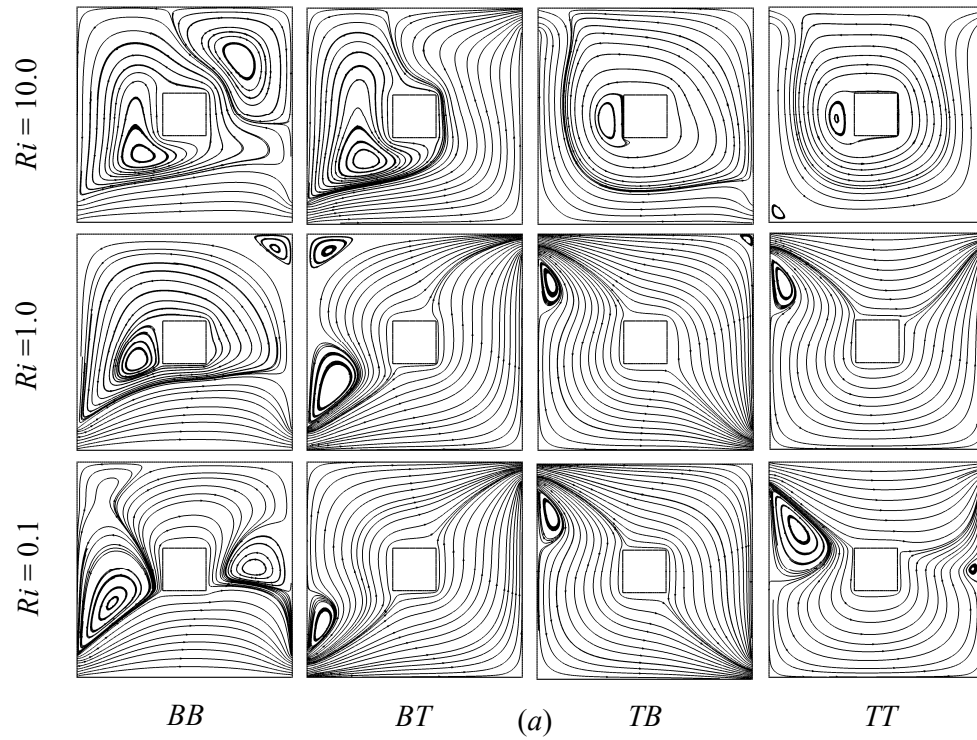
Figure 3.3: (*a*) Streamlines and (*b*) Isotherms at different inlet and outlet locations and various values of Richardson number *Ri*, while *Re* = 100, *Ha* = 10, *K* = 5, *Pr* = 0.71, *Q* = 1 and *D* = 0.2.
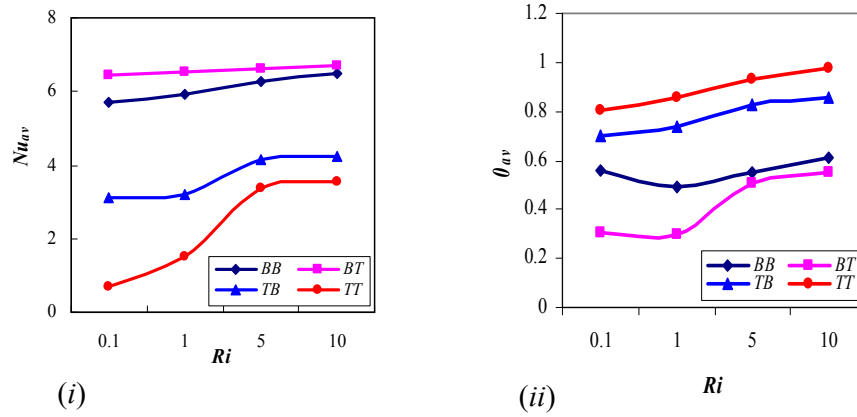
Figure 3.4: Effect of inlet and outlet locations on (*i*) average Nusselt number, (*ii*) average fluid temperature, while $Re = 100$, $Ha = 10$, $Pr = 0.71$, $D = 0.2$, $Q = 1$ and $K = 5$

Table 3.3: Variation of average Nusselt number with inlet and outlet locations

Ri	Nu_{av}			
	BB	BT	TB	TT
0.1	5.691892	6.464218	3.123972	0.690825
1.0	5.928245	6.512524	3.204073	1.499937
2.0	6.0132564	6.544932	3.494512	2.43214
3.0	6.104789	6.584512	3.731246	2.986542
4.0	6.184321	6.602143	3.945147	3.16985
5.0	6.260024	6.621028	4.137727	3.388347
6.0	6.3124563	6.642134	4.160124	3.412890
7.0	6.364571	6.664125	4.188452	3.495734
8.0	6.394587	6.681470	4.191247	3.514863
9.0	6.415321	6.701234	4.202130	3.536921
10.0	6.465167	6.70955	4.247171	3.549034

vented cavity in temperature distribution for the case of $Ri = 0.1$. It is noticed that for *BB* configuration the isothermal lines are packed at the opening and a thermal boundary layer is found near the bottom heated wall of the cavity. A little difference is followed in the case of *BT* configuration. For *TB* configuration high isothermal lines are concentrated at the hot wall indicating diffusion heat transfer in the cavity.

The temperature distribution for *TT* configuration is that all the isothermal lines are stretched out in the whole region.

At *Ri* = 1, the middle row of Fig. 3.3(*b*) shows the isotherms for four inlet and outlet position of the cavity. It is observed that for *BB* configuration round shaped high isothermal line that was seen at *Ri* = 0.1, expands below the heated block in this case. A minor change is followed in *BT* and *TB* configuration regarding *Ri* = 0.1. For *TT* configuration isotherms are stretched about diagonally.

Lastly, the isotherms for the aforesaid configurations are depicts in the first row of Fig. 3.3(*b*) where the natural convection dominates the forced convection. For *BB* configuration the isotherms are found more flattened below the obstacle. In *BT* configuration the isotherms containing the obstacle scatters comparing as that case of *Ri* = 1. Finally for *TB* and *TT* configurations the isotherms pattern change drastically regarding *Ri* = 0.1 and *Ri* = 1. Besides, a little variation is found between these two configurations. For the above mentioned four configurations, the average Nusselt number at the heated bottom wall (Nu_{av}) and the average fluid temperature (θ_{av}) in the cavity have been displayed in Fig. 3.4. It is apparent from Fig. 3.4(*i*) that the highest value of Nu_{av} is found for *BT* configuration. Also Nu_{av} increases generally with increasing *Ri* due to the rising effect of convection. In addition, the average fluid temperature (θ_{av}) in the cavity is maximum for *TT* configuration for all values of *Ri* which can be observed from Fig. 3.4(*ii*).

3.5 Concluding Remarks

A two-dimensional laminar mixed convection problem in a ventilated enclosure with a heat generating square block is studied numerically in the present work to point out the appropriate placement of inlet and outlet port for best cooling efficiency. To compare the cooling effectiveness among the considered four different cavity configurations, Nusselt number is taken as criterion. Based on the result and analysis of the numerical experiment the following summary is drawn:

In the entire domain the *BT* configuration generates more effective cooling than other configurations as obtained higher Nu_{av}.

Among the chosen four configurations, *TT* shows the highest value of θ_{av} for all values of *Ri*. Hence it can be concluded that the flow and thermal fields have strong dependence on the position of inlet and outlet openings.

Chapter 4

Effect of a Heat Generating Solid Body on Mixed Convection Flow in a Square Enclosure

In recent years mixed convection flow and heat transfer in a ventilated enclosure has become a subject of general interest of many researchers. A large number of investigations have been conducted in the past on vented cavity flow and heat transfer with regards to various combinations of the imposed temperature gradients and cavity configurations. At first the major equations of the present problem transferred into a dimensionless form by means of suitable non-dimensional variables. Then using Galerkin's finite element method the resulting non linear system of partial differential equations are solved numerically. The variation of streamlines, isotherms, average Nusselt number at the heated surface, average fluid temperature inside the cavity for the various relevant dimensionless parameters Hartmann number *Ha*, Reynolds number *Re*, Richardson number *Ri*, Prandtl number *Pr*, solid-fluid thermal conductivity ratio *K* and diameter of the inner solid body *D* are shown graphically. In addition, variation of average Nusselt number at the bottom heated surface with different relevant governing parameters are exposed in tables.

The present chapter focuses a comprehensive study about the behavior of flow and heat transfer on MHD mixed convection for a wide range of pertinent controlling parameters in a ventilated square cavity having a heat generating solid body. It was found that the flow behaviors within the cavity and heat transfer rate at hot wall are strongly affected by the presence of heat generating solid body.

The rest of this chapter consists of five sections. Section 4.1 describes the physical models of the present studied area. In section 4.2, the appropriate mathematical model for the current problem is presented. There after a brief description of solution scheme is given in the section 4.3. The results are given details in section 4.4. And last of all a conclusion is drawn in section 4.5.

4.1 Physical Model

The geometry of the present study is illustrated in Fig. 4.1 in which a Cartesian co-ordinate system is used with origin at the lower left corner of the working domain. It consists of a square enclosure of length L having a centered heat generating square solid block. The bottom wall of the cavity is subjected to hot with temperature T_h while the other sidewalls are kept insulated. The solid body with diameter d and a thermal conductivity of k_s generates uniform heat q per unit volume. The inflow opening is placed on the left bottom corner of the cavity while the outflow opening is on the right top corner as shown in the schematic and the size of each opening is $w = 0.1L$. A uniform magnetic field of strength B_0 is enforced in the horizontal direction on the right adiabatic wall. The incoming flow through the inlet is assumed at a uniform velocity u_i, ambient temperature T_i whereas the outgoing flow by the exit port is assumed to have zero diffusion flux for all variables and all solid boundaries are supposed to be rigid no-slip walls.
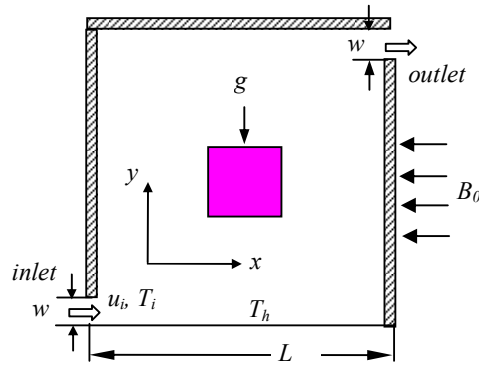
Figure 4.1: Schematic of the problem

4.2 Mathematical Formulation

The several steps of the mathematical formulation for the above problem are shown as follows.

4.2.1 Governing Equations

The working fluid within the enclosure is supposed to be incompressible, Newtonian, two-dimensional, steady and laminar with all the fluid properties assumed as constant except for density variation. The radiation effect is negligible and the viscous

dissipation is absent for the considered fluid. The governing equations for the problem under Boussinesq approximation can be described in as below:

Continuity Equation

$$\frac{\partial u}{\partial x} + \frac{\partial v}{\partial y} = 0 \tag{4.1}$$

Momentum Equations

$$u\frac{\partial u}{\partial x} + v\frac{\partial u}{\partial y} = -\frac{1}{\rho}\frac{\partial p}{\partial x} + \upsilon\left(\frac{\partial^2 u}{\partial x^2} + \frac{\partial^2 u}{\partial y^2}\right) \tag{4.2}$$

$$u\frac{\partial v}{\partial x} + v\frac{\partial v}{\partial y} = -\frac{1}{\rho}\frac{\partial p}{\partial y} + \upsilon\left(\frac{\partial^2 v}{\partial x^2} + \frac{\partial^2 v}{\partial y^2}\right) + g\beta(T - T_i) - \frac{\sigma B_0^2 v}{\rho} \tag{4.3}$$

Energy Equations

$$u\frac{\partial T}{\partial x} + v\frac{\partial T}{\partial y} = \alpha\left(\frac{\partial^2 T}{\partial x^2} + \frac{\partial^2 T}{\partial y^2}\right) \tag{4.4}$$

For solid

$$\frac{k_s}{\rho c_p}\left(\frac{\partial^2 T_s}{\partial x^2} + \frac{\partial^2 T_s}{\partial y^2}\right) + q = 0 \tag{4.5}$$

Where, x and y are the distances measured along the horizontal and vertical directions respectively; u and v are the velocity components in the x- and y-direction respectively; T denotes the temperature; ν and α are the kinematics viscosity and the thermal diffusivity respectively; p is the pressure, ρ is the density and q is the uniform constant heat flux.

4.2.2 Boundary Conditions

The boundary conditions for the present problem can be written as follows:

At the inlet: $u = u_i, v = 0, T = T_i$

At the outlet: convective boundary condition (CBC), $p = 0$

At all solid boundaries: $u = 0, v = 0$

At the heated bottom wall: $T = T_h$

At the left, right and top walls: $\dfrac{\partial T}{\partial n} = 0$

At the fluid-solid interface: $\left(\dfrac{\partial T}{\partial n} \right)_{fluid} = \dfrac{k_s}{k_f} \left(\dfrac{\partial T_s}{\partial n} \right)_{solid}$

Where, n is the non-dimensional distances either along x or y direction acting normal to the surface and k_f and k_s are the thermal conductivity of the fluid and the solid block respectively.

4.2.3 Dimensional Analysis

The above equations are made dimensionless by introducing the following non-dimensional variables

$$X = \frac{x}{L}, \; Y = \frac{y}{L}, \; U = \frac{u}{u_i}, \; V = \frac{v}{u_i}, \; P = \frac{p}{\rho u_i^2}, \; D = \frac{d}{L}, \; \theta = \frac{(T - T_i)}{(T_h - T_i)},$$

$$\theta_s = \frac{(T_s - T_i)}{(T_h - T_i)}$$

Where, X and Y are the coordinates varying along horizontal and vertical directions, respectively, U and V are the velocity components in the X and Y directions, respectively, θ is the dimensionless temperature and P is the dimensionless pressure. Taking into account the aforesaid dimensionless dependent and independent variables on the equations (4.1-4.5), the non-dimensional equations for the problem are given as follows:

Continuity Equation

$$\frac{\partial U}{\partial X} + \frac{\partial V}{\partial Y} = 0 \tag{4.6}$$

Momentum Equations

$$U \frac{\partial U}{\partial X} + V \frac{\partial U}{\partial Y} = -\frac{\partial P}{\partial X} + \frac{1}{Re} \left(\frac{\partial^2 U}{\partial X^2} + \frac{\partial^2 U}{\partial Y^2} \right) \tag{4.7}$$

$$U\frac{\partial V}{\partial X}+V\frac{\partial V}{\partial Y}=-\frac{\partial P}{\partial Y}+\frac{1}{Re}\left(\frac{\partial^2 V}{\partial X^2}+\frac{\partial^2 V}{\partial Y^2}\right)+Ri\,\theta-\frac{Ha^2}{Re}V \qquad (4.8)$$

Energy Equations

$$U\frac{\partial \theta}{\partial X}+V\frac{\partial \theta}{\partial Y}=\frac{1}{Re\,Pr}\left(\frac{\partial^2 \theta}{\partial X^2}+\frac{\partial^2 \theta}{\partial Y^2}\right) \qquad (4.9)$$

$$\frac{K}{RePr}\left(\frac{\partial^2 \theta_s}{\partial X^2}+\frac{\partial^2 \theta_s}{\partial Y^2}\right)+Q=0 \qquad (4.10)$$

Where,

$$Re=u_i L/\upsilon,\ Ha^2=\sigma B_0^2 L^2/\mu,\ Pr=v/\alpha,\ Q=qL^2/k_s\Delta T,\ Ri=Gr/Re^2,$$
$$K=k_s/k_f$$

are the Reynolds number, square of the Hartmann number, Prandtl number, heat generating parameter, Richardson number and solid fluid thermal conductivity ratio respectively. (Here $\Delta T=T_h-T_i$ and $\alpha=k_f/\rho c_p$ are respectively the temperature difference and thermal diffusivity of the fluid)

The dimensionless boundary conditions of the present problem under consideration can be written as follows:

At the inlet: $U=1$, $V=0$, $\theta=0$

At the outlet: convective boundary condition (CBC), $P=0$

At all solid boundaries: $U=0$, $V=0$,

At the heated bottom wall: $\theta=1$

At the left, right and top walls: $\dfrac{\partial \theta}{\partial N}=0$

At the fluid-solid interface: $\left(\dfrac{\partial \theta}{\partial N}\right)_{fluid}=K\left(\dfrac{\partial \theta_s}{\partial N}\right)_{solid}$

Here N is considered as the dimensionless distances either along X or Y direction that acts normal to the surface.

According to Singh and Sharif (2003), the average Nusselt number at the heated wall of the cavity based on the dimensionless variables may be expressed as $Nu_{av} = -\int\limits_{0}^{1} \dfrac{\partial \theta}{\partial Y} dX$ and the bulk average temperature of the fluid inside the cavity defined as $\theta_{av} = \int \theta \, d\overline{V} / \overline{V}$, where $\overline{V}$ is the cavity volume.

4.3 Numerical Analysis

The numerical method that has been applied in the present study is discussed briefly in this section.

4.3.1 Solution Process

The Galerkin weighted residual finite element scheme is used for the studied problem to solve the governing equations numerically. In this method, the continuum area of interest is discretized into finite element meshes, which are composed of irregular triangular elements. Six node triangular elements with quadratic interpolation functions for velocity, temperature and linear interpolation functions for pressure are used to discretize the physical domain. The coupled equations (4.6)-(4.10) are transformed into a system of integral equations using Galerkin weighted residual technique to reduce the continuum domain into discrete triangular domains. Then by imposition of boundary conditions the so obtained nonlinear algebraic equations are modified into a set of linear algebraic equations applying Newton-Raphson iteration technique. Last of all with the aid of triangular factorization method these linear equations are solved. Method of solution along with grid independent test and code validation has already been discussed in the Chapter 3 in details.

4.4 Results and Discussions

The effects of Reynolds number, Prandtl number, Hartmann number, solid fluid thermal conductivity ratio and solid block diameter for a MHD mixed convection problem in a ventilated square cavity containing a heat generating block have been investigated. The results of the present study are explained in the forms of streamlines and isotherms. In addition, the heat transfer effects inside the enclosure

are shown in terms of average Nusselt number Nu_{av} and the average fluid temperature θ_{av}

4.4.1 Effect of Reynolds Number

The streamlines and isotherms for the different values of Re with $Ha = 10$ and $Pr = 0.71$ have been presented in the Fig. 4.2. Fig. 4.2(a) shows the streamlines for the Reynolds number varied as $50 \leq Re \leq 500$, whereas the dominant forced convection effect ($Ri = 0.1$) is considered. For the lower value of $Re = 50$ it is noticed that the fluid flow absorbs the whole cavity, diverges close to the heated surface and the open lines are symmetric about diagonally. As the inertia force grows up with increasing Re, a CCW vortex is created above the inflow openings at $Re = 200$. This vortex expands sharply confining the heated block and another small clockwise vortex is found near the bottom right side of the cavity for the two higher values of Re (= 350, 500). This happened because the role of forced convection in the cavity becomes more significant with increasing Re. From this Fig. it can be highlighted that a noteworthy variation in flow behavior is found for the other two convective regimes of Ri (= 1, 10) with any particular Reynolds number.

The corresponding effect of Reynolds number Re on the thermal field is exposed in the Fig. 4.2(b). For $Re = 50$ and all Ri (= 0.1, 1, 10) it is apparent that the isotherms move out of the centered heat generating obstacle. Besides this, for the considered three different convective regimes a thermal boundary layer is formed in the neighborhood of the bottom heated wall of the cavity and high isothermal lines are crowded at the lower part of the heat generating obstacle. Moreover, plume shape isotherms are viewed at the left side of the block for $Re = 350$ and $Re = 500$ at $Ri = 0.1$ while these are found at the top of the block for $Re = 200$ with $Ri = 0.1$ as well as Re (= 200, 350, 500) at the rest two regimes of Ri. It also seen that thermal boundary-layer thickness increases as Re gets higher and the isothermal lines become denser at the adjacent area of the heated block in the mixed convection and natural convection dominated regions.

Fig. 4.3 describes the effect of Reynolds number on average Nusselt number Nu_{av} and average fluid temperature θ_{av} in the cavity as a function of Richardson number. One can observes that the value of average Nusselt number increases as Ri increases
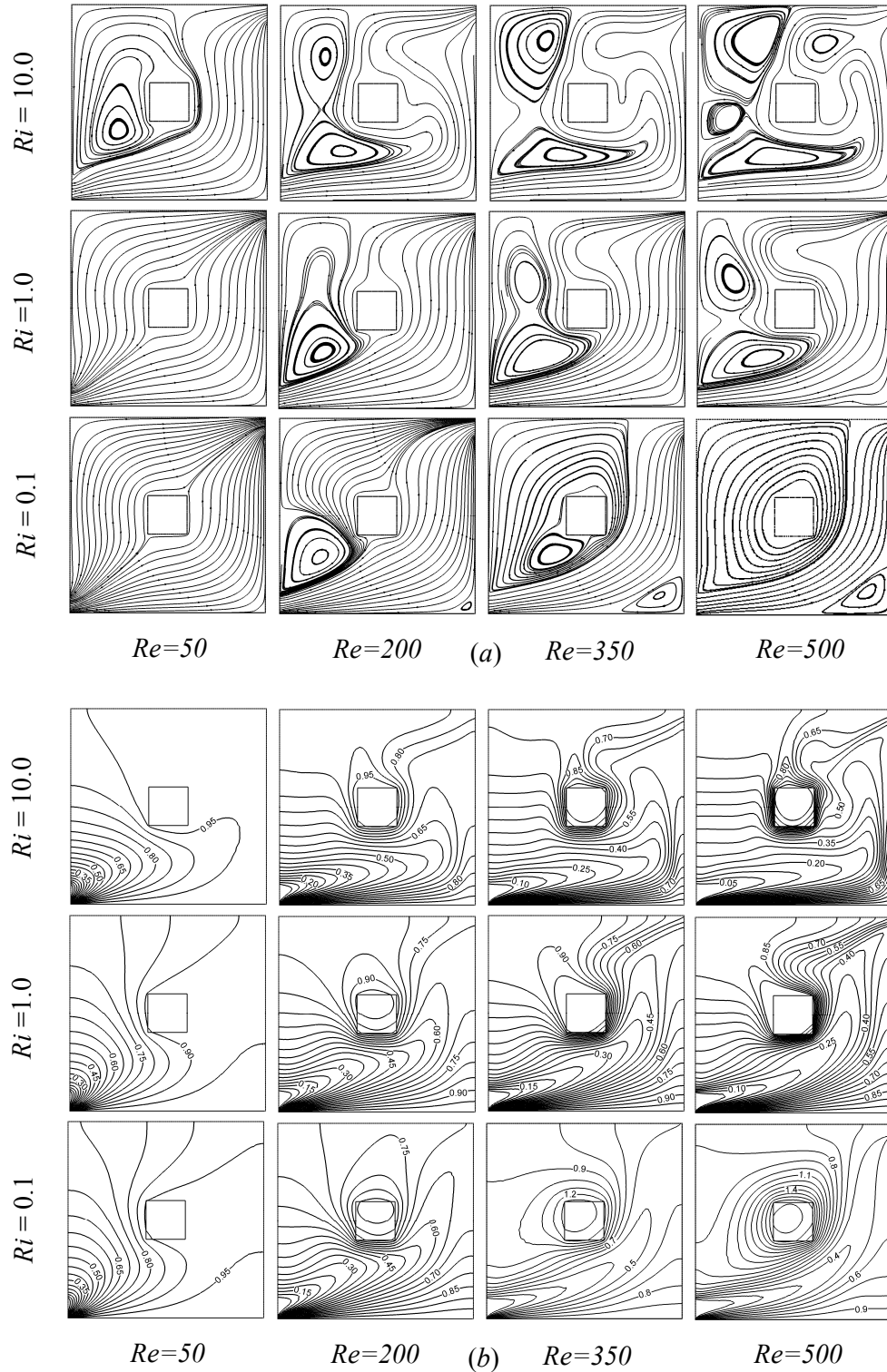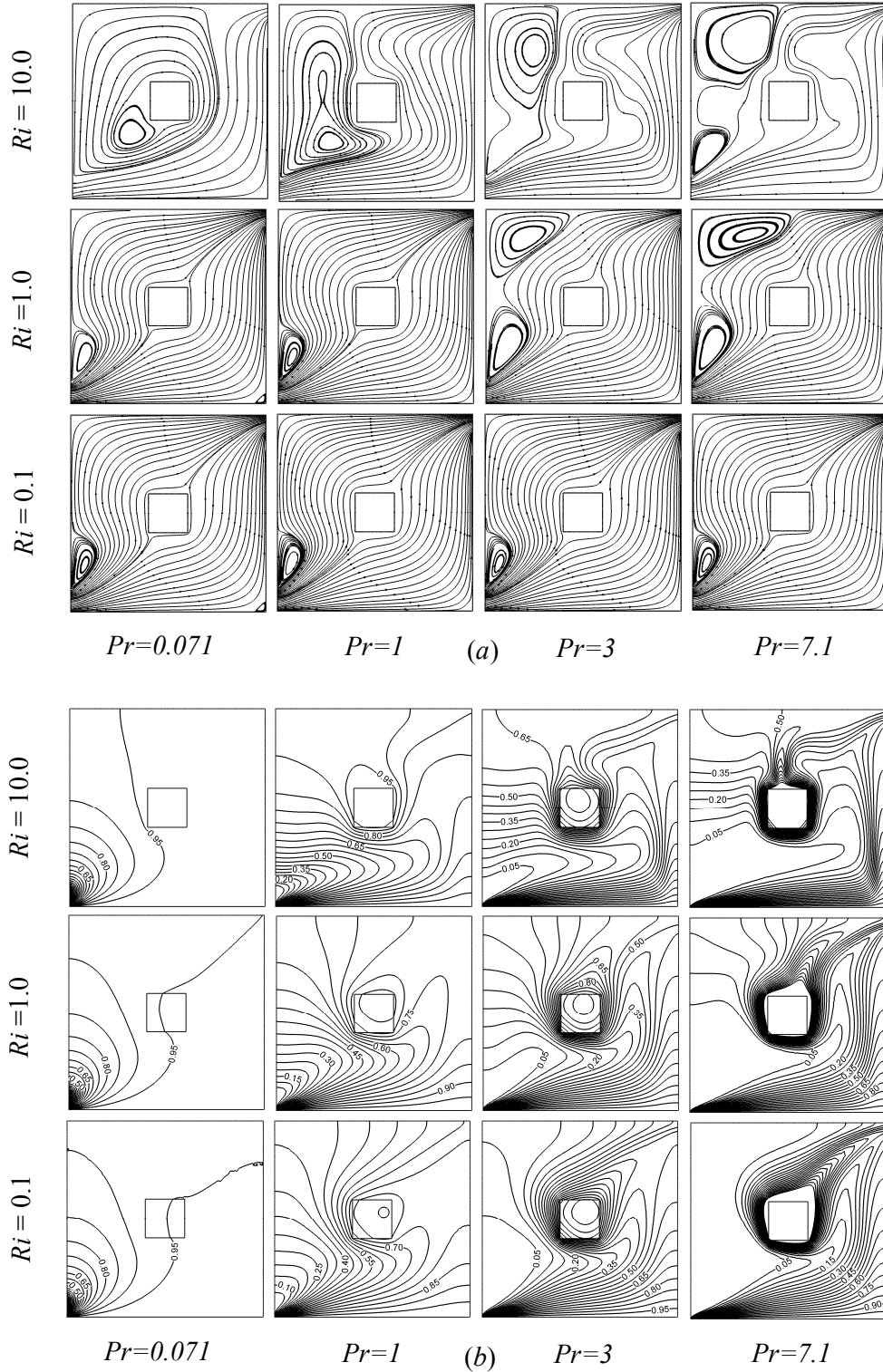
Figure 4.2: (*a*) Streamlines and (*b*) Isotherms at different Reynolds number and various values of Richardson number *Ri*, while *Ha* = 10, *K* = 5, *Pr* = 0.71, *Q* = 1 and *D* = 0.2.
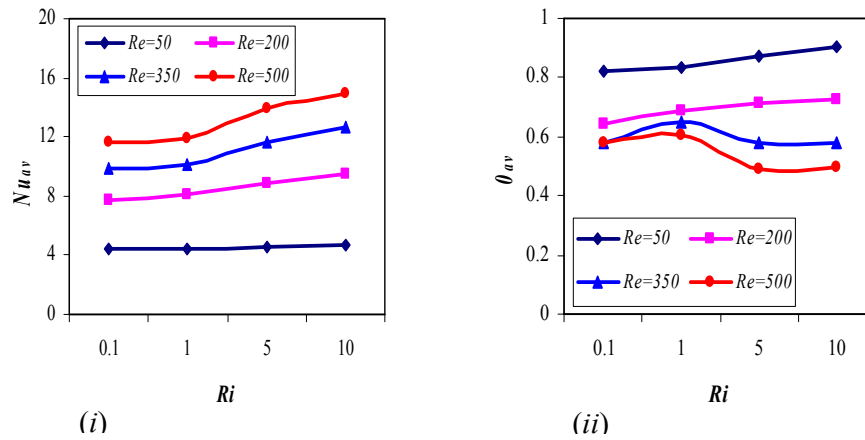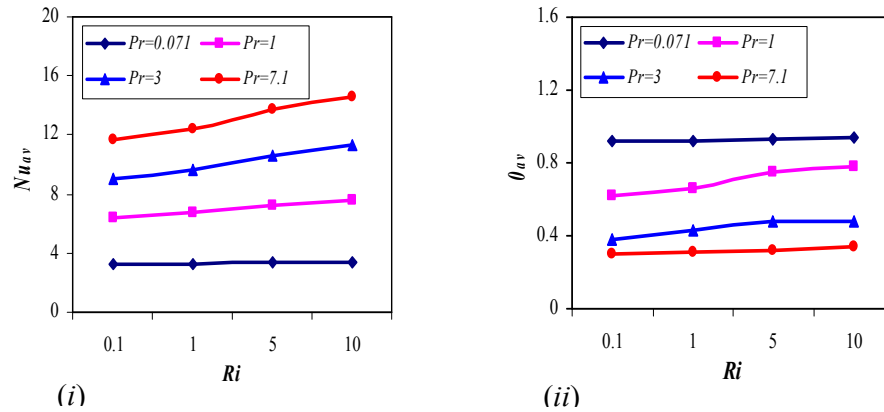
Figure 4.3: Effect of Reynolds number on (*i*) average Nusselt number, (*ii*) average fluid temperature, while $Ha = 10$, $Pr = 0.71$, $D = 0.2$, $Q = 1$ and $K = 5$.

Table 4.1: Variation of average Nusselt number with Reynolds number

Ri	Nu_{av}			
	$Re = 50$	$Re = 200$	$Re = 350$	$Re = 500$
0.1	4.388523	7.750381	9.901751	11.6910
1.0	4.443288	8.052749	10.17529	11.84686
2.0	4.485698	8.189754	10.52456	12.18456
3.0	4.502136	8.34568	10.84214	12.81458
4.0	4.534587	8.54216	11.40125	13.40216
5.0	4.591864	8.869711	11.70798	13.88068
6.0	4.625874	8.904569	11.98564	13.89751
7.0	4.632458	8.954783	12.23456	14.01235
8.0	4.642578	9.123546	12.32128	14.45681
9.0	4.657891	9.234587	12.50124	14.52136
10.0	4.669317	9.454947	12.59697	14.89302

for higher values of Re (= 200, 350 and 500) whereas for $Re = 50$, Nu_{av} is almost constant for all Ri. Thus the greatest heat transfer rate is found for the highest value of Re. On the other hand, the average fluid temperature in the cavity increases smoothly with increasing Ri for the lower values of Re (= 50, 200). But for upper Re (= 350 and 500) it is noticed that θ_{av} increases as Ri varies from 0.1 to 1, decreases in

the region $1 \leq Ri \leq 5$ and θ_{av} is about independent beyond these regions. In addition lowest average fluid temperature occurs for the largest Reynolds number.

Table 4.1 shows the variation of average Nusselt number with Reynolds number for different Richardson number. It is apparent from the table that as Ri increases heat transfer rate is higher for all values of Re.

4.4.2 Effect of Prandtl Number

The influence of Prandtl number on streamlines and isotherms are presented for fluid flow within a vented cavity of the mixed convection problem having a heat source. The Hartmann number Ha, Reynolds number Re are chosen 10 and 100 respectively while the Prandtl number is in the range $0.071 \leq Pr \leq 7.1$ for each of the three convective regimes of $Ri = 0.1, 1, 10$.

The effect of Pr at the three different values of Ri on streamlines as well as isotherms are displayed in Fig. 4.4. From Fig. 4.4(a), it is seen that at $Ri = 0.1$, a small recirculation cell is formed near the left top corner of the inlet in the cavity while $Pr = 0.071$. This indicates that the fluid flow of the enclosure has been affected by the inertia force. There is no significant change in flow patterns for the rest three higher values of Pr at the dominant forced convection region; whereas it is observed that for the mixed convection ($Ri = 1$) and the dominant natural convection ($Ri = 10$) region the flow structure is influenced by varying Pr as shown in upper two rows of Fig. 4.4(a). As the buoyancy force increases with increasing Ri; the rotating cell becomes larger for a fixed value of Pr and higher values of Ri.

Fig. 4.4(b) depicts the isotherms for the four considered values of Pr. This figure illustrates that at $Ri = 0.1$ and $Ri = 1$ with $Pr = 0.071$ the heat lines become thinner and highest isotherm line pass through the heat generating block but at the dominant free convection region the isothermal line move out from the obstacle. With higher vales of Pr (= 1, 3, 7.1) it is seen that the isotherms become denser and top right cornered plume shape isotherms are created for $Ri = 0.1, 1$ whereas at $Ri = 10$, this type of heat lines are found at the top of the centered body. Also the higher Prandtl number gives more compact isotherms in the vicinity of the heat source.

The average Nusselt number Nu_{av} and average fluid temperature θ_{av} in the studied cavity for different Prandtl numbers along with Richardson numbers has been
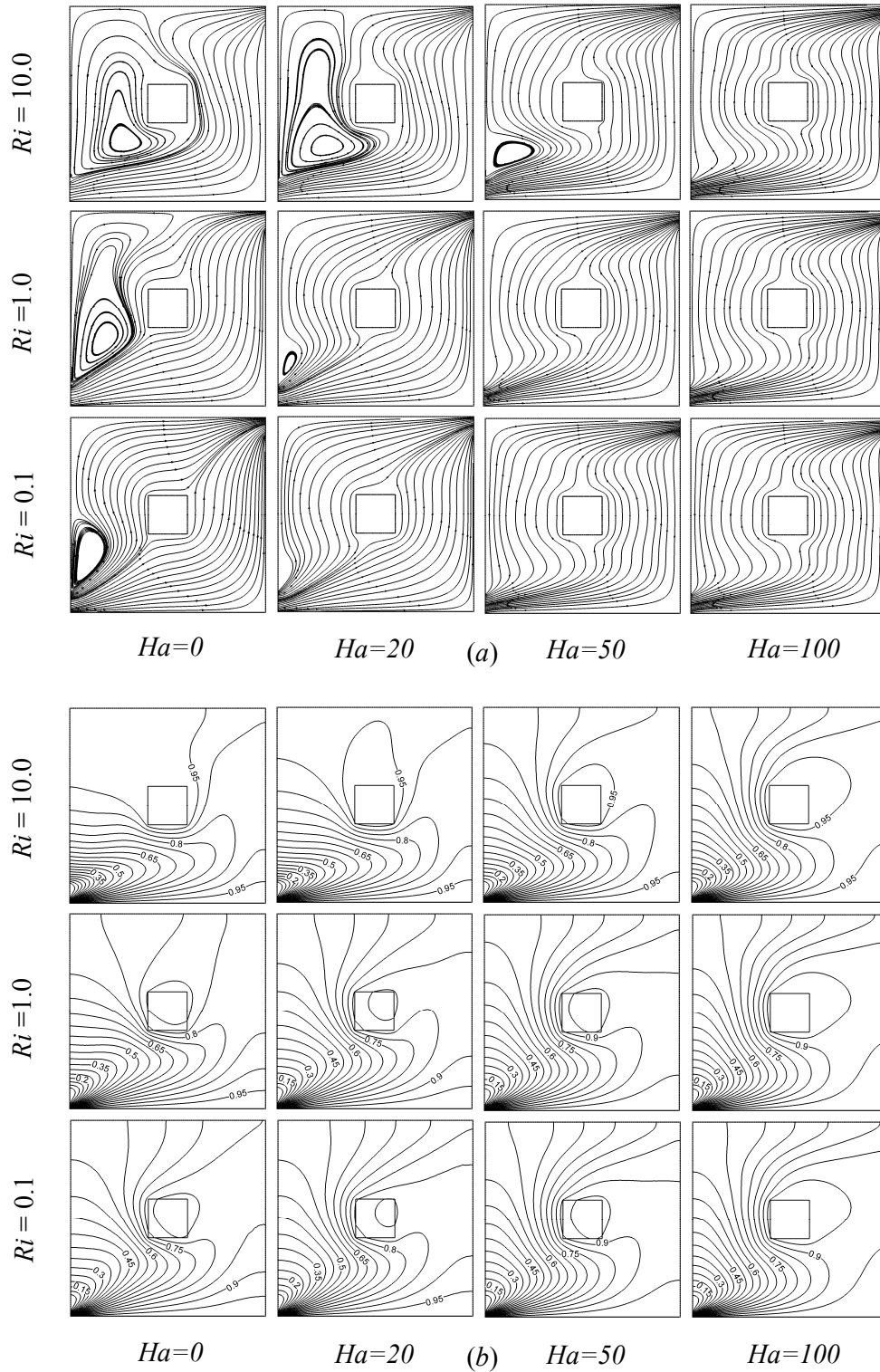
Figure 4.4: (*a*) Streamlines and (*b*) Isotherms at different Prandtl number and various values of Richardson number *Ri*, while *Re* = 100, *Ha* = 10, *K* = 5, *Q* = 1 and *D* = 0.2.
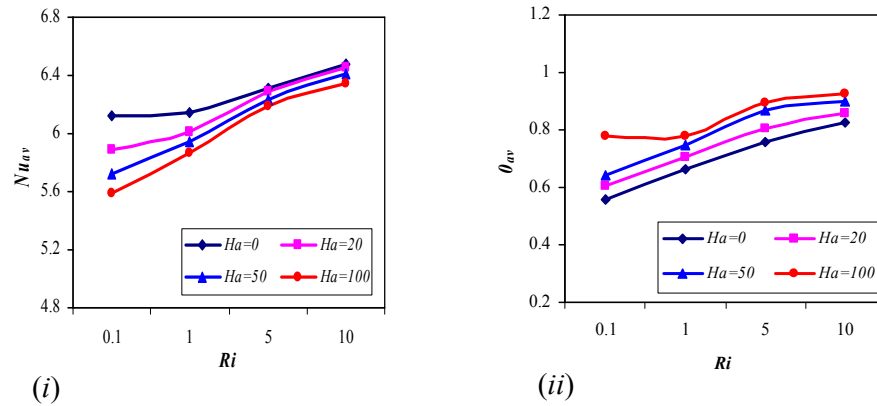
Figure 4.5: Effect of Prandtl number on (*i*) average Nusselt number, (*ii*) average fluid temperature, while *Re* = 100, *Ha* = 10, *D* = 0.2, *Q* = 1 and *K* = 5.

Table 4.2: Variation of average Nusselt number with Prandtl number

Ri	Nu_{av}			
	Pr = 0.071	*Pr* = 1	*Pr* = 3	*Pr* = 7.1
0.1	3.307886	6.401763	8.882427	11.58715
1.0	3.310394	6.734086	9.594996	12.26479
2.0	3.311246	6.814573	9.865423	12.78451
3.0	3.31548	7.01549	9.998754	12.98754
4.0	3.319854	7.132456	10.25478	13.45621
5.0	3.32025	7.231245	10.61472	13.70829
6.0	3.32145	7.334568	10.87946	13.84256
7.0	3.32456	7.421578	10.99879	13.98562
8.0	3.32514	7.501245	11.10345	14.21346
9.0	3.32789	7.542863	11.24789	14.42013
10.0	3.329817	7.580309	11.35116	14.54344

focused in Fig. 4.5. It is noted that Nu_{av} increases with the rising value of *Pr* and accordingly optimum Nu_{av} is recorded for *Pr* = 7.1, due to the capability of the fluid with the highest Prandtl number is to carry more heat away from the heat generating block and dissipated through the outlet in the cavity. Besides this it can be followed that as θ_{av} decreases while *Pr* increases, minimum average temperature is found for large Prandtl number *Pr* = 7.1.

The variation of average Nusselt number with Prandtl number is exposed in Table 4.2 for the values of Ri =0.1 to 10. It is observed that the rate of heat transfer enhances with larger values of Ri and Pr.

4.4.3 Effect of Hartmann Number

The streamlines and isotherms have been analyzed to explain the flow and thermal field structure of the mixed convection problem for different values of Hartmann number. The Prandtl number Pr, Reynolds number Re are chosen 0.71 and 100 respectively while the Hartmann number is varied from 0 to 100 for each of the three convective regimes of $Ri = 0.1, 1, 10$.

The streamlines corresponding to different Hartmann number are shown in Fig. 4.6(a). The third row of Fig. 4.6(a) displays the streamlines for dominant forced convection $Ri = 0.1$. In the absence of magnetic field ($Ha = 0$) the fluid flow is characterized by the open lines that squeezes above the inlet openings. It is also noted that a small anti-clockwise rotating vortex is developed at top just entrance of the cavity. For $Ha = 20$, the shape of the streamlines are found to be slight different and the circulating cell vanishes. Again in the case of the higher values of Ha (= 50 and 100), the streamlines are about identical and it is observed that these are almost horizontal and vertical of the cavity walls in the whole domain. When natural and forced convection are equally dominant, namely, $Ri = 1$, the effect of Hartmann number on streamlines is demonstrated in second rows of Fig 4.6(a). The mainstreams shrink from the left and top side and consequently the CCW vortex increases much and it spreads up to the top cavity wall while $Ha = 0$. For $Ha = 20$ it is seen that the open lines swell up over the whole cavity and a small eddy is found above the inlet. No vortex forms for larger values of Hartmann number and the streamlines become more vertical for $Ha = 100$. This is because most of the heat transfer process is carried out by conduction. For the convective regime $Ri = 10$, the top row of Fig. 4.6(a) depicts the fluid flow characteristics for the variation of magnetic field parameter. For $Ha = 0$, it is seen that the core vortex expands more towards the right of the cavity and occupies the block indicating the enhancement of the flow strength of the vortex. As Ha increases the flow strength of the vortices

Ha=0 *Ha=20* (*a*) *Ha=50* *Ha=100*
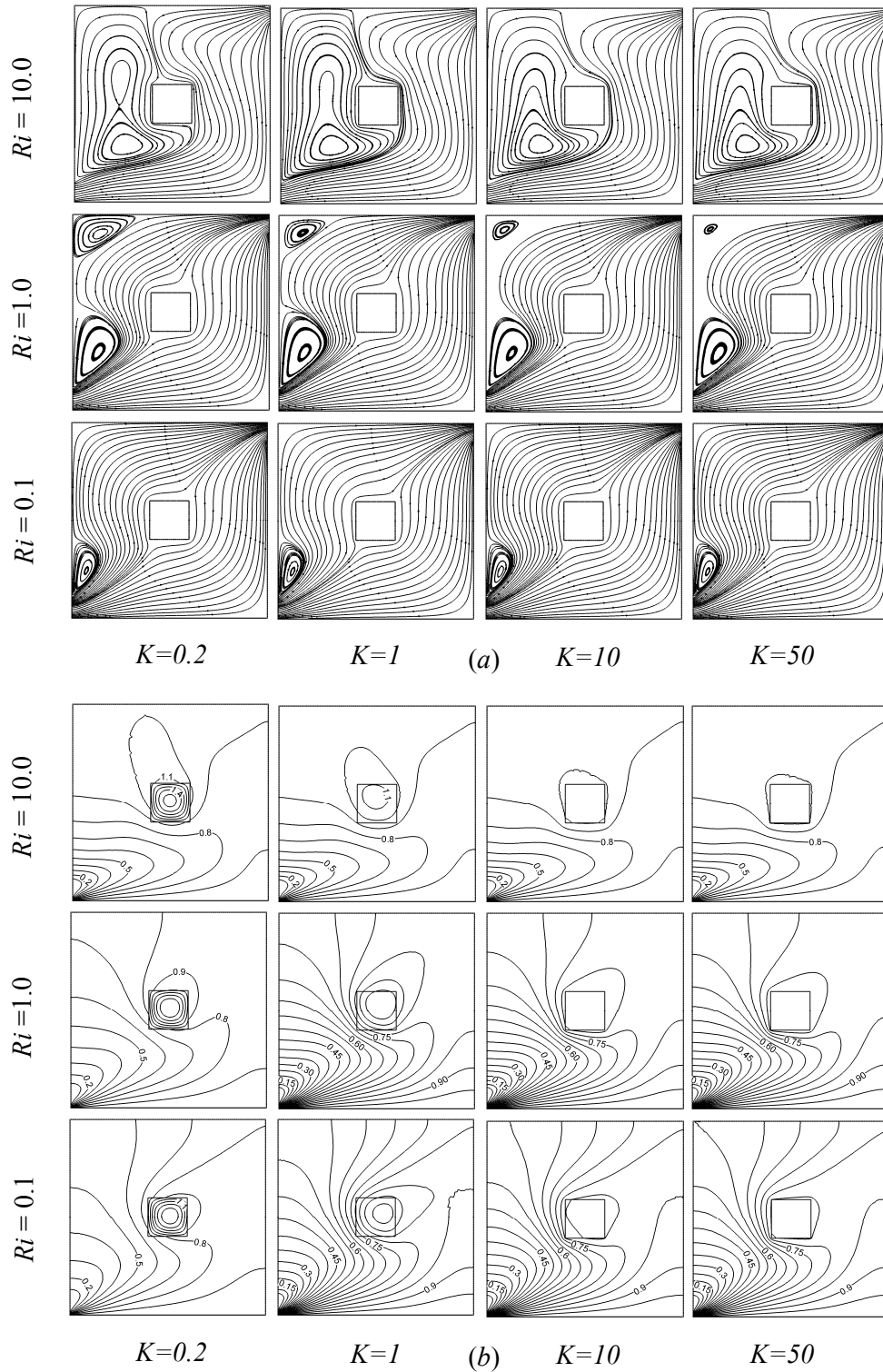

Ha=0 *Ha=20* (*b*) *Ha=50* *Ha=100*

Figure 4.6: (*a*) Streamlines and (*b*) Isotherms at different Hartmann number and various values of Richardson number *Ri,* while *Re* = 100, *Pr* = 0.71, *K* = 5, *Q* = 1 and *D* = 0.2.
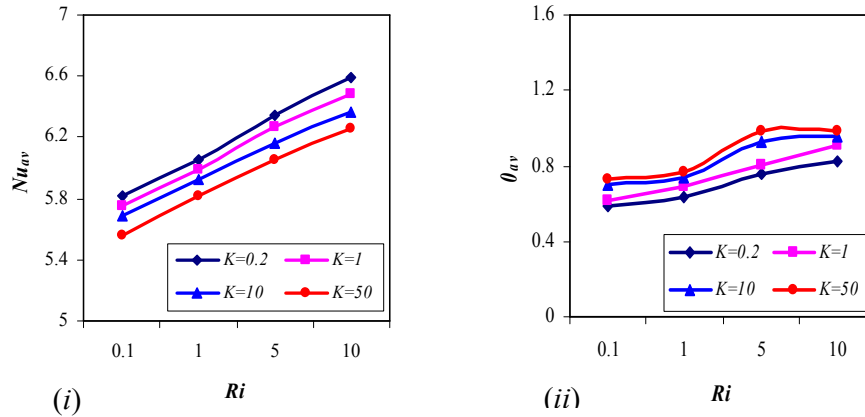
(*i*)   (*ii*)

Figure 4.7: Effect of Hartmann number on (*i*) average Nusselt number, (*ii*) average fluid temperature, while $Re = 100$, $Pr = 0.71$, $D = 0.2$, $Q = 1$ and $K = 5$.

Table 4.3: Variation of average Nusselt number with Hartmann number

Ri	Nu_{av}			
	$Ha = 0$	$Ha = 20$	$Ha = 50$	$Ha = 100$
0.1	5.921909	5.692517	5.326058	5.303347
1.0	6.139915	5.851140	5.548711	5.56483
2.0	6.195478	6.102345	5.998963	5.895842
3.0	6.231456	6.185463	6.123456	5.98421
4.0	6.294578	6.231495	6.201234	6.01548
5.0	6.316127	6.283367	6.236688	6.192215
6.0	6.384512	6.321569	6.302145	6.213694
7.0	6.408178	6.364573	6.338561	6.289756
8.0	6.411587	6.395421	6.402136	6.302145
9.0	6.431234	6.411578	6.409853	6.312579
10.0	6.449623	6.433135	6.413511	6.348449

reduces rapidly, major flows swell up and accordingly the vortex disappears while $Ha = 100$.

In Fig. 4.6(*b*), the last row displays the corresponding isotherms for the aforementioned Hartmann numbers in the regime of $Ri = 0.1$. For $Ha = 0$, the isothermal lines are crowded at the inlet and a thermal boundary layer is followed in the vicinity of the bottom hot wall of the cavity. Also a round shaped heat line

appears through the square block. The non-linearity of the temperature distribution increases with the mounting values of Hartmann number. In the case of higher magnetic field parameter it is found that high isotherms are concentrated near the heat generating block and for $Ha = 100$, the circular isotherm confines the centered block. For $Ri = 1$, the temperature distribution inside the enclosure are presented in the middle row of Fig. 4.6(b). In the case of lowest magnetic field the isotherms pattern changes above the heat generating block. But no significant change is found for growing magnetic field parameter comparatively with those of the case at $Ri = 0.1$. Lastly from the top row of Fig. 4.6(b) for $Ri = 10$, it is noticed that at $Ha = 0$ the heat lines are packed below the block. The non-linearity of isotherms increases and the heat generating block is curbed by the topmost isothermal line for the cases of growing Ha.

From Fig. 4.7(i) it is seen that as the magnetic field Ha decreases average Nusselt number Nu_{av} increases for all values of Ri. Thus higher Nu_{av} that is maximum heat transfer is found in the absence of magnetic field. Moreover for the increasing value of Ri, Nu_{av} increases for each of the four chosen values of Ha which is expected because of the supremacy of natural convection. In addition average fluid temperature is shown in Fig. 4.7(ii) and from this figure it can be concluded that θ_{av} is about uniformly increased for the values of $Ha = 20, 50, 100$. But for $Ha = 0$, average temperature is identical in the region $0.1 \leq Ri \leq 1$ and it increases in the dominant natural convection domain. It is also observed that average temperature is lowest for $Ha = 0$.

Table 4.3 reveals the variation of heat transfer rate at the heated surface among the different Hartmann number along with Richardson number. As Ri increases Nu_{av} increases but it decreases with the larger value of Ha.

4.4.4 Effect of Solid Fluid Thermal Conductivity Ratio

Fig. 4.8(a) presents the streamlines for different values of K for the convective regimes of Ri (0.1, 1, 10) while $Re = 100$, $Ha = 10$, and $Pr = 0.71$ are kept fixed. At $Ri = 0.1$ and $K = 0.2$ it is observed that the mainstreams capture almost the cavity and a counter-clockwise rotating cell develops just above the inlet openings. This is the

$Ri = 10.0$ $Ri = 1.0$ $Ri = 0.1$

K=0.2   *K=1*   (*a*)   *K=10*   *K=50*

K=0.2   *K=1*   (*b*)   *K=10*   *K=50*

Figure 4.8: (*a*) Streamlines and (*b*) Isotherms at different thermal conductivity ratio and various values of Richardson number *Ri*, while *Re* = 100, *Pr* = 0.71, *Ha* = 10, *Q* = 1 and *D* = 0.2

Figure 4.9: Effect of thermal conductivity ratio on (*i*) average Nusselt number, (*ii*) average fluid temperature, while $Re = 100$, $Pr = 0.71$, $D = 0.2$, $Q = 1$ and $Ha = 10$.

Table 4.4: Variation of average Nusselt number with thermal conductivity ratio

Ri	Nu_{av}			
	$K = 0.2$	$K = 1$	$K = 10$	$K = 50$
0.1	5.812649	5.753399	5.688583	5.555065
1.0	6.058879	5.985485	5.896423	5.817765
2.0	6.184789	6.012345	5.923185	5.904563
3.0	6.234567	6.135469	6.012456	5.994658
4.0	6.302145	6.201456	6.12349	6.012348
5.0	6.345561	6.268571	6.157524	6.054824
6.0	6.398745	6.298457	6.197845	6.13458
7.0	6.482589	6.326985	6.285469	6.184793
8.0	6.512378	6.412578	6.301297	6.201346
9.0	6.55789	6.457892	6.35698	6.21459
10.0	6.593505	6.480545	6.360907	6.256456

reason that outer fresh and colder fluids which enters the cavity cannot come into intimate mixing with the inner hotter fluids. There is no disparity in the streamlines for the rest higher values of *K*. In the mixed convection domain ($Ri = 1$) for $K = 0.2$ it follows that the size of lower vortex increases and the top-left cornered open lines squeezes, as a result another anti- clockwise vortex appears occupying that region.

But it can be noticed that with the increasing of thermal conductivity ratio the upper vortex reduces in size. A drastic change in flow lines is found at the higher value of $Ri = 10$. The main flow is found merely the right side of the obstacle and an extremely large vortex is created starting just above the inlet that spreads up to the top wall of the enclosure confining the obstacle.

The corresponding isothermal lines for the chosen values of K in the range $0.1 \leq Ri \leq 10$ are displayed in Fig. 4.8(b). In the forced convection dominated region, highest circular thermal lines are distributed inside the centered solid block for the lowest value of $K = 0.2$. As the value of K increases from 0.2 to 1 it is noticed that the isotherms are dispersed all over the cavity and the compactness of heat lines inside the block reduces. It can be summarized that with increasing the value of K isothermal lines move out gradually from the solid obstacle and as a result it disappears at $K = 50$. With the comparison of $Ri = 0.1$, a minor change including right-top cornered plume shaped heat line is found in the patterns of isotherms at $Ri = 1$. For the free convection dominated region ($Ri = 10$) the behavior of temperature distribution changes markedly. The majority of isothermal lines are distributed below the heat generating block and plume shaped isotherm alters it direction from the right-top corner to left-top corner.

In order to investigate the effect of thermal conductivity ratio K at solid fluid interface on heat transfer manner, average Nusselt number Nu_{av} at the bottom heated surface and average fluid temperature θ_{av} in the cavity are shown in Fig. 4.9. From this it can be observed that average Nusselt number enhances sharply as the value of K decreases and Ri increases. Therefore the rate of heat transfer is found optimum for the smallest value of K. On the other hand, θ_{av} increases for the rising value K and minimum average temperature is occurred when $K = 0.2$. Also for the lower values of K ($= 0.2, 1$) it is apparent that θ_{av} raises with the increasing value of all Ri but θ_{av} is seen about stationary in the domain $0.1 \leq Ri \leq 1$ and $5 \leq Ri \leq 10$ while it grows up in the area $1 \leq Ri \leq 5$ in the case of upper values $K = 10$ and $K = 50$.

Table 4.4 shows the variation of heat transfer rate at the hot bottom surface with thermal conductivity ratio for the values of $Ri = 0.1$ - 10. Comparatively higher heat transfer rate is found for the upper value of Ri and it decreases as the value of K increases.

4.4.5 Effect of Block Diameter

The streamlines for different block size are depicts in Fig. 4.10(a) in the range of Richardson number $0.1 \leq Ri \leq 10$. At $Ri = 0.1$ and $D = 0.1$ the major streams stretched diagonally from the inlet to the exit opening and a recirculation cell is created just above the inlet of the cavity as expected. As the value of D increases the vortex becomes smaller and consequently it diminishes at the largest value of $D = 0.7$ due to the space availability in the cavity. Besides, streamlines are found to be nearly flat and vertical between the cavity and centered solid block for larger values of D (= 0.5, 0.7). In the pure mixed convection case ($Ri = 1$) the vortex expands rapidly at D = 0.1 and this recirculation cell sharply reduces and finally disappears for the maximum blocked size ($D = 0.7$) with the similar flow structures as seen at $Ri = 0.1$. One can easily be observed that for $D = 0.1$ the intensity of the vortex in the cavity increases too much and it captures the obstacle in the case of higher value of $Ri = 10$, this is happened since buoyancy effect increases. For $D = 0.3$ the counter-clockwise vortex shrinks from the right side and it vacates the block. A bi-cellular recirculation cell is created at $D = 0.5$ and it becomes narrow regarding $D = 0.1$ and $D = 0.3$. There is no change in flow patterns for $D = 0.7$ with the comparison of $Ri = 0.1$ and $Ri = 1$. Fig. 4.10(b) illustrates the temperature distribution inside the vented enclosure for the four chosen values of block diameter D. For all the convective regimes of Richardson number Ri (= 0.1, 1, 10) it is noticed that at $D = 0.1$ isotherms are concentrated near the inlet and a thermal boundary layer is formed in the vicinity of the bottom hot wall. The heat lines are scattered in the whole domain for the lower values of Ri (= 0.1, 1) while these are seems to be curved below the heat generating block at $Ri = 10$ and $D = 0.1$. For higher values of D the heat lines are almost similar in all the selected range of Richardson number.

Average Nusselt number and average fluid cavity temperature are displayed in Fig. 4.11 to expose the heat transfer efficiency for the inner heat generating body. From Fig. 4.11(i) it is noticed that average Nusselt number is higher for the smallest value of D and a little difference in heat transfer is found for the two consecutive values of $D = 0.1$ and $D = 0.3$. On the other hand, largest sized solid body gives the maximum cavity temperature that is seen in Fig. 4.11(ii).
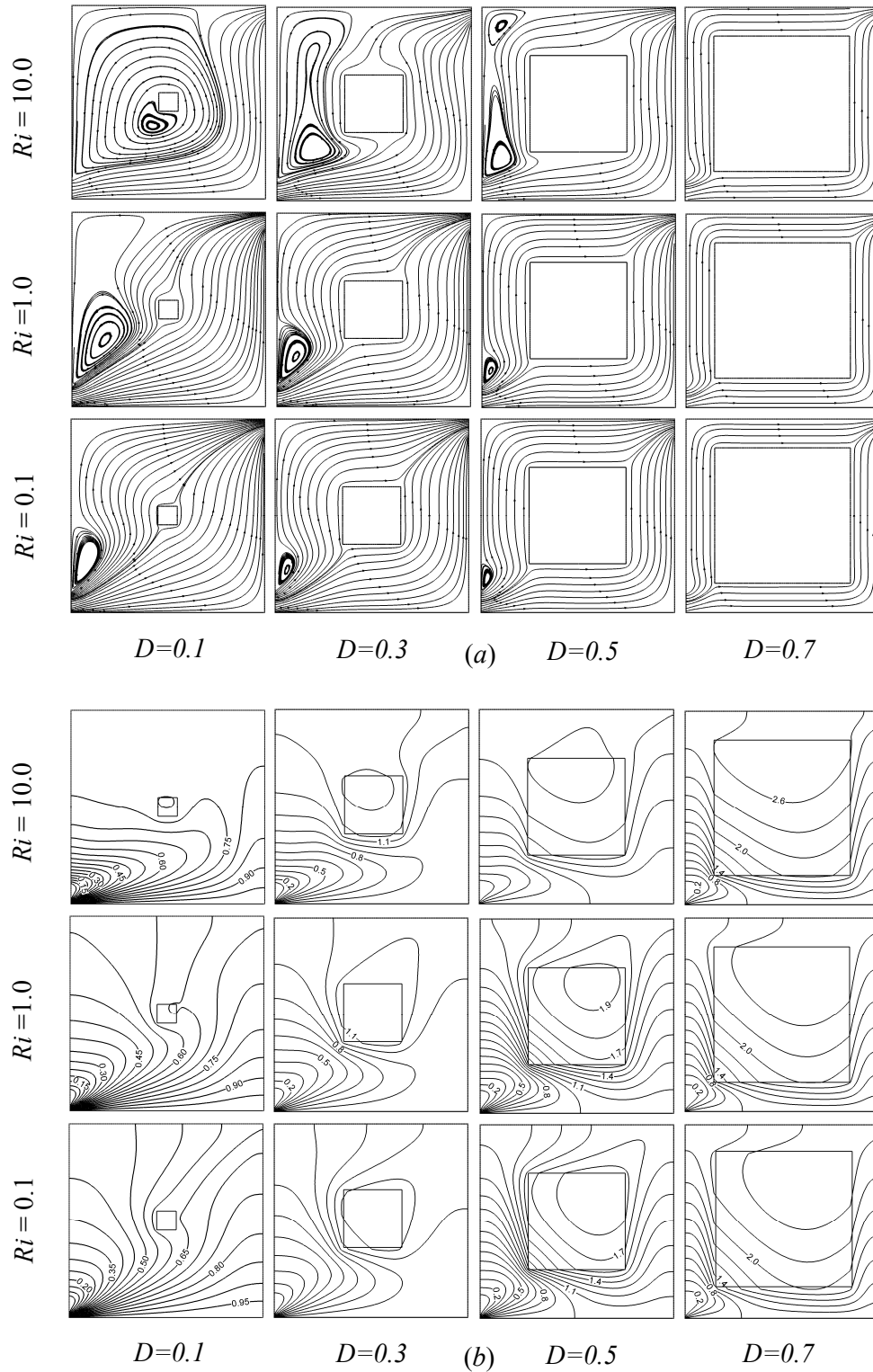
Figure 4.10: (*a*) Streamlines and (*b*) Isotherms at different block diameter and various values of Richardson number *Ri*, while *Re* = 100, *Pr* = 0.71, *Ha* = 10, *Q* = 1 and *K* = 5.
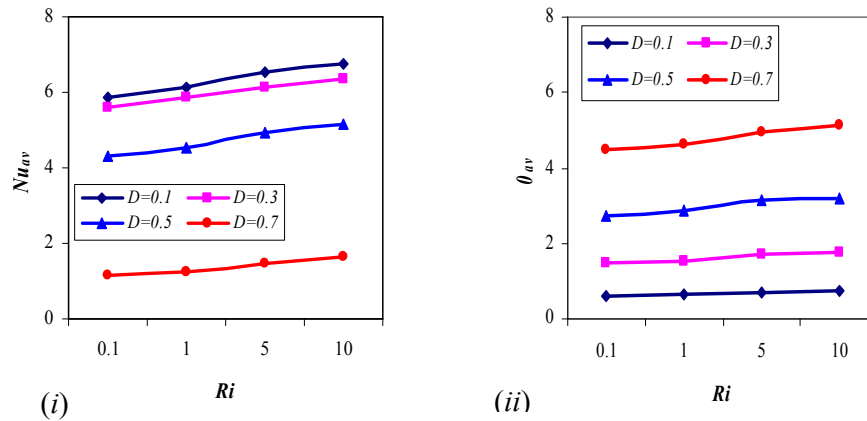
Figure 4.11: Effect of block diameter on (*i*) average Nusselt number, (*ii*) average fluid temperature, while $Re = 100$, $Pr = 0.71$, $K = 5$, $Q = 1$ and $Ha = 10$.

Table 4.5: Variation of average Nusselt number with block diameter

Ri	Nu_{av}			
	$D = 0.1$	$D = 0.3$	$D = 0.5$	$D = 0.7$
0.1	5.86043	5.613745	4.304263	1.134105
1.0	6.115497	5.854553	4.552257	1.229502
2.0	6.21343	5.912346	4.62351	1.293046
3.0	6.315479	6.012145	4.78623	1.304568
4.0	6.416312	6.10879	4.821364	1.358764
5.0	6.544416	6.147784	4.919997	1.48240
6.0	6.59215	6.195476	4.995689	1.598761
7.0	6.612456	6.201347	5.012345	1.612486
8.0	6.685421	6.254987	5.10246	1.620439
9.0	6.704236	6.301249	5.11879	1.63254
10.0	6.774454	6.335527	5.138711	1.646546

Variation of average Nusselt number for block diameter along with *Ri* is given in Table 4.5. It can easily be seen that heat transfer rate decreases as *D* increases. Also when *Ri* increases heat transfer also increases.

71

4.5 Concluding Remarks

The present analysis addresses a problem on mixed convection two-dimensional laminar flow in a ventilated square enclosure with the variation of governing parameters such as Reynolds numbers ($50 \leq Re \leq 500$), Prandtl number ($0.071 \leq Pr \leq 7.1$), Hartmann number ($0 \leq Ha \leq 100$), thermal conductivity ratio ($0.2 \leq K \leq 50$), solid body diameter ($0.1 \leq D \leq 0.7$) and Richardson numbers ($0.1 \leq Ri \leq 10$). Combined convection flow along with thermal field is analyzed here numerically in the presence of heat generating obstacle located in the ventilated enclosure. Detailed computations for the distribution of streamlines, isotherms, average Nusselt number at the heated wall and average fluid temperature in the cavity were performed to explore the effect of the mentioned parameters. In view of the obtained results, the following conclusions may be summarized**.**

The Reynolds number Re always plays a crucial role on both flow and thermal fields. The highest value of Re gives the ceiling average Nusselt number and minimum average temperature in the cavity.

The effects of Prandtl number Pr on streamlines are insignificant in the forced convection dominated region but significant in other two convective regimes. On the other hand, in all convective regimes the temperature distributions in the cavity are influenced much by Prandtl number. The average Nusselt number becomes higher and average temperature in the cavity becomes lower for the larger values of Pr.

The flow field and temperature distribution are affected from the magnetic field. The decreasing of Hartmann number Ha increases the average Nusselt number but decreases the average fluid temperature in the cavity.

The highest heat transfer is recorded for the lowest value of K and it increases with increasing Ri. Lower thermal conductivity ratio shows the minimum average fluid temperature in the cavity.

A small size of obstacle gives the maximum average Nusselt number. Average fluid temperature in the cavity is about independent of Ri and it is lowest for the smaller value of D.

Chapter 5

Effect of a Heat Conducting Solid Body on Mixed Convection Flow in a Square Enclosure

Combined free and forced convection flow through a square vented enclosure with heated bottom wall is often encountered in air conditioning system for room space. Various aspects of flow and heat transfer in enclosures with and without obstacle was extensively studied in past and some of them have been reported in the literature. The present chapter deals with a numerical investigation on mixed convection in a ventilated enclosure containing a heat conducting solid body that was carried out using a finite element method.

A comprehensive study about the behavior of flow and heat transfer on MHD mixed convection for a wide range of various influencing parameters in a ventilated square cavity with internal heat conducting obstacle has been focused in this contents. The results showed that the flow and thermal behaviors within the cavity and heat transfer rate at hot wall are affected by the presence of heat conducting solid body.

There are five consecutive sections that are described in this chapter. Among these section 5.1 contains the physical configuration of the considered model. The mathematical formulation of the present problem is described in few steps in section 5.2. The numerical method that is applied in the studied problem is discussed in brief in section 5.3. Section 5.4 presents the outcome of this analysis in details. In view of the obtained results a conclusion is summarized finally in section 5.5.

5.1 Physical Configuration

The physical model of the studied problem is shown in Fig. 5.1 that consists of a square enclosure of length L with a heat conducting solid block located at the center. Except the bottom surface which is kept at a constant temperature T_h all sides of the cavity were taken as thermally isolated. The inlet port is placed on the bottom of the left wall, exit port is situated at the top of the right wall and the magnitude of each port is $w = 0.1L$. For all solid boundaries rigid no-slip walls assumed that is velocity components u and v are set to be zero. The flow of a uniform velocity, u_i and the

ambient temperature, T_i enters into the cavity and the outgoing flow is considered to have zero diffusion flux for all dependent variables.
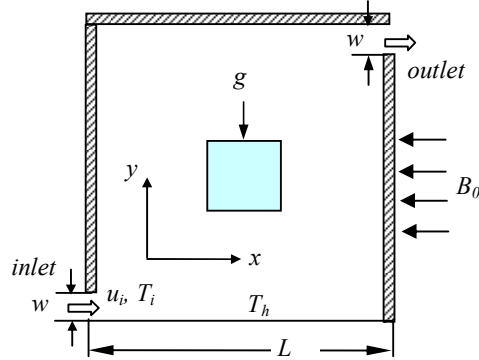
Figure 5.1: Schematic of the problem

5.2 Mathematical Formulation

Mathematical formulation for the current problem is described step by step in this section.

5.2.1 Governing Equations

The studied fluid is treated as laminar, Newtonian and incompressible with the flow on the mixed convection problem which possesses constant thermo physical properties. Under the Boussinesq approximation the governing equations for steady mixed convection flow using conservation of mass, momentum, and energy can be written in the dimensionless form as follows:

Continuity Equation

$$\frac{\partial U}{\partial X} + \frac{\partial V}{\partial Y} = 0 \qquad (5.6)$$

Momentum Equations

$$U\frac{\partial U}{\partial X} + V\frac{\partial U}{\partial Y} = -\frac{\partial P}{\partial X} + \frac{1}{Re}\left(\frac{\partial^2 U}{\partial X^2} + \frac{\partial^2 U}{\partial Y^2}\right) \qquad (5.7)$$

$$U\frac{\partial V}{\partial X} + V\frac{\partial V}{\partial Y} = -\frac{\partial P}{\partial Y} + \frac{1}{Re}\left(\frac{\partial^2 V}{\partial X^2} + \frac{\partial^2 V}{\partial Y^2}\right) + \frac{Ra}{Re^2 Pr}\theta - \frac{Ha^2}{Re}V \qquad (5.8)$$

74

Energy Equations

$$U\frac{\partial \theta}{\partial X}+V\frac{\partial \theta}{\partial Y}=\frac{1}{Re\,Pr}\left(\frac{\partial^2 \theta}{\partial X^2}+\frac{\partial^2 \theta}{\partial Y^2}\right)$$

(5.9)

$$\frac{K}{RePr}\left(\frac{\partial^2 \theta_s}{\partial X^2}+\frac{\partial^2 \theta_s}{\partial Y^2}\right)=0$$

(5.10)

Where, the dimensionless parameters involving the equations (5.6) - (5.10) are the Reynolds number, Rayleigh number, square of Hartmann number, Prandtl number, Richardson number, solid fluid thermal conductivity ratio and these are defined respectively as follows

$$Re=u_i L/\upsilon,\ Ra=g\,\beta\,\Delta T\,L^3\big/\upsilon\alpha,\ Ha^2=\sigma\,B_0^2 L^2\big/\mu,\ Pr=v/\alpha,\ Ri=Gr\big/Re^2$$
$$\text{and } K=k_s\big/k_f$$

In addition, $\Delta T=T_h-T_i$ is temperature difference and $\alpha=k_f\big/\rho c_p$ is fluid thermal diffusivity.

5.2.2 Boundary Conditions

The non-dimensional boundary conditions which are used in the current work can be set as follows:-

At the inlet: $U=1$, $V=0$, $\theta=0$

At the outlet: convective boundary condition (CBC), $P=0$

At all solid boundaries: $U=0$, $V=0$

At the heated bottom wall: $\theta=1$

At the left, right and top walls: $\dfrac{\partial \theta}{\partial N}=0$

At the fluid-solid interface: $\left(\dfrac{\partial \theta}{\partial N}\right)_{fluid}=K\left(\dfrac{\partial \theta_s}{\partial N}\right)_{solid}$

Here N is the dimensionless distances either along X or Y direction that acts normal to the surface.

The average Nusselt number at the hot wall of the enclosure based on the dimensionless variables may be expressed as $Nu_{av} = -\int_{0}^{1} \frac{\partial \theta}{\partial Y} dX$ and the average fluid temperature of the cavity defined as $\theta_{av} = \int \theta \, d\overline{V} / \overline{V}$, where $\overline{V}$ is the volume of the cavity that was recommended by Singh and Sharif (2003).

5.3 Numerical Analysis

In this section, the numerical scheme adopted in the present study together with grid refinement test and validity of computational code is discussed briefly.

5.3.1 Method of Solution

The Galerkin weighted residual based finite element scheme is applied in this study to solve the governing equations numerically. Firstly, the problem is defined as a two dimensional enclosure and the solution domain is discretized into finite element meshes, which are composed of non-uniform triangular elements. The coupled equations (5.6) - (5.10) are transformed into a system of integral equations using Galerkin weighted residual technique and then using appropriate boundary conditions the so obtained nonlinear algebraic equations are modified into a set of linear algebraic equations with the help of Newton-Raphson iteration technique. Last of all, these linear equations are solved by means of triangular factorization method.

5.3.2 Grid Size Sensitivity Test

For grid refinement check five different non-uniform grid systems with 2312, 3976,
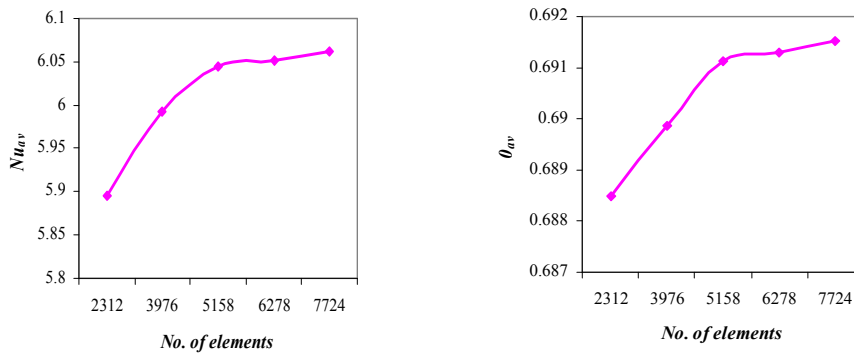
Figure 5.2: Grid test for average Nusselt number and average fluid temperature

5158, 6278 and 7724 number of elements are examined in the present simulation. Fig. 5.2 shows that average Nusselt number at the hot wall and average fluid temperature in the cavity for 5158 elements gives a little difference with the corresponding outcomes for the other denser grids and thus the grid system of 5158 elements is selected for the computation of all cases for optimum results.

5.3.3 Validation of the Numerical Scheme

In order to validate the computational code, the average Nusselt number on the bottom heated wall obtained form the current code and those performed by House et al. (1990) are tabulated in Table 5.1. The comparison was carried out for the Rayleigh number $Ra = 0.0$ and 10^5 and three values of $K = 0.2$, 1.0 and 5.0. House et al. (1990) studied a problem of square vertical cavity of length L with a heat conducting body where the top, bottom walls were insulated and the vertical walls were isothermal and differentially heated. The mean deviations between the Nu_{av} calculated by the present simulations and those of the aforementioned study House et al. (1990) were less than 1% that established the reliability of the present solver.

Table 5.1: Comparison of average Nusselt number with House et al. (1990)

Ra	K	Nu_{av}		Error (%)
		Present study	House et al. (1990)	
0	0.2	0.7082	0.7063	0.19
0	1.0	1.0001	1.0000	0.01
0	5.0	1.4153	1.4125	0.28
10^5	0.2	4.6228	4.6239	0.11
10^5	1.0	4.5041	4.5061	0.20
10^5	5.0	4.3187	4.3249	0.62

5.4 Results and Discussions

In order to investigate the flow behaviors, thermal fields and heat transfer performance affected by the Reynolds number, Prandtl number, Hartmann number,

solid fluid thermal conductivity ratio and diameter of the centered block; a mixed convection problem in a vented enclosure with heat conductive block has been performed numerically. Computations are performed for considered parameters in the range of *Ri* varies from 0.1 to 10 and findings are presented in terms of streamlines, isotherms, average Nusselt number at the hot wall as well as average cavity fluid temperature.

5.4.1 Effect of Reynolds Number

The influence of Reynolds number on the overall flow pattern and heat lines arrangements are depicted in Fig. 5.3. Here the value of *Pr* is chosen as 0.71which corresponds to air. These figures show the streamlines and isotherm contours for various Reynolds number varied from 50 to 500. From Fig. 5.3(*a*) it is observed that at low Reynolds number *Re* = 50, the mainstream occupies the whole domain for *Ri* (= 0.1, 1) whereas a very large counter clockwise vortex is developed confining the centered block for *Ri* = 10. When *Re* = 200 and *Ri* = 0.1, a unicellular vortex is found above the inlet opening and it expands very sharply for the higher values of *Ri*. In the dominant forced convection region a very big sized anticlockwise rotating cell is created and another small clockwise vortex is seen at the right bottom corner for *Re* = 350. Large vortex swells up and small one disappears as *Ri* increases. At *Re* = 500 a minor change is followed in flow patterns with the comparison of *Re* = 350 for all *Ri*. The corresponding isotherms for different Reynolds numbers are displayed in Fig. 5.3(*b*). For the lower value of *Re* = 50 the heat lines are nonlinear that stretched the whole cavity and a small variation is noticed for different values of Richardson numbers. The isotherms are packed at the inlet and form a boundary layer in the vicinity of bottom hot wall of the cavity at *Re* = 200. As the Reynolds number increases (*Re* = 350, 500) the isothermal lines move away to the right wall and high isotherms are crowded at the heated surface of the cavity. In the case of two upper values of *Ri* (= 1, 10), a tendency is observable for the low temperature heat lines is coming back towards the left wall of the enclosure.

Fig. 5.4 illustrates average Nusselt number at the heated wall and bulk average fluid temperature in the cavity for different values of *Re*. It is seen that for low Reynolds number heat transfer rate at the bottom wall is about stationary with respect to *Ri* and
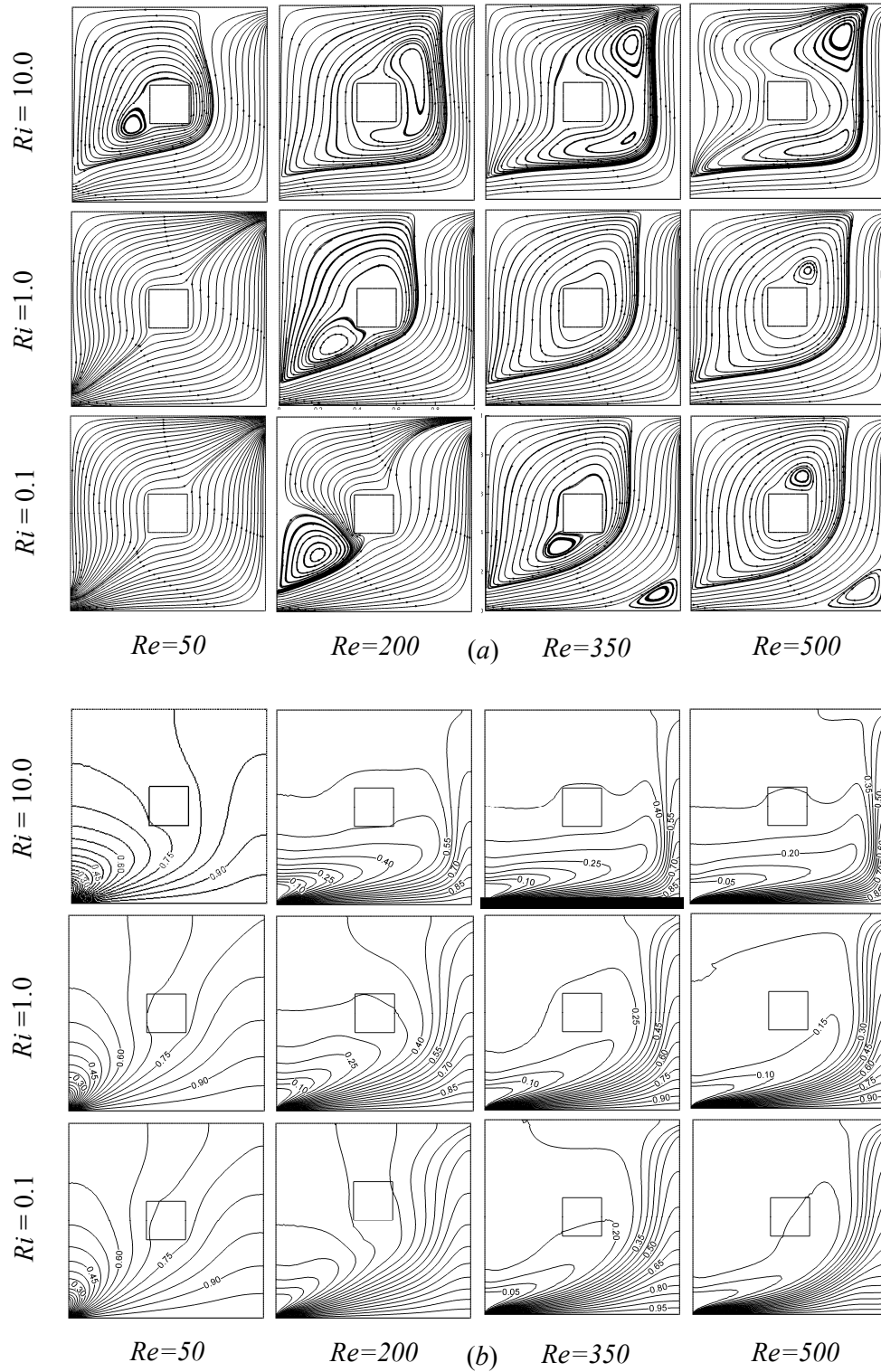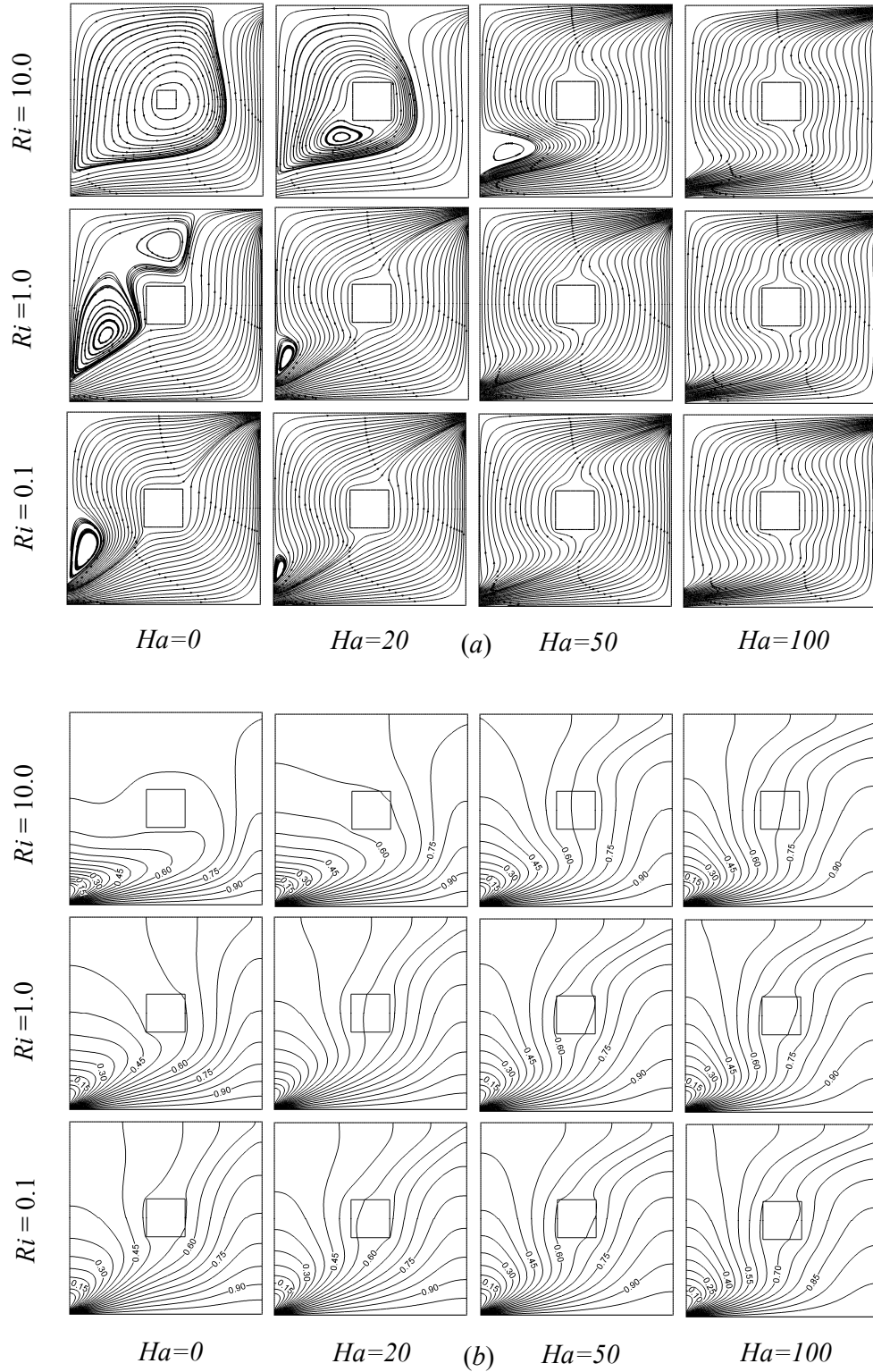
Figure 5.3: (a) Streamlines and (b) Isotherms at different Reynolds number and various values of Richardson number *Ri*, while *Ha* = 10, *K* = 5, *Pr* = 0.71, *Q* = 1 and *D* = 0.2
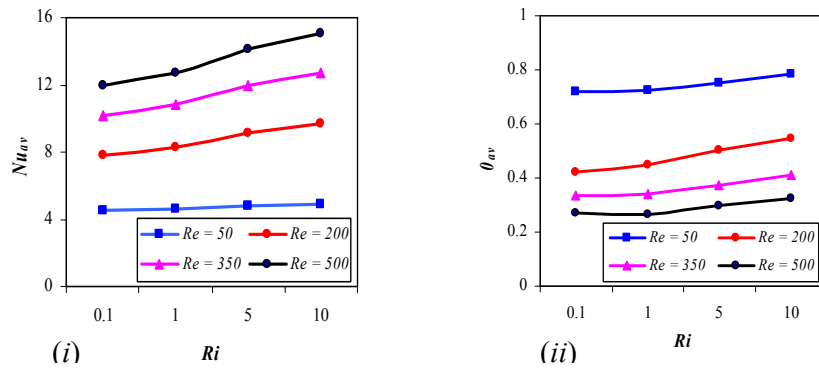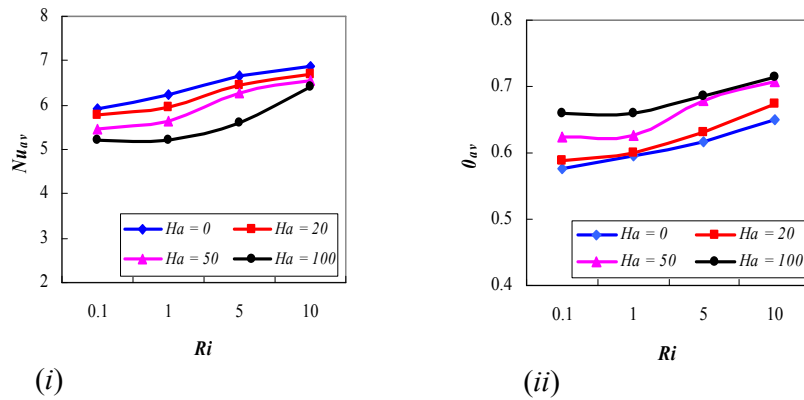
Figure 5.4: Effect of Reynolds number on (*i*) average Nusselt number, (*ii*) average fluid temperature, while *Ha* = 10, *Pr* = 0.71, *D* = 0.2, *Q* = 1 and *K* = 5.

Table 5.2: Variation of average Nusselt number with Reynolds number

Ri	Nu_{av}			
	Re = 50	*Re* = 200	*Re* = 350	*Re* = 500
0.1	4.553039	7.851059	10.16745	11.93826
1.0	4.610437	8.326203	10.79475	12.69623
2.0	4.654871	8.564213	11.02432	12.98754
3.0	4.685423	8.754621	11.35487	13.21458
4.0	4.712583	8.956471	11.58742	13.84573
5.0	4.778768	9.155231	11.97403	14.11736
6.0	4.798564	9.354612	12.03457	14.32134
7.0	4.821346	9.48761	12.31257	14.58451
8.0	4.85423	9.587423	12.54217	14.69752
9.0	4.875243	9.63241	12.71045	14.89866
10.0	4.921946	9.672471	12.76067	15.07491

maximum heat transfer is found for the largest value of *Re* which is reasonable. A reverse effect is followed for the case of average temperature of the fluid inside the cavity.

Table 5.2 shows the variation of average Nusselt number at the hot bottom surface with Reynolds number for the values of *Ri* = 0.1 to 10. Comparatively higher heat transfer rate is found for the upper value of *Re* and for larger values of *Ri*.

5.4.2 Effect of Prandtl Number

The effect of Prandtl number in the range 0.071 - 7.1 on flow and thermal fields inside a vented enclosure with heat conductive block placed at the center are presented in Fig. 5.5; the other parameters are kept fixed at $Re = 100$ and $Ha = 10$. The flow characteristics that are represented by streamlines for four different values of Prandtl number are shown in Fig. 5.5(a). At $Ri = 0.1$ and for all selected values of Pr it is seen that a recirculation cell is formed just above the inflow opening and open lines are identical. There is no significant change except extended vortex size is observed for the different Prandtl numbers in the case of pure mixed convection $Ri = 1$. But when $Ri = 10$ a dramatically variation in flow patterns is noticed for the studied Prandtl numbers. Major streams minimize towards the right-bottom walls and consequently size of the various shaped vortices expand very swiftly and surrounded the inner block.

In order to examine the mode of temperature distribution heat line contours are plotted in Fig. 5.5(b). At $Pr = 0.071$ a small number of high isotherms only are observed for all the considered values of Ri. On the other hand, for $Ri = 0.1$, 1, and 10 temperature distributions are followed almost the whole domain with thermal boundary layer at the bottom wall when $Pr = 1$. As Prandtl number increases a noteworthy change occurs in the isotherms pattern. For larger values of Pr ($= 3, 7.1$) hot wall is jammed by heat lines and gradually these became isolate from the heat conducting solid in the case of all chosen Richardson numbers.

Lastly average heat transfer rate is presented in Fig. 5.6 along the heated wall at different Prandtl numbers. Heat transfer rate is highest and it slowly rises up with increasing of Richardson number when $Pr = 7.1$. Also it follows that smallest value of Pr gives minimum heat transfer which is independent of Ri. On the other hand, average temperature of fluid inside the enclosure decreases as Prandtl number increases.

A numerical data is presented in Table 5.3 for showing the effect of Prandtl number on average Nusselt number at the heated surface of the square enclosure. It is observed that heat transfer rate increases very slowly as Ri increases whereas it increases rapidly with the upper values of Pr.
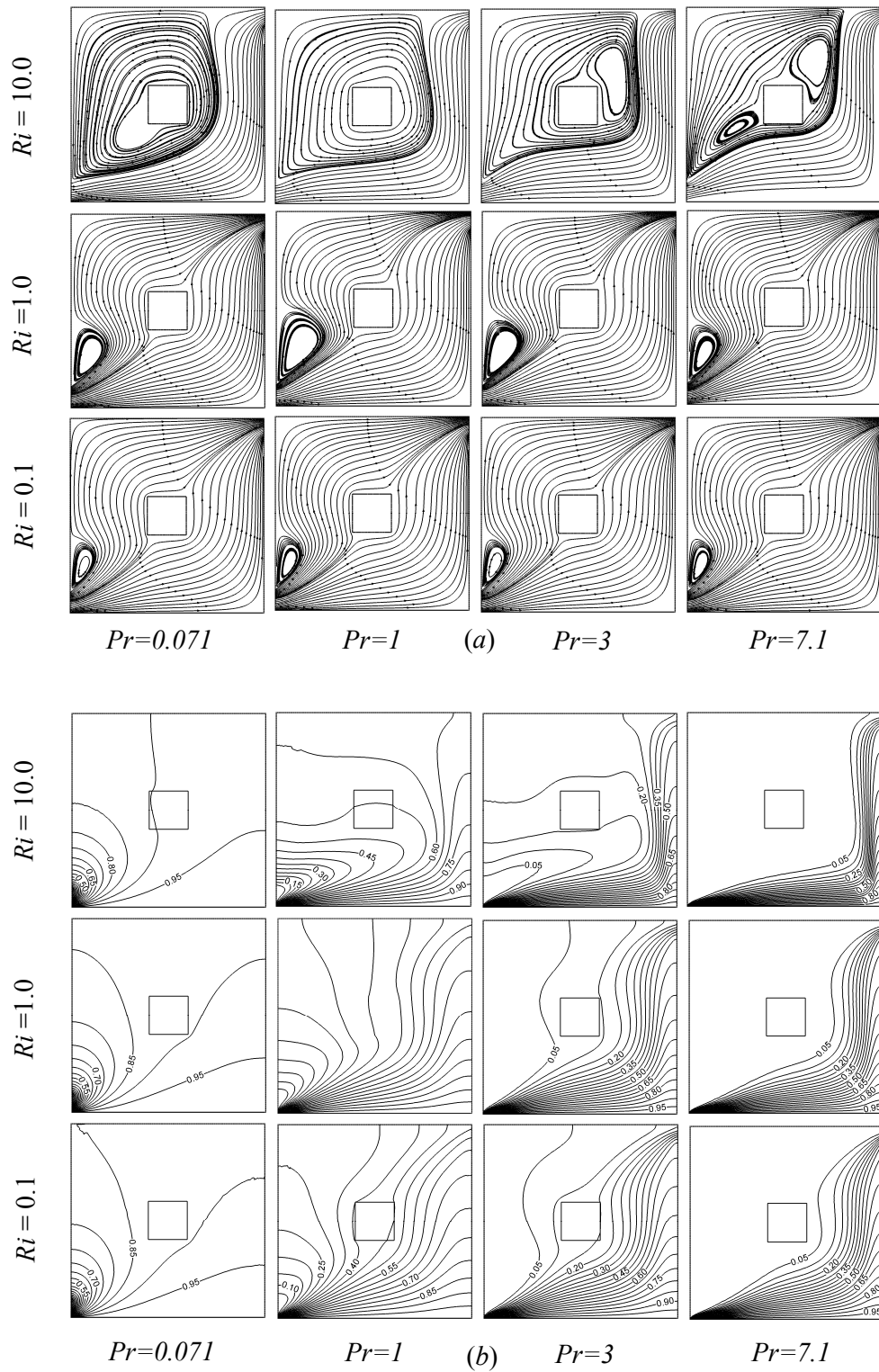
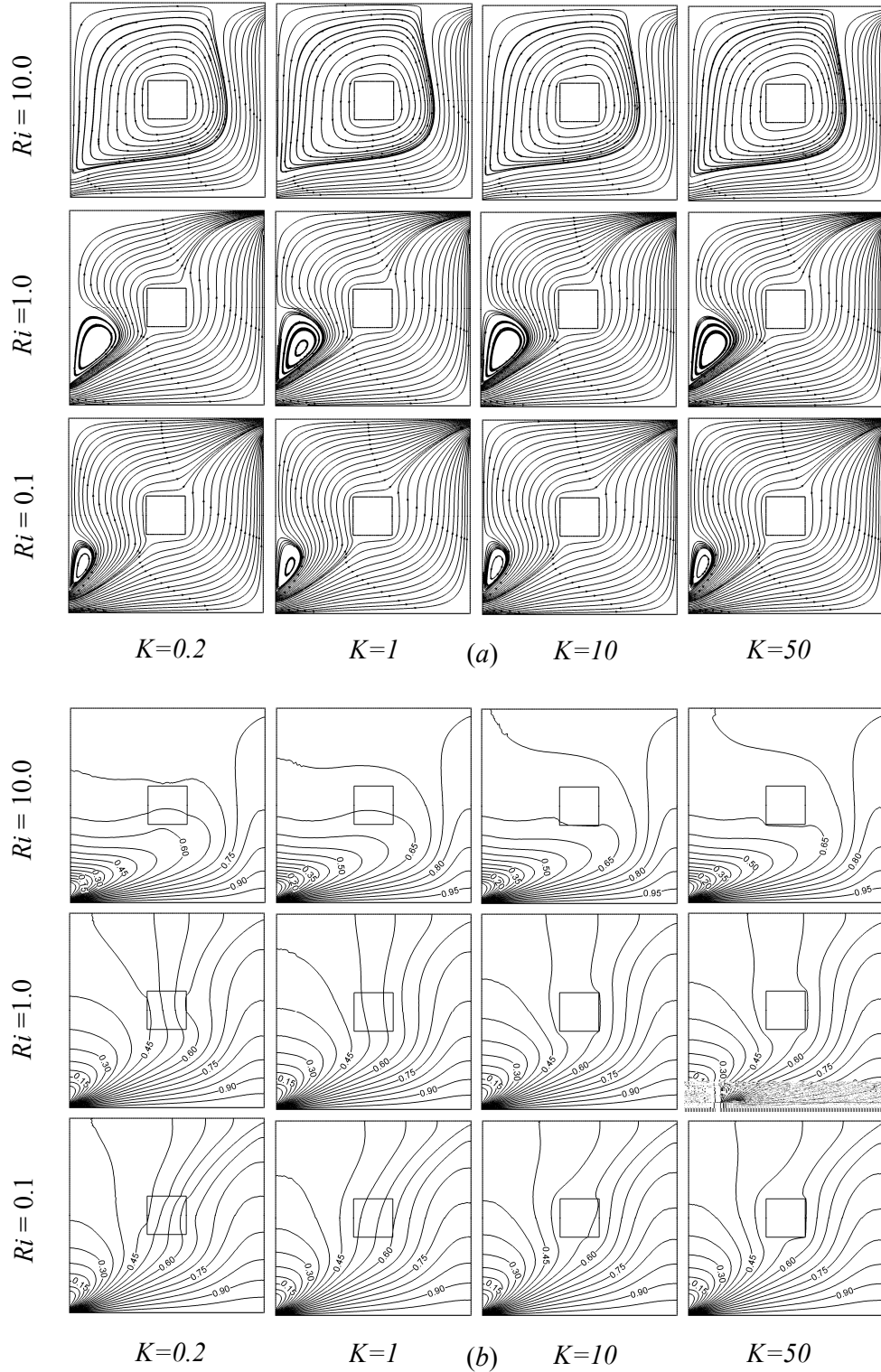**Figure 5.5:** (*a*) Streamlines and (*b*) Isotherms at different Prandtl number and various values of Richardson number *Ri*, while *Re* = 100, *Ha* = 10, *K* = 5, *Q* = 1 and *D* = 0.2.
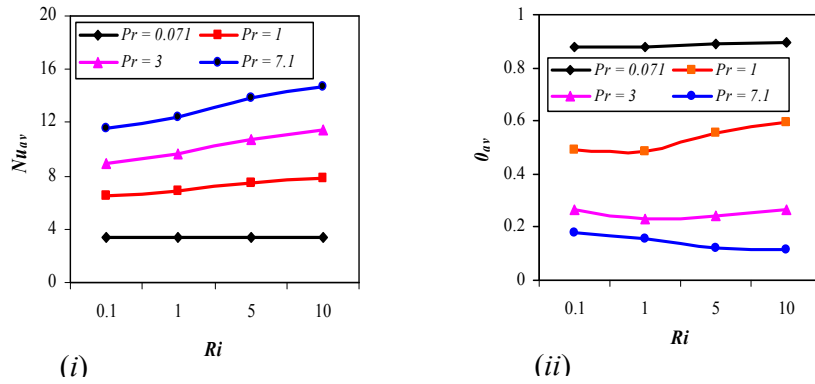
Figure 5.6: Effect of Prandtl number on (*i*) average Nusselt number, (*ii*) average fluid temperature, while $Re = 100$, $Ha = 10$, $D = 0.2$, $Q = 1$ and $K = 5$.

Table 5.3: Variation of average Nusselt number with Prandtl number

Ri	Nu_{av}			
	$Pr = 0.071$	$Pr = 1$	$Pr = 3$	$Pr = 7.1$
0.1	3.403973	6.469222	8.975492	11.60556
1.0	3.406295	6.861754	9.617635	12.36946
2.0	3.408124	6.921346	9.721458	12.57896
3.0	3.409854	7.125478	9.985473	12.78456
4.0	3.410456	7.31245	10.24587	13.01246
5.0	3.415927	7.481586	10.78206	13.88605
6.0	3.416547	7.598647	11.02436	13.99854
7.0	3.417864	7.654782	11.12458	14.02316
8.0	3.419854	7.784572	11.23547	14.33215
9.0	3.42214	7.801246	11.35648	14.53217
10.0	3.432531	7.838668	11.45531	14.73343

5.4.3 Effect of Hartmann Number

Fig. 5.7(*a*) illustrates the effect of Hartmann number in terms of streamlines. For the dominant forced convection area , at $Ha = 0$ it is followed that the fluid flow characterizes by the major streams through the cavity and a small vortex is found in the lower left side of the cavity. While the Hartmann number increases by $Ha = 20,$ the size of the vortex reduces and as a result the open lines expands towards the left

Figure 5.7: (*a*) Streamlines and (*b*) Isotherms at different Hartmann number and various values of Richardson number *Ri*, while *Re* = 100, *Pr* = 0.71, *K* = 5, *Q* = 1 and *D* = 0.2.
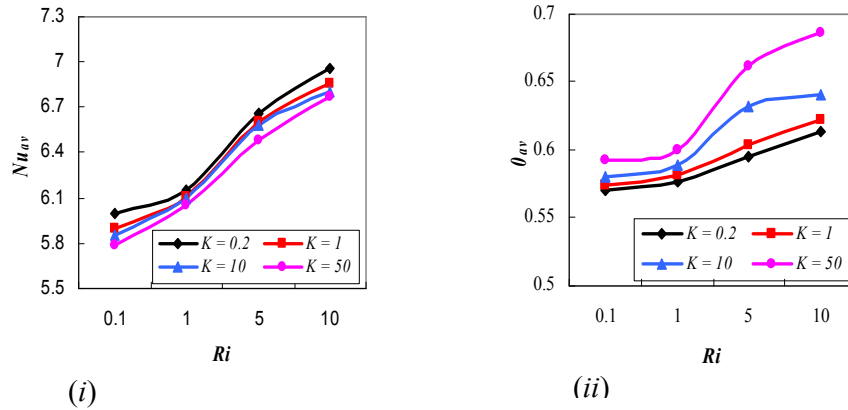
(*i*)   (*ii*)

Figure 5.8: Effect of Hartmann number on (*i*) average Nusselt number, (*ii*) average fluid temperature, while $Re = 100$, $Pr = 0.71$, $D = 0.2$, $Q = 1$ and $K = 5$.

Table 5.4: Variation of average Nusselt number with Hartmann number

Ri	Nu_{av}			
	$Ha = 0$	$Ha = 20$	$Ha = 50$	$Ha = 100$
0.1	6.189092	5.791037	5.663728	5.595915
1.0	6.235082	5.958862	5.728370	5.617554
2.0	6.35421	6.132456	5.801248	5.34216
3.0	6.45782	6.254781	5.987321	5.468721
4.0	6.521367	6.34127	6.13248	5.54213
5.0	6.651435	6.455524	6.280295	5.612085
6.0	6.698741	6.501248	6.31245	5.789214
7.0	6.724135	6.552413	6.42157	5.98752
8.0	6.784592	6.602145	6.485721	6.12345
9.0	6.832142	6.654217	6.502143	6.3241
10.0	6.870787	6.680713	6.538633	6.425373

bottom side of the cavity. On the other hand, the rotating cell disappears and streamlines are nearly similar for the rest two values of Hartmann number $Ha = 50$ and $Ha = 100$. In the domain $Ri = 1$, a large bi-cellular re-circulation cell is created ($Ha = 0$) that spreads from the lower left side to the upper side of the cavity. At $Ha =$

20, the vortex increases slightly regarding the same case of $Ri = 0.1$. In addition, there is no significant change in the patterns of fluid contours for the higher values of Hartmann number ($Ha = 50, 100$). For the convective regime $Ri = 10$, in the absence of magnetic force ($Ha = 0$) the vortex expands drastically and it confines the centered block. This indicates the enhancement of the flow strength of the vortex. At $Ha = 20$, the vortex shrinks from the right side and another vortex is seen below the obstacle. The flow strength of the rotating cell reduces sharply and the open lines swell up with the rising values of Ha and as a consequence the vortex moves out while $Ha = 100$.

The corresponding isotherms are displayed in Fig. 5.7(b). For the lower Hartmann number $Ha = 0$, the heat lines are distributed through all over the cavity and isotherms are packed at the opening in the domain $Ri = 0.1$. Also a thermal boundary layer is formed in the vicinity of the bottom heated surface of the cavity. A minor change is noticed in temperature distribution inside the cavity for the case of upper values of $Ha = 20, 50, 100$. While $Ri = 1$, the isothermal lines are slight different for $Ha = 0, 20$ but these are identical for the two larger values of Ha (= 50. 100). Lastly, in the dominant free convective regime $Ri = 10$, a markable change is observed in the case of $Ha = 0$. Comparatively low temperatured heat lines reflect towards the left wall of the cavity. As Ha increases the non-linearity of the isotherms increases and a little variation is found among the three consecutive values of $Ha = 20, 50, 100$.

Fig. 5.8 depicts the heat transfer performance of the enclosure for different values of Hartmann number that are presented in terms of average Nusselt number Nu_{av} at hot wall and the average bulk temperature of fluid θ_{av} inside the enclosure. It is observed from Fig. 5.8(i) that heat transfer rate decreases as the value of Ha increases within the range of $0.1 \leq Ri \leq 10$. On the other hand, an opposite result is found for the average fluid temperature in the cavity from Fig. 5.8(ii) which reveals that heat transfer rate enhances as the value of Ha increases.

Table 5.4 gives the variation of average Nusselt number with different Hartmann number and it is found that rate of heat transfer decreases with the increasing of Ha but it increases as Ri increase.

5.4.4 Effect of Solid Fluid Thermal Conductivity Ratio

Fig. 5.9(a) shows the streamlines for the considered four values of thermal conductivity ratio in the three convective regimes of Richardson number. In the convective domain $Ri = 0.1$, for $K = 0.2$ it is noticed that the open lines stretched from the inlet to the exit inside the cavity and a small vortex is created at the top of the inlet. This is happened as the fresh and colder fluids entering the cavity cannot mix immediately with the hot fluids of the cavity. For the other three higher values of K, there is no significant dissimilarity in the streamline patterns. While $Ri = 1$, the vortex size increases and the major stream squeezes from the left-top corner at $K = 0.2$. A very minor variation can be followed in the streamlines for the thermal conductivity ratio $K = 1$, 10 and 50. Interestingly, for all the chosen values of K a noteworthy change is occurred in streamlines where the free convection dominates the forced convection ($Ri = 10$). In these cases, the vortex expands very sharply that captures the centered heat conducting block and consequently open lines suppress towards the bottom right wall of the cavity. This is due to the supremacy of the natural convection.

The corresponding temperature distributions are depicted in Fig. 5.9(b). The isotherms are found to be scattered through the whole cavity in the two convective regimes of Richardson number namely $Ri = 0.1$, 1 for the considered values of thermal conductivity ratio $K = 0.2$, 1, 10 and 50. In close observation it can be noted that there exists a little disparity in temperature distribution inside the cavity as K varies from 0.2 to 50. In the region $Ri = 10$ where the dominant natural convection is considered, heat lines show an observable variation regarding that of $Ri = 0.1$, 1. With a variety in the midst of different values of K, a large number of isothermal lines are seen to be folded that returns the left wall of the cavity.

Average Nusselt number Nu_{av} at the bottom heated surface and average fluid temperature θ_{av} in the cavity are depicted in Fig. 5.10 for showing the effect of thermal conductivity ratio K at solid fluid interface on heat transfer mode. From this it can be followed that Nu_{av} enhances sharply as Ri increases with decreasing value of K. Therefore highest heat transfer is recorded for the smallest value of K. In addition, θ_{av} increases with the higher values of K and minimum average fluid temperature inside the cavity is found when $K = 0.2$.

Figure 5.9: (*a*) Streamlines and (*b*) Isotherms at different thermal conductivity ratio and various values of Richardson number *Ri* while, *Re* = 100, *Pr* = 0.71, *Ha* = 10, *Q* = 1 and *D* = 0.2

(*i*)　　　　　　　　　　　　　(*ii*)

Figure 5.10: Effect of thermal conductivity ratio on (*i*) average Nusselt number, (*ii*) average fluid temperature, while $Re = 100$, $Pr = 0.71$, $D = 0.2$, $Q = 1$ and $Ha = 10$.

Table 5.5: Variation of average Nusselt number with thermal conductivity ratio

Ri	Nu_{av}			
	$K = 0.2$	$K = 1$	$K = 10$	$K = 50$
0.1	5.996055	5.894875	5.852833	5.792311
1.0	6.15619	6.106777	6.096624	6.052123
2.0	6.34578	6.301245	6.297541	6.201245
3.0	6.45476	6.410213	6.402134	6.39875
4.0	6.54217	6.51247	6.49857	6.42157
5.0	6.654277	6.60185	6.583809	6.482992
6.0	6.698547	6.68542	6.601248	6.542178
7.0	6.721453	6.70102	6.684572	6.621345
8.0	6.852143	6.801243	6.754128	6.675482
9.0	6.901243	6.83214	6.785496	6.702143
10.0	6.959192	6.861843	6.804503	6.764881

Deviation of average Nusselt number for different thermal conductivity ratio with respect to Ri is tabulated in Table 5.5. From the table it is noticed that Nu_{av} decreases slightly as K increases and it gives higher values with the increasing of Richardson number.

5.4.5 Effect of Block Diameter

The streamline and isotherm patterns due to the variation for solid block diameter D are presented in Fig. 5.11. It is seen from Fig. 5.11(a), when $Ri = 0.1$ the open lines are found throughout the cavity and a small recirculation cell is developed at the top of the inlet port for $D = 0.1$. As the Richardson number increases, the intensity of flow circulation within the cavity enhanced owing to the increase in buoyancy effect. For the largest value of Ri it can easily be noticed that the vortex swells up drastically confining the centered body so that the open streams are suppressed in the lower-right corner of the cavity which is very reasonable. The second column of Fig. 5.11(a) shows how the behavior of the flow fields are affected under the influence of block dimension $D = 0.3$ in the range of Richardson number $0.1 \leq Ri \leq 10$. At $Ri = 0.1$ the fluid streams are nearly identical with the same case for $D = 0.1$. On the other hand, in mixed convection area ($Ri = 1$) it is followed that the bi-cellular vortex reduces to unicellular and relatively it becomes very small and so main streams spread out at the left side of the block. There is no significant change in flow characteristics for $Ri = 10$ regarding to $D = 0.1$. The effects of the internal block dimension $D = 0.5$ at three convective regimes of Ri ($= 0.1, 1, 10$) on the streamline patterns are displayed in third column of Fig. 5.11(a). At $Ri = 0.1$ and $Ri = 1$, a very small eddy is created at the left side of the cavity situated above the injection port and the solid body is fully surrounded with major streams. For high value of Ri, where free convection dominates a large counter clockwise vortex is appeared that confines the obstacle. In this case open lines are seen only the bottom and right side of the cavity. Last column of Fig. 5.11(a) depicts the streamlines for block size $D = 0.7$ at three selected values of Ri. From this figure it can be reported that as the value of D increases the vortex becomes smaller and accordingly it disappears at $D = 0.7$ for all values of Ri. This is the reason that for larger values of D space availability in the cavity reduces. Further, streamlines are similar in the range of $0.1 \leq Ri \leq 10$ and these are found in two parts; one is bottom-right sided while the other is left-top sided of the cavity.

In addition, the first column of Fig. 5.11(b) shows that for the dominant forced convection and mixed convection area the heat lines patterns become scatter except
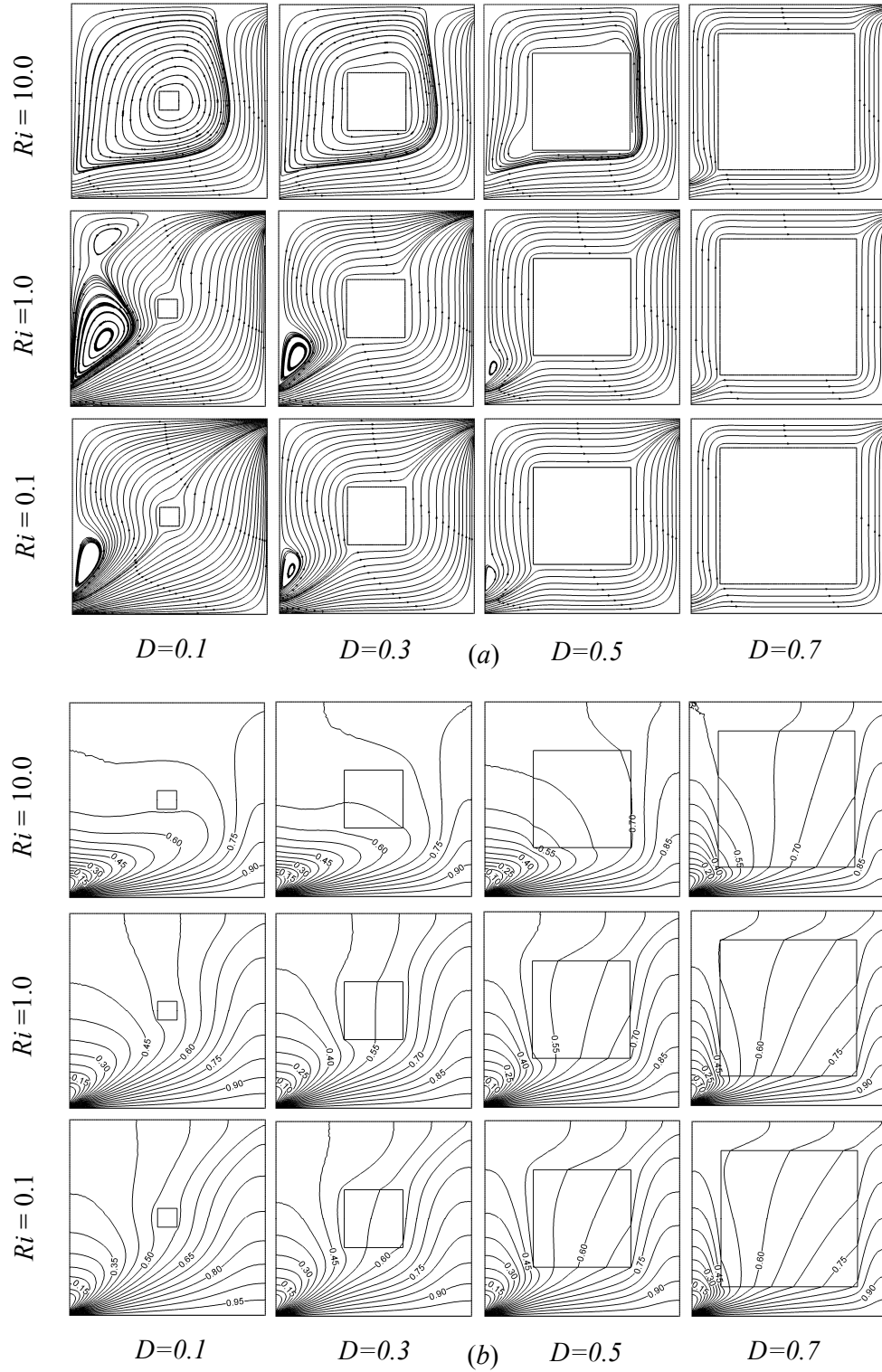
Figure 5.11: (*a*) Streamlines and (*b*) Isotherms at different block diameter and various values of Richardson number *Ri*, while *Re* = 100, *Pr* = 0.71, *Ha* = 10, *Q* = 1 and *K* = 5

(*i*)   (*ii*)
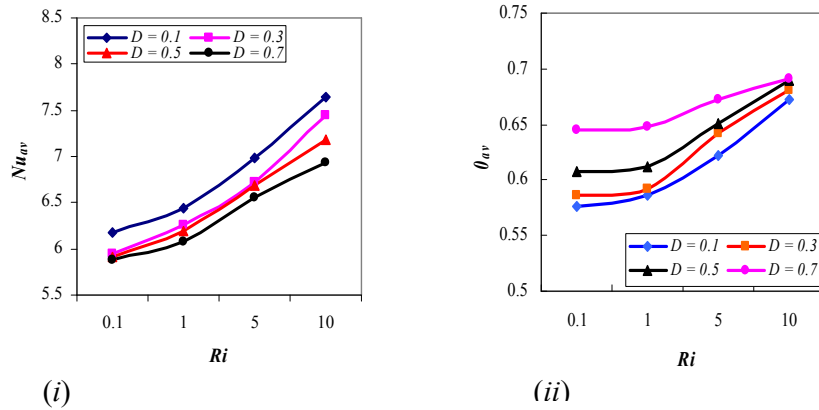
Figure 5.12: Effect of block diameter on (*i*) average Nusselt number, (*ii*) average fluid temperature, while $Re = 100$, $Pr = 0.71$, $K = 5$, $Q = 1$ and $Ha = 10$.

Table 5.6: Variation of average Nusselt number with block diameter

Ri	Nu_{av}			
	$D = 0.1$	$D = 0.3$	$D = 0.5$	$D = 0.7$
0.1	6.168909	5.938528	5.918809	5.878331
1.0	6.446465	6.255076	6.188468	6.075355
2.0	6.592357	6.370531	6.274562	6.184572
3.0	6.704987	6.487892	6.381245	6.294578
4.0	6.818792	6.614246	6.540872	6.421573
5.0	6.991182	6.726170	6.684877	6.550595
6.0	7.1071246	6.870453	6.792456	6.685782
7.0	7.221246	7.022145	6.861247	6.771245
8.0	7.420241	7.191472	6.971234	6.814893
9.0	7.537841	7.314712	7.082145	6.881243
10.0	7.636104	7.446213	7.184350	6.929178

in the vicinity of the bottom hot surface for $D = 0.1$. But as the natural convection becomes dominant ($Ri = 10$), isotherms are found to be folded below the inner body. Also for all the considered values of Richardson number the high-isothermal lines are more concentrated near the hot wall and the temperature distribution is more uniform in the lower right parts of the cavity. The second column of Fig. 5.11(*b*) represents

the temperature distribution for $D = 0.3$. Close examination of the temperature field for the working domain it reveals that except a minor difference the same is reflected in heat lines as was observed for $D = 0.1$. The thermal fields characteristics inside the cavity for $D = 0.5$ are displayed in the third column of Fig. 5.11(b). For the whole domain of Ri (= 0.1-10) the isotherms are clustered close to the bottom wall specially at the inlet openings, which indicates the existence of high temperature gradients in the vertical direction. Besides, thermal boundary layer is created near the hot wall and it increases in thickness slowly as Ri gets higher value. Finally from the last column it is noted that for all the considered values of Richardson number heat lines are distributed about uniformly over the whole enclosure and these are almost similar relative to Ri for the case of $D = 0.7$.

In order to evaluate how the center lined solid block of the cavity affects the average heat transfer along the hot wall; average Nusselt number is plotted as a function of Richardson number in Fig. 5.12(i) for different block diameter D. This figure reveals that average Nusselt number increases rapidly with the increase of Ri. Highest heat transfer is found at the lowest value of $D = 0.1$ and it reduces as the value of D increases. A closer examination of Fig. 5.12(i) shows that there is a slight variation in average Nusselt number for the two consecutive values of D (= 0.3 and 0.5). On the other hand, Fig. 5.12(ii) presents the average temperature of the fluid (θ_{av}) inside the enclosure. The θ_{av} is almost invariant at low Ri ($0.1 \leq Ri \leq 1$) whereas it increases with higher Ri ($1 \leq Ri \leq 10$) for all of the chosen values of D. Another important observation is that minimum cavity fluid temperature is found for the smallest size of the block.

In addition Table 5.6 gives an idea about the effect of centered heat conducting block dimension D in case of some selected mixed convection parameter on the average Nusselt number at the hot surface of the cavity. It is clear that as D increases Nu_{av} decreases for fixed Ri. On the other hand for a stationary value of D, Nu_{av} increases with the rising value of Ri.

5.5 Concluding Remarks

A two-dimensional numerical study is carried out to explain the flow patterns and heat transfer phenomena of an electrically conducting fluid subjected to externally imposed magnetic field.

— The results show that there is a considerable enhancement in heat transfer from the heated wall due to higher values of Reynolds number.

— Prandtl number effects in flow behaviors are more significant in free convection dominated region than other two regimes. Heat transfer at the bottom heated surface increases with increasing of Prandtl number.

— Optimum cooling that is lowest cavity fluid temperature can be obtained in absence of magnetic field parameter ($Ha = 0$).

— A slight dissimilarity is found in flow and thermal fields for the variation of thermal conductivity ratio that is flow and thermal fields are not much affected by the parameter K. Highest heat transfer rate is found in case of lowest value of $K = 0.2$.

— The flow visualization results show that in the dominant natural convection domain comparatively larger vortex is developed for the smaller block diameter D. The heat transfer at heated wall increases gradually as the value of D reduces with all the Richardson numbers. Last of all, it can be summarized that maximum cooling effectiveness is achieved if the dimension of the centered block is minimized.

Chapter 6

Effect of an Adiabatic Solid Body on Mixed Convection Flow in a Square Enclosure

Interest in mixed convection fluid flow and heat transfer in ventilated systems has been motivated by a broad range of applications, including thermal design of buildings, air conditioning and recently the cooling of electronic equipments. The flow and heat transfer characteristics of combined free and forced convection in a two-dimensional square enclosure with internal thermally isolated solid body is studied in the present chapter. A finite element method is used for solving the governing equations. The involved parameters are Reynolds number, Prandtl number, Hartmann number and diameter of the solid body.

Hence, the objective of the present study is to investigate streamlines and heat lines for the mixed convection flow and heat transfer in such a system, idealized as a square enclosure filled with a centered adiabatic block.

The current chapter is divided in five sections, of which section 6.1 covers the physical model of the considered geometry. Section 6.2 presents the mathematical formulation of the problem. The method of solution is deliberated briefly in section 6.3. Section 6.4 exposes the findings of this research elaborately and lastly the summary of this chapter is given in section 6.5.

6.1 Physical Configuration

A square enclosure containing incompressible fluid with a centered insulated obstacle is shown in the Fig. 6.1. The cavity dimensions are defined by L for each side. The bottom wall is heated while the remaining walls are considered perfectly adiabatic. The entrance and outlet of the enclosure are positioned at the bottom of the left wall and at the top of the right wall respectively. A magnetic field of strength B_0 is assumed to be applied transversely to the opposite of flow direction. The size of each opening is equal to one-tenth of the cavity length. The inflow state is (u_i, T_i) while zero diffusion flux is assumed for outflow.
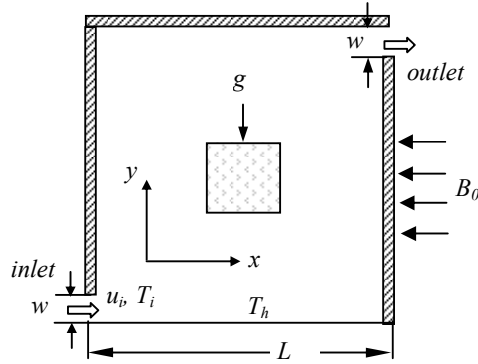
Figure 6.1: Schematic of the problem

6.2 Mathematical Modeling

Mathematical model for the present work is designed by the following some steps.

6.2.1 Governing Equations

The fluid inside the square enclosure is assumed as laminar, incompressible and steady-state. Two-dimensional mass, momentum and energy conservation equations are considered as the governing equations in the present work and airflow is assumed to obey the Boussinesq approximation with constant physical properties. Taking into account the above mentioned assumptions, the dimensionless governing equations are described as follows:

Continuity Equation

$$\frac{\partial U}{\partial X} + \frac{\partial V}{\partial Y} = 0 \tag{6.5}$$

Momentum Equations

$$U\frac{\partial U}{\partial X} + V\frac{\partial U}{\partial Y} = -\frac{\partial P}{\partial X} + \frac{1}{Re}\left(\frac{\partial^2 U}{\partial X^2} + \frac{\partial^2 U}{\partial Y^2}\right) \tag{6.6}$$

$$U\frac{\partial V}{\partial X} + V\frac{\partial V}{\partial Y} = -\frac{\partial P}{\partial Y} + \frac{1}{Re}\left(\frac{\partial^2 V}{\partial X^2} + \frac{\partial^2 V}{\partial Y^2}\right) + Ri\,\theta - \frac{Ha^2}{Re}V \tag{6.7}$$

Energy Equations

$$U\frac{\partial \theta}{\partial X} + V\frac{\partial \theta}{\partial Y} = \frac{1}{Re\,Pr}\left(\frac{\partial^2 \theta}{\partial X^2} + \frac{\partial^2 \theta}{\partial Y^2}\right) \tag{6.8}$$

Where, the Reynolds number, square of Hartmann number, Prandtl number, Richardson number are defined respectively as

$$Re = u_i L / \upsilon, \ Ha^2 = \sigma B_0^2 L^2 / \mu, \ Pr = v / \alpha, \ Ri = Gr / Re^2$$

6.2.2 Boundary Conditions

The concerning boundary conditions in the dimensionless form are given below:

At the inlet: $U = 1, V = 0, \theta = 0$

At the outlet: convective boundary condition (CBC), $P = 0$

At all solid boundaries: $U = 0, V = 0$

At the heated bottom wall: $\theta = 1$

At the left, right and top walls: $\dfrac{\partial \theta}{\partial N} = 0$

At the surface of the block: $U = 0, V = 0, \dfrac{\partial \theta}{\partial N} = 0$

Where, N is the non-dimensional distances either along X or Y direction acting normal to the surface.

According to Singh and Sharif (2003), the average Nusselt number at the hot wall of the cavity based on the dimensionless quantities may be expressed by

$Nu = -\int_0^1 \dfrac{\partial \theta}{\partial X} dY$ and the average temperature of the fluid in the cavity is defined by

$\theta_{av} = \int \theta \, d\overline{V} / \overline{V}$, where $\overline{V}$ is the cavity volume.

6.3 Numerical Procedure

The procedure of solution that is applied in solving the considered problem is explained here briefly.

6.3.1 Solution Technique

The solution of the governing equations along with boundary conditions are obtained through the Galerkin weighted residual based finite element method. The continuum domain is discretized into finite element meshes, which are consists of non-uniform

triangular elements. The principal conservation of mass, momentum and energy equations are transferred into a system of integral equations by using Galerkin weighted residual method. Gauss quadrature method executes the integration concerning each term of these equations. Boundary conditions are then imposed and the nonlinear equations are transferred into linear algebraic equations with the aid of Newton Raphson method which are finally solved by triangular factorization method.

6.3.2 Grid Size Sensitivity Test

In order to obtain the grid independence solution, a grid refinement study is conducted to select proper grid resolution. Various size of grid having 2024, 3540, 4508, 5554 and 7160 elements are used to determine the average rate of heat transfer at the heated wall of the cavity. The average heat transfer rate at the hot wall with grid elements is revealed in Table 6.1 and Fig. 6.2. As it is seen that there is no significant discrepancy ahead of 5554 elements, all computations are performed using this grid resolution.

Table 6.1: Grid Sensitivity Check at $Re = 100$, $Ri = 1$, $K = 5$, $D = 0.2$ and $Pr = 0.71$

Elements	Nu_{av}	Discrepancy (%)
2024	6.201839	---
3540	6.202839	0.02
4508	6.212839	0.17
5554	6.213839	0.19
7160	6.213939	0.19
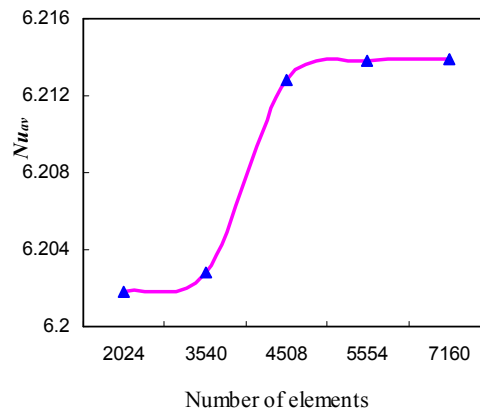
Figure 6.2: Average Nusselt number for different grid elements while $Ri = 1$, $Ha = 10$, $D = 0.2$, $Re = 100$ and $Pr = 0.71$

6.3.3 Validation of the Numerical Scheme

The solution procedure has been validated against the numerical results of Oztop et al. (2009) is shown in the Fig. 6.3. This figure shows that the streamline and isotherm patterns in the present work have excellent agreement with those obtained by Oztop et al. (2009). Thus the numerical code used in this analysis can perform the present problem with logical agreement.

| Present | | | Present | | |
| $D = 0.3$ | $D = 0.4$ | $D = 0.5$ | $D = 0.3$ | $D = 0.4$ | $D = 0.5$ |
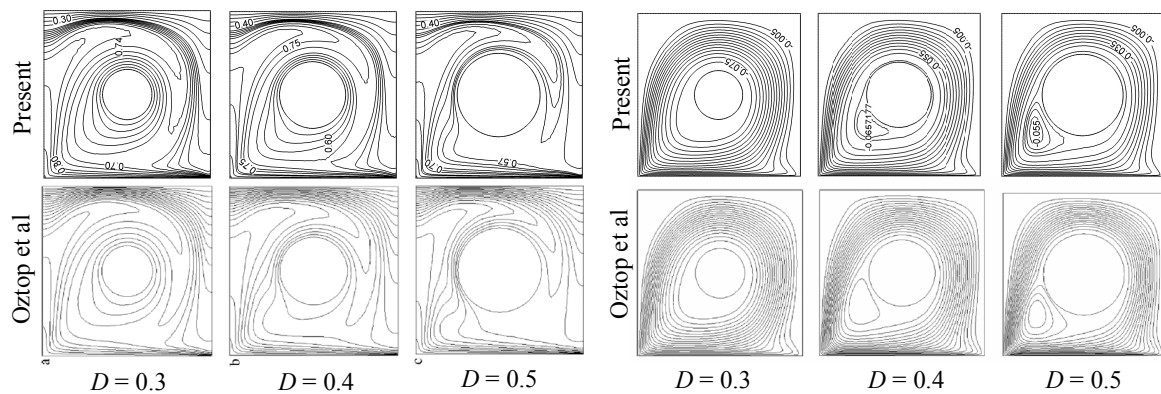
Figure 6.3: Comparison of streamlines (left) and isotherms (right) between the work of Oztop et al. (2009) and present while $Gr = 10^5$, $Pr = 0.71$, $C = 0.5$ and $Re = 1000$

6.4 Results and Discussions

As stated earlier, the overall aim of the current investigation is to explore steady laminar mixed convection flow and heat transfer in a ventilated square enclosure with an inner adiabatic solid body. The MHD mixed convection phenomenon inside a vented enclosure having an adiabatic obstacle is influenced by different controlling parameters such as Re, Pr, Ha, D, and Ri. Analysis of the results is made here for the mentioned parameters varied as $50 \leq Re \leq 500$, $0.071 \leq Pr \leq 7.1$, $0 \leq Ha \leq 100$, $0.1 \leq D \leq 0.7$ and each of the cases the mixed convection parameter Ri is chosen in the range of $0.1 \leq Ri \leq 10$. The outcomes of the present study are discussed here in different steps in order to focus the characteristic of flow field, temperature distribution inside the ventilated cavity as well as heat transfer performance within the cavity in terms of average Nusselt number at the hot surface, average temperature of the fluid inside the enclosure.

6.4.1 Effect of Reynolds Number

A general observation concerning the influence of Reynolds number on streamlines has been demonstrated in Fig. 6.4(a). In the dominant and pure mixed convection region the flow patterns inside the enclosure appear as an onion shape that elongated from the entry to the exit port at Re=50, while a large anti-clockwise rotating cell formed occupying the centered block for the case $Ri = 10$. When $Re = 200$, a vortex is seen near the lower left side of the cavity, consequently open lines shrinks towards the obstacle at $Ri = 0.1$ and this vortex enlarges very fast as Ri increases. For higher values of $Re = 350, 500$ the vortices expand in size and number of small eddies and these are nearly similar in all the ranges of $0.1 \leq Ri \leq 10$. This figure is also indicating that the Reynolds number is an effective parameter on streamlines.

In order to clearly exhibit the thermal field characteristic of the working area for the different Reynolds number the corresponding isotherms are displayed in Fig. 6.4(b). At smaller value of Reynolds number ($Re = 50$) temperature distribution inside the cavity shows non-linearity for all the values of Ri varies as 0.1-10 with a minor change in $Ri = 10$. In the dominant forced convection and pure mixed convection area it can be easily followed that isotherms are shrink gradually in the direction of bottom-right sided wall with the increasing values of Reynolds number from 200 to 500 as the basis of higher Re shows more suppression. In addition, for these three values of Reynolds number the tendency of heat lines minimization is more visible in the case of $Ri = 10$ and some folding isotherms are returned to the left wall.

To show the effect of Reynolds number, Fig. 6.5 records the variations of Nu_{av} and θ_{av} as the function of Ri within the range of 0.1–10 for different values of Re. It is evident from Fig. 6.5(i) that average Nusselt number increases with the mounting values of Reynolds number Re. In addition, heat transfer rate at heated wall is about invariant for lowest value of Re with respect to Ri. Logically, Fig. 6.5(ii) shows a reverse effect in the case of average temperature of cavity fluid.

Table 6.2 gives the variation of average Nusselt number with Reynolds number. As Re increases, Nu_{av} increases with the rising value of Ri.
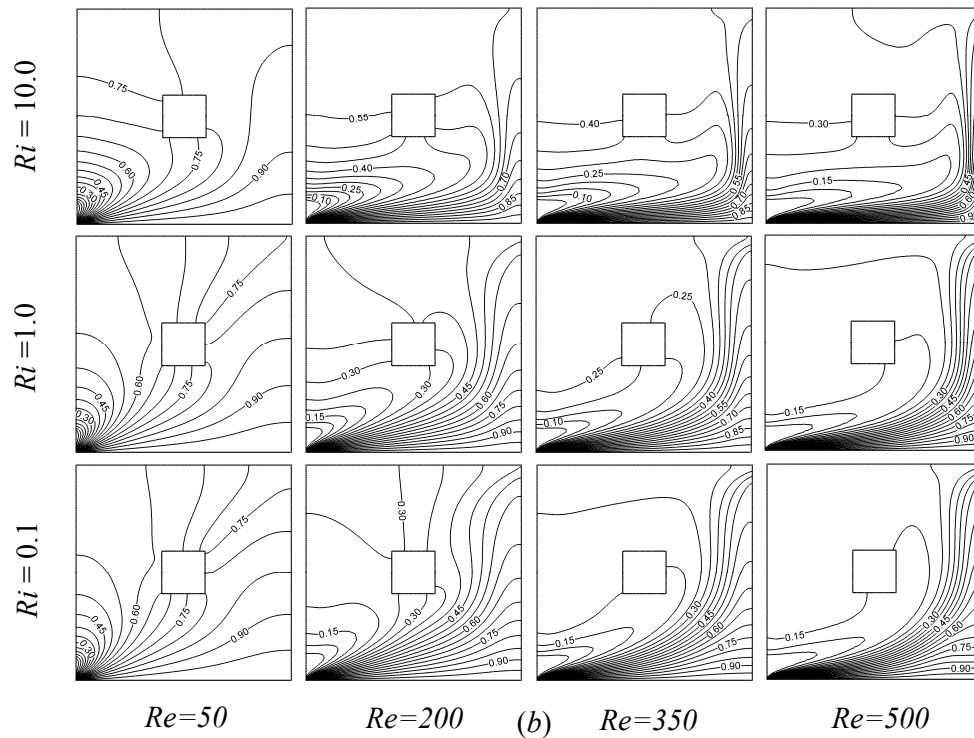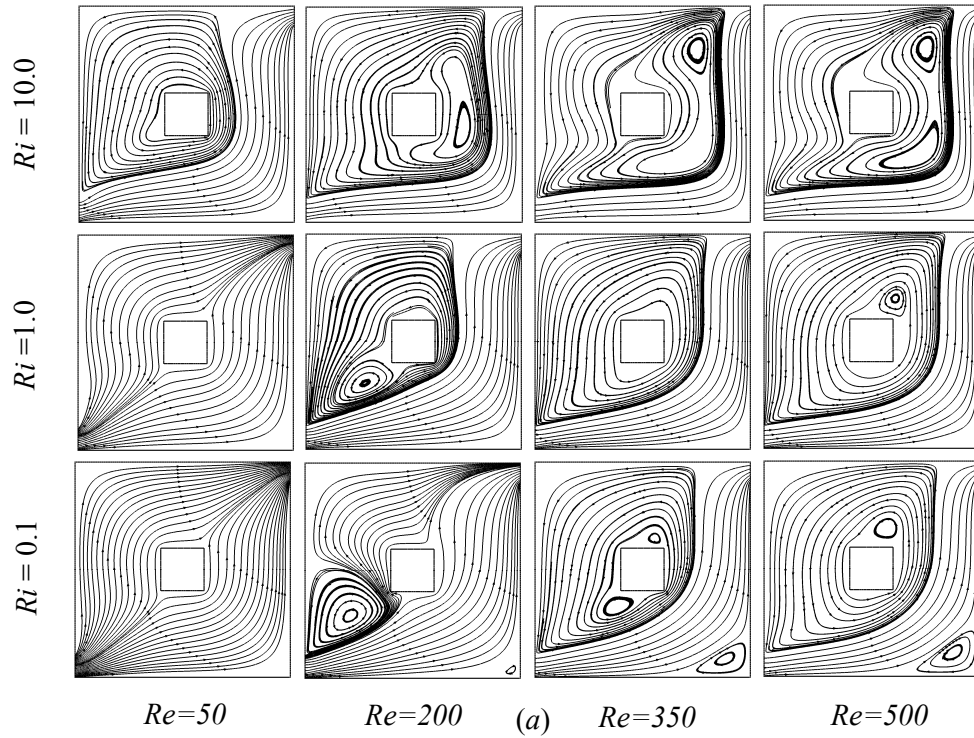
Figure 6.4: (*a*) Streamlines and (*b*) Isotherms at different Reynolds number and various values of Richardson number *Ri*, while *Ha* = 10, *K* = 5, *Pr* = 0.71, *Q* = 1 and *D* = 0.2
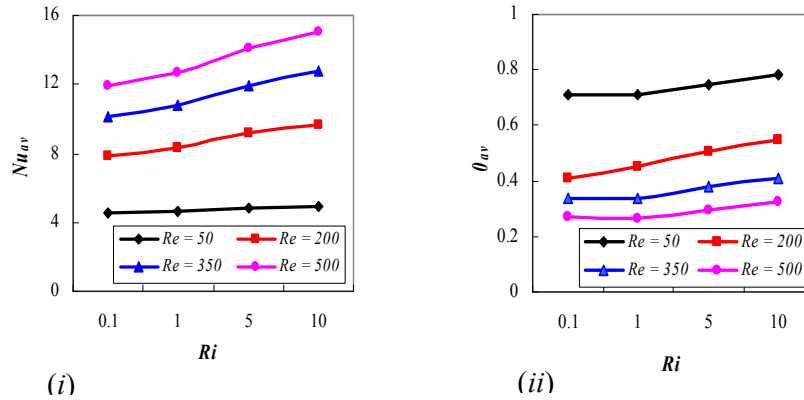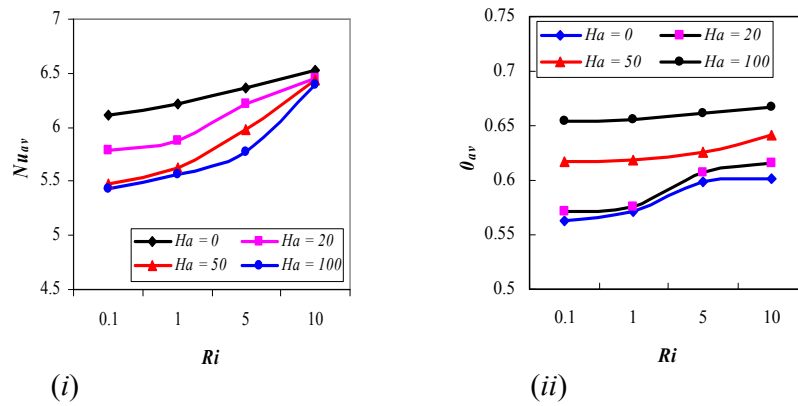
Figure 6.5: Effect of Reynolds number on (*i*) average Nusselt number, (*ii*) average fluid temperature, while $Ha = 10$, $Pr = 0.71$, $D = 0.2$, $Q = 1$ and $K = 5$.

Table 6.2: Variation of average Nusselt number with Reynolds number

Ri	Nu_{av}			
	$Re = 50$	$Re = 200$	$Re = 350$	$Re = 500$
0.1	4.542412	7.839311	10.16379	11.93755
1.0	4.601385	8.320327	10.78297	12.69044
2.0	4.65145	8.56349	10.99854	12.87125
3.0	4.690142	8.75421	11.22436	13.24587
4.0	4.735423	8.98654	11.54287	13.78542
5.0	4.782014	9.143034	11.97443	14.12518
6.0	4.812456	9.321457	12.02136	14.59861
7.0	4.838754	9.46257	12.24587	14.75217
8.0	4.852785	9.52143	12.43568	14.88237
9.0	4.880245	9.60241	12.59857	14.99021
10.0	4.895953	9.671546	12.74836	15.03054

6.4.2 Effect of Prandtl Number

The effect of Prandtl number ($0.071 \leq Pr \leq 7.1$) on flow patterns and temperature distribution in an enclosure vented having an adiabatic block are displayed in Fig. 6.6, where Re and Ha are kept constant at 100 and 10 respectively. The streamlines that are the representative of flow behavior are shown in Fig. 6.6(*a*). From the third row of Fig. 6.6(*a*) it is seen that in the dominant forced convection regime ($Ri = 0.1$)
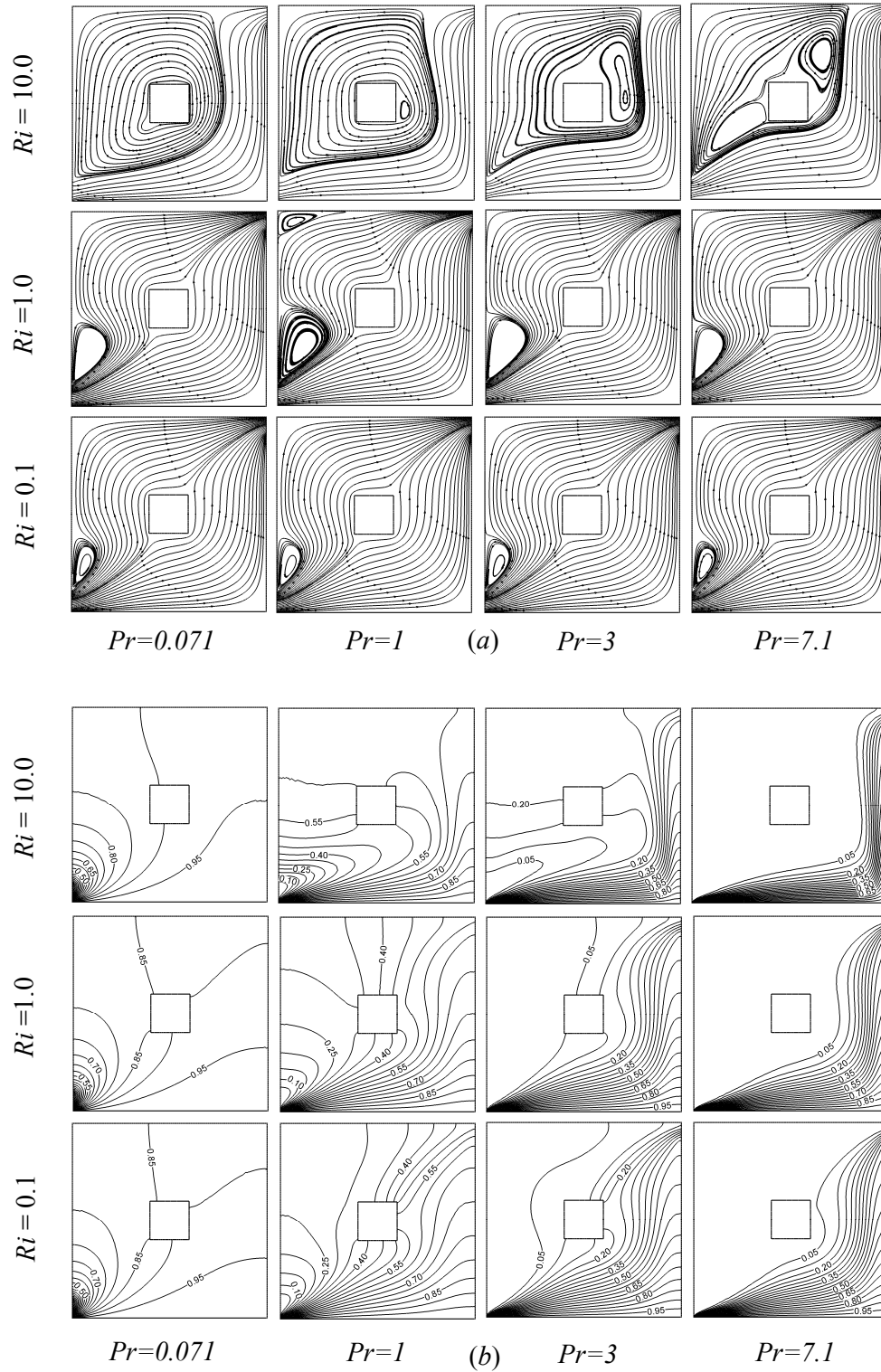
Figure 6.6: (*a*) Streamlines and (*b*) Isotherms at different Prandtl number and various values of Richardson number *Ri*, while *Re* = 100, *Ha* = 10, *K* = 5, *Q* = 1 and *D* = 0.2.

(i) (ii)
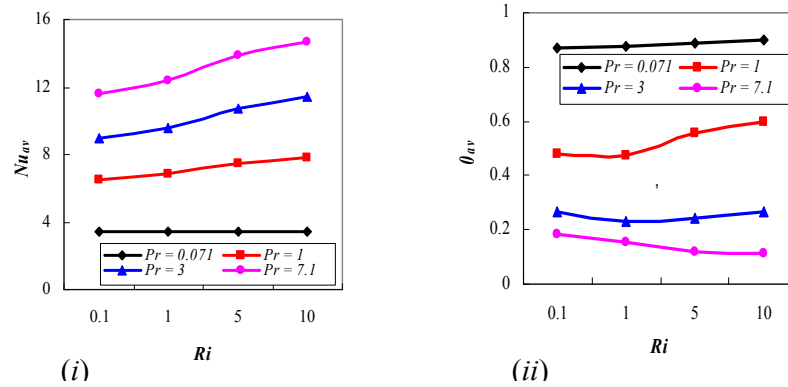
Figure 6.7: Effect of Prandtl number on (*i*) average Nusselt number, (*ii*) average fluid temperature, while $Re = 100$, $Ha = 10$, $D = 0.2$, $Q = 1$ and $K = 5$.

Table 6.3: Variation of average Nusselt number with Prandtl number

Ri	Nu_{av}			
	$Pr = 0.071$	$Pr = 1$	$Pr = 3$	$Pr = 7.1$
0.1	3.401222	6.46578	8.974533	11.60541
1.0	3.40483	6.831039	9.60981	12.36013
2.0	3.40593	6.924561	9.723654	12.87453
3.0	3.407842	7.1124	9.89754	13.01279
4.0	3.409875	7.34217	10.24563	13.54789
5.0	3.419237	7.471625	10.76878	13.88735
6.0	3.419982	7.54213	10.85467	13.98547
7.0	3.421025	7.685423	10.93215	14.12135
8.0	3.4228	7.72413	11.02436	14.35647
9.0	3.43012	7.752463	11.23546	14.56871
10.0	3.426057	7.827903	11.43939	14.72438

and for all of the four different values of *Pr*, a small sized vortex is created above the inlet and open lines are stretched over the whole domain. When $Ri = 1$ (second row), the lower vortex enlarges for all selected values of *Pr* and a small eddy is found at the left-top corner of the cavity for $Pr = 1$. In dominant free convection regime ($Ri = 10$) the top row shows a noticeable change in flow characteristics for all *Pr*. Size of

the vortices increase very rapidly confining the centered body and thus main flow minimizes towards the bottom-right sides of the cavity.

The temperature distributions for the four considered values of *Pr* are displayed in Fig. 6.6(*b*). It is seen that for all convective regimes of *Ri* = 0.1, 1, 10 and at *Pr* = 0.071 a few number of heat lines are created. Among them some semi-circular shaped isotherms are found at the left wall of the cavity. When *Pr* = 1 the temperature distribution are found over the whole cavity for *Ri* = 0.1, 1 and for *Ri* = 10 heat lines are found to be reflected to the left wall. A significant change is followed for higher value of *Pr* = 3 and *Ri* = 0.1, 1; isotherms are crowded to the right bottom side of the enclosure. At *Ri* = 10 and *Pr* = 3 low temperatured isothermal lines returns to the left wall of the cavity. For all convective regimes of *Ri* isotherms are suppressed towards the hot bottom surface and right wall of the cavity when *Pr* = 7.1 and comparatively more suppression is noted for larger values of *Ri*. Moreover for largest value of *Pr* = 7.1, isotherms are found to be isolated from the centered obstacle of the cavity.

Average Nusselt number and average fluid temperature inside the cavity are shown in Fig. 6.7. From Fig. 6.7(*i*) it is seen that highest value of *Pr* = 7.1 gives the maximum heat transfer rate and lowest value of *Pr* = 0.071 gives the minimum heat transfer rate at the heated surface. An opposite effect is found to the average fluid temperature that is depicted in Fig. 6.7(*ii*).

The variations of average Nusselt number with Prandtl number are tabulated in Table 6.3. From this table it is seen that Nu_{av} increases with both of the rising values of *Pr* (rapidly) and *Ri* (slowly).

6.4.3 Effect of Hartmann Number

Fig. 6.8(*a*) depicts the effects of the magnetic field parameter on streamlines at different Richardson number. At low Hartmann number *Ha* = 0, a rotating cell is created just above the inlet in the domain *Ri* = 0.1 and it increases rapidly for the consecutive value of *Ri* = 1. On the other hand it is followed that for the above two convective regimes of Richardson number the flow structures are almost identical at the rest three considered values of *Ha* (= 20, 50, 100). Interestingly, in the dominant free convection domain the patterns of the cavity flow change dramatically for the
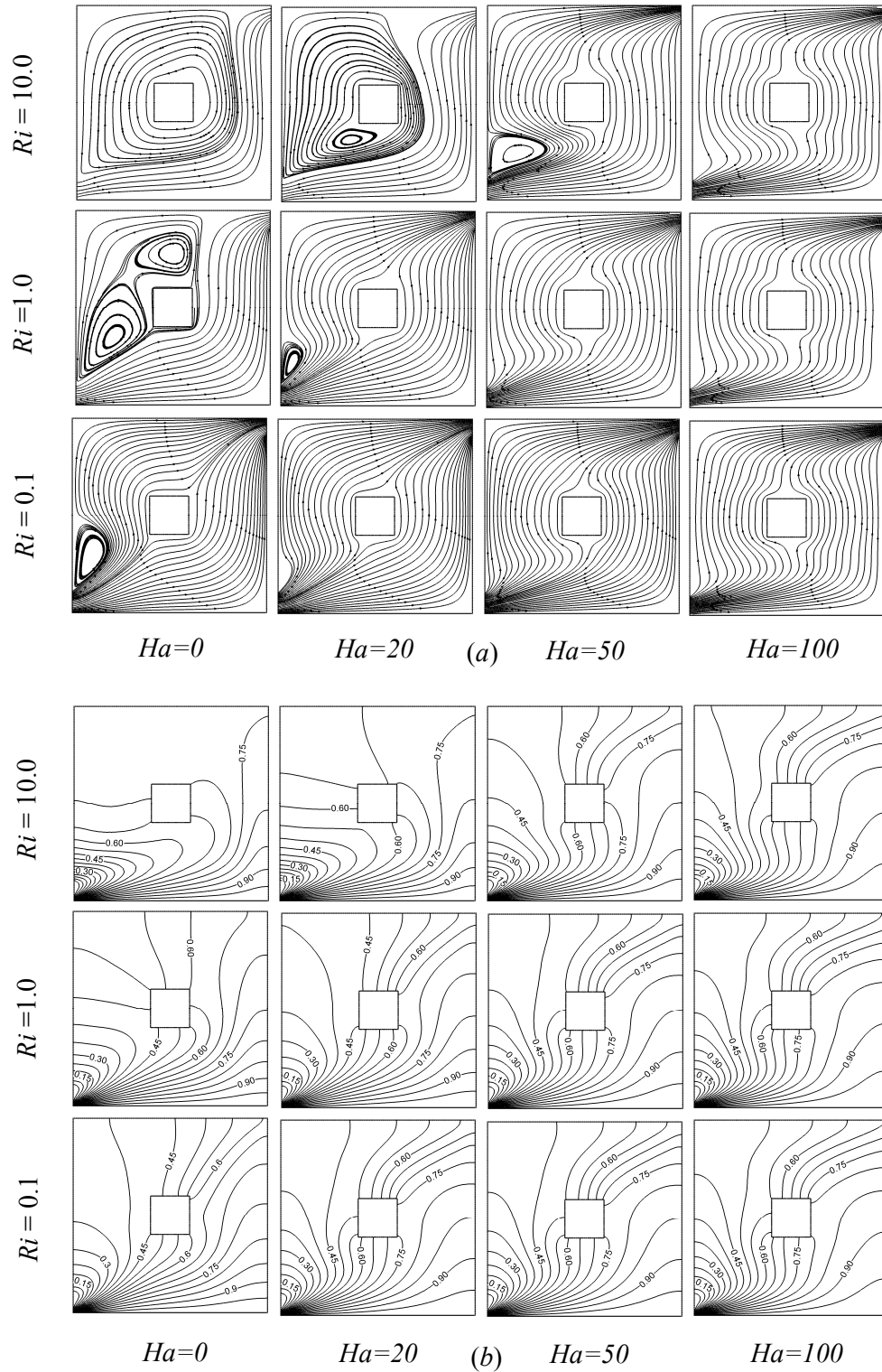
Figure 6.8: (*a*) Streamlines and (*b*) Isotherms at different Hartmann number and various values of Richardson number *Ri*, while *Re* = 100, *Pr* = 0.71, *K* = 5, *Q* = 1 and *D* = 0.2.

(*i*) (*ii*)

Figure 6.9: Effect of Hartmann number on (*i*) average Nusselt number, (*ii*) average fluid temperature, while *Re* = 100, *Pr* = 0.71, *D* = 0.2, *Q* = 1 and *K* = 5.

Table 6.4: Variation of average Nusselt number with Hartmann number

Ri	Nu_{av}			
	Ha = 0	*Ha* = 20	*Ha* = 50	*Ha* = 100
0.1	6.117298	5.788497	5.470473	5.438015
1.0	6.211818	5.878837	5.630361	5.56877
2.0	6.26431	5.941346	5.784562	5.604578
3.0	6.30457	6.12243	5.854136	5.66213
4.0	6.32872	6.17243	5.921234	5.72475
5.0	6.360872	6.215266	5.976642	5.779284
6.0	6.382157	6.258542	6.044782	5.834762
7.0	6.43871	6.291403	6.139754	5.901245
8.0	6.47021	6.324315	6.211354	6.113145
9.0	6.49287	6.38458	6.305416	6.238740
10.0	6.52927	6.452779	6.433060	6.38791

cases of lower *Ha* than those of higher values of *Ha*. The reality established here is that the application of transverse magnetic field acting as Lorentz's force which retards the flow. As expected, the flow strength is reduced with increasing the Hartmann number.

The inspection of the heat lines profile relating to these various values of the Hartmann number are illustrated in Fig. 6.8(*b*). The isothermal lines are scattered

through all over the enclosure for the choosing values of four Hartmann number as $Ha = 0, 20, 50, 100$ in the different values of Richardson number regimes with the exception of two cases. However a significant change is found for the lowest value of $Ha = 0$, that is in the absence of magnetic field parameter along with $Ri = 10$. Also a noticeable variation is observed in the dominant natural convective domain at $Ha = 20$. Moreover, it is seen that heat lines are crowded at the bottom wall near the inlet port and a boundary layer is created at the vicinity of the heated surface of the cavity for each case.

At last the heat transfer efficiency of the enclosure for the above discussed parameter is presented in terms of average Nusselt number Nu_{av} and the dimensionless average bulk temperature θ_{av}. Fig. 6.9 plots the variation of both average Nusselt number and average fluid temperature for different values of Hartmann number. The variation profile indicates that heat transfer rate decreases as the value of Ha increases within the range of $0.1 \leq Ri \leq 10$ and so an opposite result is found for the average fluid temperature in the cavity. The higher the Hartmann number the smaller are the fluctuations in the average temperature.

Table 6.4 shows the rate of heat transfer at the bottom hot wall along with Hartmann number. As Ha becomes higher Nu_{av} decreases slowly, but it increases very slowly when Ri increases.

6.4.4 Effect of Block Diameter

Diameter $D = 0.1$ that is for a smaller solid block, an anti-clockwise vortex is developed above the inlet at the value of $Ri = 0.1$ whereas it increases very sharply for the higher value of $Ri = 1$. But in the dominant free convective regime $Ri = 10$, the flow patterns inside the cavity change dramatically. The vortex swells up and captures the block, open lines move away along the bottom right side of the cavity, as expected. Also a small eddy is seen inside the vortex and at the right side of the adiabatic obstacle. As D increases from 0.1 to 0.3, the size of the re-circulation cell decreases for all of the three chosen values of mixed convection parameters Ri (0.1, 1, 10). When $D = 0.5$, small sized vortex vanishes in the dominant forced convection and mixed convection domain but in the region where free convection dominates forced convection the flow strength of the vortex is reduced regarding to same case
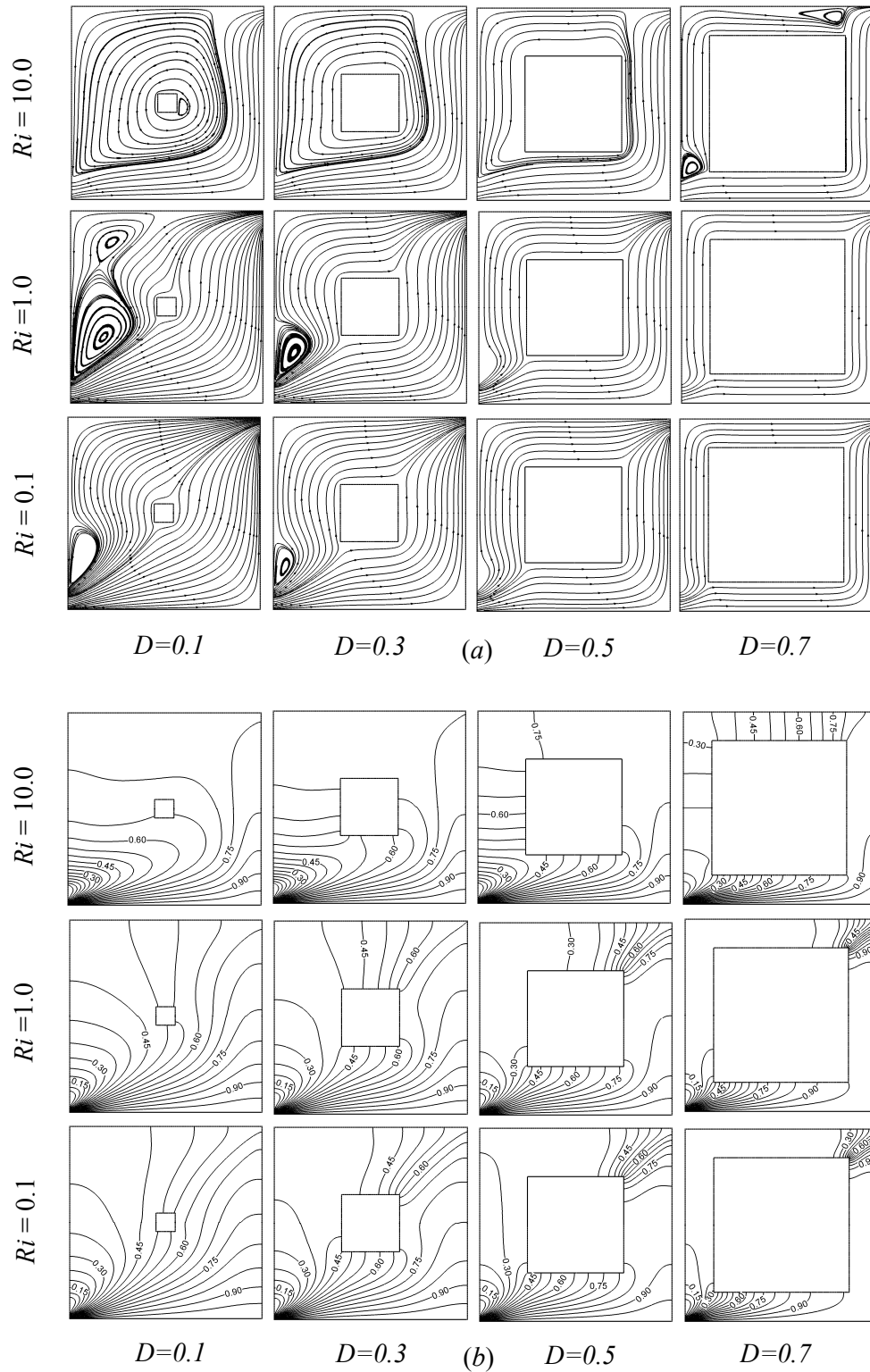
Figure 6.10: (*a*) Streamlines and (*b*) Isotherms at different block diameter and various values of Richardson number *Ri*, while *Re* = 100, *Pr* = 0.71, *Ha* = 10, *Q* = 1 and *K* = 5.
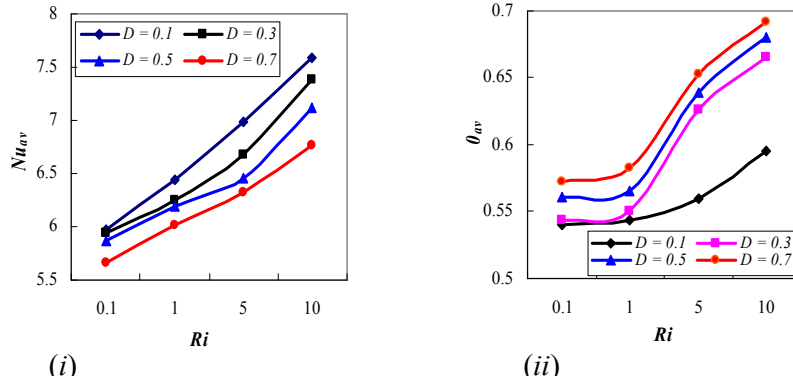
Figure 6.11: Effect of block diameter on (*i*) average Nusselt number, (*ii*) average fluid temperature, while $Re = 100$, $Pr = 0.71$, $K = 5$, $Q = 1$ and $Ha = 10$.

Table 6.5: Variation of average Nusselt number with block diameter

Ri	Nu_{av}			
	$D = 0.1$	$D = 0.3$	$D = 0.5$	$D = 0.7$
0.1	5.96388	5.936496	5.870495	5.659744
1.0	6.320079	6.173956	6.145851	6.014219
2.0	6.564872	6.362145	6.21345	6.113024
3.0	6.721436	6.451278	6.32104	6.19784
4.0	6.835421	6.574213	6.398742	6.26894
5.0	6.984043	6.67612	6.455061	6.322963
6.0	7.012354	6.874512	6.56871	6.42157
7.0	7.112354	6.985462	6.70321	6.53214
8.0	7.352136	7.12354	6.89214	6.60124
9.0	7.46873	7.204321	7.01249	6.68942
10.0	7.58193	7.387842	7.114406	6.771448

with $D = 0.3$ due to the lackness of space availability inside the cavity. For the largest value of $D = 0.7$ there is no vortex in the domain $Ri = 0.1, 1$ whereas in the domain $Ri = 10$ two small vortex is appeared instead of single large vortex.

The first column of Fig. 6.10(*b*) depicts the isotherms for $D = 0.1$ and it shows that for the dominant forced convection and mixed convection domain the heat lines patterns become scatter except in the vicinity of the bottom hot surface of the enclosure. On the other hand, isotherms are found to be folded below the inner body

when the natural convection becomes dominant (Ri = 10). Moreover, the high-isothermal lines are seen more concentrated near the hot wall and the thermal field is more uniform in the lower right parts of the enclosure for all the considered values of Richardson number. From the second column of Fig. 6.10(b) it is seen that a significant change in isotherm patterns is occurred for the two lower values of Ri = 0.1 and Ri = 1.0 when D = 0.3. But in the dominant free convection region temperature distribution inside the enclosure is almost identical that was found for D = 0.1. A noteworthy variation is followed in thermal fields for the larger value of D (= 0.5) in all the considered values of mixed convection parameter Ri. A large number of packed heat lines are noticed at the top right corner of the cavity for the dominant forced convection and mixed convection domain. When Ri = 10, except some high isothermal lines all isotherms are seen to be folded to the left wall of the enclosure. When D = 0.7, a little dissimilarity in heat lines is observed in the case of Ri = 10 but for the other two values of Ri isotherms are about same that was seen in the case of D = 0.5.

The average heat transfer rate at the hot wall of the enclosure and average fluid temperature inside the cavity are displayed in Fig. 6.11 for different block diameter D. Fig. 6.11(i) shows heat transfer rate is maximum at the lowest value of D = 0.1 and it minimizes as the value of D increases. Besides that, from Fig. 6.11(ii) it is noticed that the average fluid temperature θ_{av} inside the enclosure is about stationary in the range of Richardson number $0.1 \leq Ri \leq 1$. But it increases rapidly for three larger values of D and smoothly for the smallest D with higher Ri ($1 \leq Ri \leq 10$). And smallest block shows the minimum cavity fluid temperature.

Table 6.5 shows the variation of Nu_{av} with centered adiabatic block diameter D. Average Nusselt number gives the higher value for upper values of Ri and it decreases very gradually with higher values of D.

6.5 Concluding Remarks

The pertinent parameters of this work have provided some reliable information on the condition on flow and heat transfer for the enclosure vented confining a thermally isolated obstacle and it may be concluded that the considered parameters in this study can be treated as heat transfer controlling parameter.

From the present investigation it is seen that for different Reynolds number *Re* while Hartmann number *Ha*, Prandtl number *Pr* and adiabatic solid body diameter *D* are kept stationary; heat transfer rate at the hot wall of the cavity is larger for upper values of *Re*. In addition, the flow and thermal fields in the case of Reynolds number are much affected than those of other considering parameters.

Flow fields are much affected by Prandtl number in dominant free convection domain than the other two convective regimes of Richardson number. On the other hand, a significant effect is followed in thermal fields for all the considered values of *Pr* with all values of *Ri*. The rate of heat transfer is ceiling for the largest Prandtl number.

But an opposite effect is noticed for the case of different Hartmann number *Ha* with fixed Reynolds number *Re*, Prandtl number *Pr* and block diameter *D*; that is, rate of heat transfer reduces as *Ha* increases.

The heat transfer rate can be enhanced by reducing the diameter of the adiabatic obstacle and thus optimum cooling in the enclosure is achieved for the smallest value of *D*.

Chapter 7

Conclusions

A mixed convection problem on two dimensional steady, laminar, incompressible viscous flow in an obstructed ventilated enclosure have been investigated numerically to explain the flow and heat transfer characteristics of an electrically conducting fluid subjected to externally imposed magnetic field. The Reynolds number, Prandtl number, Hartmann number, thermal conductivity ratio and solid block diameter are treated as governing parameters in this dissertation. The present work is mainly based on three types of internal solid block as heat generating, heat conducting and adiabatic. Detailed analysis for visualization of streamlines, isotherms, average Nusselt number at the heated surface and average fluid temperature in the cavity were carried out to explore the effect of mentioned three obstacles along with studied parameters. The results are presented details in the relevant chapters and in view of the obtained results a data for heat transfer performance in the case of mixed convection regime ($Ri = 1$) is presented in this chapter.

In chapter 3, the effect of inlet and outlet position of an obstructed ventilated cavity has been investigated. It was found that the BT configuration that is the enclosure having bottom inlet and top outlet gives the optimum cooling inside the cavity as the rate of heat transfer at the hot wall is maximum. In addition, TT configuration shows the ceiling cavity fluid temperature. In mixed convection regime BT configuration shows that heat transfer rate is 76.96% higher than TT configuration.

The effect of heat generating block with different governing parameters has been analyzed in chapter 4. A variation of Nu_{av} between lowest value and upper value of considering parameters is presented here for $Ri = 1$. In case of Reynolds number, average Nusselt number increases 166.62% when Re varies from 50 to 500. When Prandtl number rises to 7.1 from 0.071, it is found that Nu_{av} increases 270.49%. For the case of two values of Hartmann number; absence of magnetic field parameter ($Ha = 0$) and highest Hartmann number ($Ha = 100$), a little difference of 9.37% decreasing is found. High thermal conductivity ratio gives low heat transfer rate and

it is noticed that Nu_{av} decreases 3.98% when $K = 0.2$ increases to $K = 50$. Also it is revealed that largest size heat generating block minimizes heat transfer rate and 79.90% decreasing is found when D varies from 0.1 to 0.7.

The effect of heat conducting block along with considered parameters in this work has been carried out in chapter 5. A comparison of Nu_{av} between the lowest and highest value of various parameters is summarized here for the mixed convection domain. For the forced convection parameter Re, it is observed that Nu_{av} increases 175.38% when Re increases from 50 to 500. Average Nusselt number increases 263.14% for the variation of Prandtl number $Pr = 0.071$ & $Pr = 7.1$. When $Ha = 0$ reaches to $Ha = 100$, Nu_{av} decreases 9.90%. If thermal conductivity ratio $K = 0.2$ goes to $K = 50$, Nu_{av} decreases 1.69%. For the variation of block diameter D from 0.1 to 0.7, it is clear that average Nusselt number decreases 5.76%.

Chapter 6 presents the effect of adiabatic solid body together with the related parameters. For mixed convection region, the rate of heat transfer variation is shown for the studied parameters. Average Nusselt number enhances 175.80% for the difference of $Re = 50$ & $Re = 500$. Also when $Pr = 0.071$ rises up to $Pr = 7.1$, Nu_{av} increases 263.02%. For the variation of Hartmann number ($Ha = 0$ to $Ha = 100$), Nu_{av} decreases 10.35%. It is noticed that if the dimension of solid block increases, Nu_{av} decreases and it is decreased 4.84%, when the diameter of the solid block reaches its highest value $D = 0.7$ from the lowest value $D = 0.1$.

Last of all, a comparison of heat transfer rate at the heated surface of the enclosure for the studied three types of obstacle has been computed here in tabular form.

From these tables it can be followed that for the case of heat conducting block highest heat transfer rate is found for all convective regimes and all considered parameters. This is due to the fact that as it conducts heat it is helpful for heat transfer. The second highest heat transfer rate is marked for the adiabatic block for all the cases. It is reliable because it neither produces heat nor conducts heat and thus it acts an obstacle. Finally, the comparison table shows that heat generating block gives the lowest heat transfer rate as it generates heat itself and consequently rate of heat transfer reduces.

Table-7.1

Ri		Nu_{av}		
		HG Block	*HC* Block	*AD* Block
0.1	*Re*=500	11.6910	11.93826	11.93755
	Pr=7.1	11.58715	11.60556	11.60541
	Ha=100	5.303347	5.595915	5.438015
	K=50	5.555065	5.792311	---
	D=0.7	1.134105	5.878331	5.659744
1.0	*Re*=500	11.84686	12.69623	12.69044
	Pr=7.1	12.26479	12.36946	12.36013
	Ha=100	5.56483	5.617554	5.56877
	K=50	5.817765	6.052123	---
	D=0.7	1.229502	6.075355	6.014219
10.0	*Re*=500	14.89302	15.07491	15.03054
	Pr=7.1	14.54344	14.73343	14.72438
	Ha=100	6.348449	6.425373	6.38791
	K=50	6.256456	6.764881	---
	D=0.7	1.646546	6.929178	6.771448

Table-7.2

Ri		Nu_{av}		
		HG Block	*HC* Block	*AD* Block
0.1	*Re*=350	9.901751	10.16745	10.16379
	Pr=3.0	8.882427	8.975492	8.974533
	Ha=50	5.326058	5.663728	5.470473
	K=10	5.688583	5.852833	--
	D=0.5	4.304263	5.918809	5.870495
1.0	*Re*=350	10.17529	10.79475	10.78297
	Pr=3.0	9.594996	9.617635	9.60981
	Ha=50	5.548711	5.728370	5.630361
	K=10	5.896423	6.096624	--
	D=0.5	4.552257	6.188468	6.145851
10.0	*Re*=350	12.59697	12.76067	12.74836
	Pr=3.0	11.35116	11.45531	11.43939
	Ha=50	6.413511	6.538633	6.433060
	K=10	6.360907	6.804503	--
	D=0.5	5.138711	7.184350	7.114406

Table-7.3

Ri		Nu_{av}		
		HG Block	HC Block	AD Block
0.1	Re=200	7.750381	7.851059	7.839311
	Pr=1.0	6.401763	6.469222	6.46578
	Ha=20	5.692517	5.791037	5.788497
	K=1	5.753399	5.894875	--
	D=0.3	5.613745	5.938528	5.936496
1.0	Re=200	8.052749	8.326203	8.320327
	Pr=1.0	6.734086	6.861754	6.831039
	Ha=20	5.85114	5.958862	5.878837
	K=1	5.985485	6.106777	--
	D=0.3	5.854553	6.255076	6.173956
10.0	Re=200	9.454947	9.672471	9.671546
	Pr=1.0	7.580309	7.838668	7.827903
	Ha=20	6.433135	6.680713	6.452779
	K=1	6.480545	6.861843	--
	D=0.3	6.335527	7.446213	7.387842

Table-7.4

Ri		Nu_{av}		
		HG Block	HC Block	AD Block
0.1	Re=50	4.388523	4.553039	4.542412
	Pr=0.071	3.307886	3.403973	3.401222
	Ha=0	5.921909	6.189092	6.117298
	K=0.2	5.812649	5.996055	--
	D=0.1	5.86043	6.168909	5.96388
1.0	Re=50	4.443288	4.610437	4.601385
	Pr=0.071	3.310394	3.406295	3.40483
	Ha=0	6.139915	6.235082	6.211818
	K=0.2	6.058879	6.15619	--
	D=0.1	6.115497	6.446465	6.320079
10.0	Re=50	4.669317	4.921946	4.895953
	Pr=0.071	3.329817	3.432531	3.426057
	Ha=0	6.449623	6.870787	6.52927
	K=0.2	6.593505	6.959192	--
	D=0.1	6.774454	7.636104	7.58193

7.1 Further Works

The following can be put forward for the further works as follow-ups of the present research as

❖ In the future, the study can be extended by incorporating different types of nano-fluids.

❖ Double diffusive combined free and forced convection can be analyzed through including the governing equation of concentration conservation.

❖ Analysis can be executed by using magnetic fluid instead of electrically conducting fluid within the porous medium and varying the boundary conditions of the cavity's walls.

❖ The problem can be performed for turbulent flow and unsteady flow using various fluids with different thermal boundary conditions.

❖ In this work, the fluid flow and heat transfer has been analyzed only for two-dimensional case. So this research work may be extended to three-dimensional analyses to investigate the effects of considered parameters on flow fields and heat transfer in enclosures. In addition, the problem of fluid flow and heat transfer along with three types of solid body may be studied also in three-dimensional cases.

<u>Contents</u>

Nomenclature

B_0	magnetic induction (Wb/m^2)
c_p	specific heat at constant pressure ($J/kg.K$)
d	dimensional diameter of the cylinder (m)
D	dimensionless diameter of the cylinder
g	gravitational acceleration (ms^{-2})
Gr	Grashof number
h	convective heat transfer coefficient ($W/m^2.K$)
L	length of the cavity (m)
Ha	Hartmann number
H_λ	linear shape function
k_f	thermal conductivity of fluid ($Wm^{-1}K^{-1}$)
k_s	thermal conductivity of solid ($Wm^{-1}K^{-1}$)
K	Solid fluid thermal conductivity ratio
L	length of the cavity (m)
n	dimensional distance either along x or y direction (m)
N	non-dimensional distance either along X or Y direction
N_α	quadratic shape function
Nu	Nusselt number
p	pressure
P	non-dimensional pressure
Pr	Prandtl number
q_w	heat flux
Ra	Raleigh number
Re	Reynolds number
Ri	Richardson number
S_x	surface tractions along X-axis
S_y	surface tractions along Y-axis
T	dimensional fluid temperature (K)
T_s	dimensional solid temperature (K)
ΔT	dimensional temperature difference (K)
u	velocity in x-direction (m/s)
v	velocity in y-direction (m/s)
U	dimensionless horizontal velocity
V	dimensionless vertical velocity
$\overline{V}$	cavity volume (m^3)
x, y	Cartesian coordinates (m)
X, Y	dimensionless Cartesian coordinates
$\square$	square cylinder

Greek symbols

α thermal diffusivity $(m^2 s^{-1})$

β coefficient of thermal expansion (K^{-1})

θ dimensionless fluid temperature

θ_s dimensionless solid temperature

$\Delta\theta$ dimensionless temperature difference

μ dynamic viscosity of the fluid $(m^2 s^{-1})$

v kinematic viscosity of the fluid $(m^2 s^{-1})$

ρ density of the fluid (kgm^{-3})

σ fluid electrical conductivity $(\Omega^{-1}.m^{-1})$

Subscripts

av average

h heated wall

i inlet state

s solid

Abbreviation

CBC   convective boundary conditions

BB   bottom inlet and bottom outlet

BT   bottom inlet and top outlet

TB   top inlet and bottom outlet

TT   top inlet and top outlet

HG   heat generating block

HC   heat conducting block

AD   adiabatic block

List of Tables

List of Figures

References

Amir Hossein Zarei, Seyed Hadi Rostamian, Mohammad Hemmat Esfe, "heat transfer behavior of mixed convection flow in lid driven cavity containing hot obstacle subjected to nano-fluid with variable properties", Journal of Basic and Applied Scientific Research, Vol.3, No. 2, pp. 713-721, 2013.

Angirasa, D., "Mixed convection in a vented enclosure with isothermal vertical surface", Fluid Dyn. Res. Vol. 26, pp. 219-233, 2000.

Anderson, J. D., "Computational fluid dynamics", International Ed., McGraw-Hill, 1995.

Bhave, P., Narasimhan, A., and Ress, D. A. S., "Natural convection heat transfer enhancement using adiabatic block: Optimal block size and Prandtl number effect", Int. J. of Heat and Mass Transfer, Vol. 49, pp. 3807-3818, 2006.

Bilgen, E., "Natural convection in cavities with a thin fin on the hat wall", Int. J. of Heat and Mass Transfer, Vol. 48, pp. 3493-3505, 2005.

Bilgen, E., and Yamane, T., "Conjugate heat transfer in enclosures with openings for ventilation", Heat and Mass Transfer, Vol. 40, pp. 401-411, 2004.

Braga, E. J., and de Lemos, M. J. S., "Laminar natural convection in cavities filed with circular and square rods", Int. Commun. in Heat and Mass Transfer, Vol. 32, pp. 1289-1297, 2005.

Carlos Alberto Chaves, Jose Rui Camargo and Valesca Alves Correa, "Combined forced and free convection heat transfer in a semi porous open cavity", Scientific Research and Essay, Vol.3, No. 8, pp. 333-337, 2008.

Cengel, Y. A., "Heat and mass transfer", Third Ed., Tata McGraw-Hill, 2007.

Chamkha, A. J., "Hydromagnetic combined convection flow in a vertical lid-driven cavity with internal heat generation or absorption", Numer. Heat Transfer, Part A, Vol. 41, pp. 529-546, 2002.

Chung, T. J., "Computational fluid dynamics", First Ed., Cambridge University Press, 2002.

Srinivasacharya Darbhasayanam and Kaladhar Kolla, "Analytical solution of mixed convection flow of couple stress fluid between two circular cylinders with Hall and ion-slip effects", Turkish J. Eng. Env. Sci., Vol. 36, pp. 226 – 235, 2012.

Das, M. K., and Reddy, K. S. K., "Conjugate natural convection heat transfer in an inclined square cavity containing a conducting block", Int. J. of Heat and Mass Transfer, Vol. 49, pp. 4987-5000, 2006.

Deng, Q. H., and Tang, G. F., "Numerical visualization of mass and heat transport for conjugate natural convection/ heat conduction by streamline and heat line", Int. J. of Heat Mass Transfer, Vol. 45, pp. 2373-2385, 2002.

Dechaumphai, P., "Finite Element Method in Engineering", second Ed., Chulalongkorn University Press, Bangkok, 1999.

Ferziger, J. H. and Perić, M., "Computational methods for fluid dynamics", Second Ed., Springer Verlag, Berlin Hedelberg, 1997.

Fletcher, C. A. J., "Computational techniques for fluid dynamics 1", Second Ed., Springer Verlag, Berlin Hedelberg, 1991.

Gaikwad, S. N. and Kamble, S. S., "An analytical study of combined free and forced convection through vertical channel with porous media", Bulletin of the Marathwada Mathematical Society, Vol. 12, No. 1, pp. 37–46, 2011.

Garandet, J. P., Alboussiere, T., and Moreau, R., "Buoyancy driven convection in a rectangular enclosure with a transverse magnetic field", Int. J. of Heat Mass Transfer, Vol. 35, pp. 741-748, 1992.

Gau, C., Jeng, Y.C., and Liu, C.G., "An experimental study on mixed convection in a horizontal rectangular channel heated from a side", ASME J. Heat Transfer, Vol. 122, pp. 701–707, 2000.

Gowda, Y. T. K., Narayana, P. A. A., and Seetharamu, K. N., "Mixed convection heat transfer past in-line cylinders in a vertical duct", Numer. Heat Transfer, Part A, Vol. 31, pp. 551-562, 1997.

Gau, G., Sharif, M. A. R., "Mixed convection in rectangular cavities at various aspect ratios with moving isothermal side walls and constant flux heat source on the bottom wall", Int. J. of Thermal Sciences, Vol. 43, pp. 465-475, 2004.

Ha, M. Y., Jung, M. J., and Kim, Y.S., "Numerical study on transient heat transfer and fluid flow of natural convection in an enclosure with a heat-generating conducting body", Numer. Heat Transfer, Part A, Vol. 35, pp. 415-434, 1999.

Saleh Habibis , Hashim Ishak , and Basriati Sri , "Flow reversal of fully developed mixed convection in a vertical channel with chemical reaction", International Journal of Chemical Engineering, Vol. 2013, Article ID 310273, 4 pages, 2013.

Hagen, K. D., "Heat transfer with applications", First Ed., Prentice-Hall International, 1999.

Hossain, M. A., and Gorla, R. S. R., "Effect of viscous dissipation on mixed convection flow of water near its density maximum in a rectangular enclosure with isothermal wall", Int. J. of Numer. Methods for Heat and Fluid Flow, Vol. 16, No. 1, pp. 5-17, 2006.

House, J. M., Beckermann, C. and Smith, T. F., "Effect of a centered conducting body on natural convection heat transfer in an enclosure", Numer. Heat Transfer, Part A, Vol. 18, pp. 213-225, 1990.

How, S.P. and Hsu, T.H., "Transient mixed convection in a partially divided enclosure", Comput. Math. Appl. Vol. 36, pp. 95-115, 1998.

Hsu, T.H., and How, S. P., "Mixed convection in an enclosure with a heat-conducting body", Acta Mechanica, Vol. 133, pp. 87-104, 1999.

Hsu, T.H., and Wang, S. G., "Mixed convection in a rectangular enclosure with discrete heat sources", Numer. Heat Transfer, Part A, Vol. 38, pp. 627-652, 2000.

Hsu, T.H., Hsu, P.T., How, S.P., "Mixed convection in a partially divided rectangular enclosure", Numer. Heat Transfer, Part A, Vol. 31, pp. 655-683, 1997.

Jami, M., Mezrhab, A. Bouzidi, M and Lallemand, P., "Lattice boltzmann method applied to the laminar natural convection conduction in an enclosure with a heat generating cylinder conducting body", Int. J. of Thermal Sciences, Vol. 46, pp. 38–47, 2007.

Joshi, N. D. and Sukhatme, S. P., "An analysis of combined free and forced convection heat transfer from a horizontal circular cylinder to a transverse flow", J. Heat Transfer, Vol. 93, No. 4, pp. 441-448, 2010.

Kalam, A., Munshi, J. H., Rahman, M., Chowdhury, M., M. K., "Analysis of combined convection in an open cavity under constant heat flux boundary conditions and magnetic field using finite element method", Journal of scientific research, Vol. 6, No. 2, pp. 243-256, 2014.

Kumar De, A., and Dalal, A., "A numerical study of natural convection around a square, horizontal, heated cylinder placed in an enclosure", Int. J. of Heat and Mass Transfer, Vol. 49, pp. 4608-4623, 2006.

Khanafer, K., Vafai, K., and Lightstone, M., "Mixed convection heat transfer in two-dimensional open-ended enclosure", Int. J. of Heat and Mass Transfer, Vol. 45, pp. 5171-5190, 2002.

Lacroix, M., and Joyeux, A., "Natural convection heat transfer around heated cylinders inside a cavity with conducting walls", Numer. Heat Transfer, Part A, Vol. 27, pp. 335-349, 1995.

Lee, J. R., and Ha, M. Y., "A numerical study of natural convection in a horizontal enclosure with a conducting body", Int. J. of Heat and Mass Transfer, Vol. 48, pp. 3308-3318, 2005.

Lee, J. R., and Ha, M. Y., "Numerical simulation of natural convection in a horizontal enclosure with a heat-generating conducting body", Int. J. of Heat and Mass Transfer, Vol. 49, pp. 2684-2702, 2006.

Xianglong Liu, Guangcai Gong, and Hengsheng Cheng, "Combined natural convection and radiation heat transfer of various absorbing-emitting-scattering media in a square cavity", Advances in Mechanical Engineering, Vol. 2014, 10 pages, Article ID 403690, 2014.

Mahmud, S., Tasnim, S. H., and Mamun, M. A. H., "Thermodynamic analysis of mixed convection in a channel with transverse hydromagnetic effect", Int. J. of Thermal Sciences, Vol. 42, pp. 731-740, 2003.

Manca, O., Nardini, S., Khanafer, K., and Vafai, K., "Effect of heated wall position on mixed convection in a channel with an open cavity", Numer. Heat Transfer, Part A, Vol. 43, pp. 259–282, 2003.

Manca, O., Nardini, S., and Vafai, K., "Experimental investigation mixed convection in a channel with an open cavity", Experimental Heat Transfer, Vol. 19, pp. 53–68, 2006.

Mansour Kalbasi and Alireza Saeedi, "Numerical investigation into the convective heat transfer of CuO nanofluids flowing through a straight tube with uniform heat flux" Indian Journal of Science and Technology, Vol. 5, No. S3, pp. 2455-2458, 2012.

Merrikh, A. A., and Lage, J. L., "Natural convection in an enclosure with disconnected and conducting solid blocks", Int. J. Heat Mass Transfer, Vol. 48, No. 7, pp. 1361-1372, 2005.

Misra, D., and Sarkar, A., "Finite element analysis of conjugate natural convection in a square enclosure with a conducting vertical wall", Comput. Methods Appl. Mech. Engg., Vol. 141, pp. 205-219, 1997.

Nakhi, A. B., and Chamkha, A. J., "Conjugate natural convection around a finned pipe in a square enclosure with internal heat generation", Int. J. of Heat and Mass Transfer, Vol. 50, pp. 2260-2271, 2007.

Oh, J. Y., Ha, M. Y., and Kim, K. C., "Numerical study of heat transfer and flow of natural convection in an enclosure with a heat generating conducting body", Numer. Heat Transfer, Part A, Vol. 31, pp. 289-304, 1997.

Olumuyiwa A. Lasode' "Mixed convection heat transfer in rotating vertical elliptic ducts", J. of the Braz. Soc. of Mech. Sci. & Eng., Vol. XXIX, No. 2, pp 142-151, 2007.

Omri, A., and Nasrallah, S. B., "Control volume finite element numerical simulation of mixed convection in an air-cooled cavity", Numer. Heat Transfer, Part A, Vol. 36, pp. 615–637, 1999.

Oreper, G. M., Szekely, J., "The effect of an externally imposed magnetic field on buoyancy driven flow in a rectangular cavity", J. of Crystal Growth, Vol. 64, pp. 505-515, 1983.

Oztop, H. F., and Dagtekin, I., "Comparison of position of heated thin plate located in a cavity for natural convection", Int. Commun. in Heat Mass Transfer, Vol. 31, No. 1, pp. 121-132, 2004.

Oztop, H. F., Zhao, Z., and Yu, B., "Fluid flow due to combined convection in lid-driven enclosure having a circular body," International journal Heat and Fluid Flow, Vol. 30, pp. 886–901, 2009.

Oztop, H., and Bilgen, E., "Natural convection in differentially heated and partially divided square cavities with internal heat generation", Int. J. of Heat and Fluid Flow, Vol. 27, pp. 466-475, 2006.

Papanicolaou, E., and Jaluria, Y., "Mixed convection from an isolated heat source in a rectangular enclosure", Numer. Heat Transfer, Part A, Vol. 18, pp. 427–461, 1990.

Papanicolaou, E., and Jaluria, Y., "Transition to a periodic regime in mixed convection in a square cavity", J. Fluid Mech., Vol. 239, pp. 489–509, 1992.

Papanicolaou, E., and Jaluria, Y., "Mixed convection from a localized heat source in a cavity with conducting walls: A numerical study", Numer. Heat Transfer, Part A, Vol. 23, pp. 463–484, 1993.

Papanicolaou, E., and Jaluria, Y., "Mixed convection from simulated electronic components at varying relative positions in a cavity", J. Heat Transfer, Vol. 116, pp. 960–970, 1994.

Patankar, S. V., "Numerical heat transfer and fluid flow", Second Ed., Washington, D. C. Homisphere, 1980.

Pop, Grosan, T. and Cornelia, R. "Effect of heat generated an exothermic reaction on the fully developed mixed convection flow in a vertical channel", Communications in Nonlinear Science and Numerical Simulation, Vol. 15, No. 3, pp. 471–474, 2010.

Prakash, D. and Ravikumar, P., "Study of thermal comfort in a room with windows at adjacent walls along with additional vents", Indian Journal of Science and Technology, Vol. 6, No. 6, pp. 4659-4669, 2013.

Radhakrishnan, T.V., Verma, A.K., Balaji, C., and Venkateshan, S.P., "An experimental and numerical investigation of mixed convection from a heat generating element in a ventilated cavity," Experimental Thermal and Fluid Science, vol. 32, pp. 502–520, 2007.

Rahman, M. M., Alim, M. A., Saha, S. and Chowdhury, M. K., "A numerical study of mixed convection in a square cavity with a heat conducting square cylinder at different locations", J. of Mechanical Engineering, The Institution of Engineers, Bangladesh, Vol. ME 39, No. 2, pp. 78 - 85, 2008a.

Rahman, M. M., Alim, M. A., Saha, S. and Chowdhury, M. K., "Mixed convection in a vented square cavity with a heat conducting horizontal solid circular cylinder", Journal of Naval Architecture and Marine Engineering, Vol. 5, No. 2, pp.37 - 46, 2008b.

Rahman, M. M., Alim, M. A. and Mamun, M. A. H. "Finite element analysis of mixed convection in a rectangular cavity with a heat-conducting horizontal circular cylinder", Nonlinear analysis: Modeling and Control, Vol.14, No. 2, pp. 217-247, 2009.

Raji, A., and Hasnaoui, M., "Mixed convection heat transfer in a rectangular cavity ventilated and heated from the side", Numer. Heat Transfer, Part A, Vol. 33, pp. 533–548, 1998a.

Raji, A., and Hasnaoui, M., "Correlations on mixed convection in ventilated cavities". Revue Ge´ne´rale de Thermique, Vol. 37, pp. 874–884, 1998b.

Raji, A., and Hasnaoui, M., "Mixed convection heat transfer in ventilated cavities with opposing and assisting flows", Int. J. Computer-Aided Eng. Software, Vol. 17, No. 5, pp. 556–572, 2000.

Reddy, J. N. and Gartling, D. K., "The Finite Element Method in Heat Transfer and Fluid Dynamics", CRC Press, Inc., Boca Raton, Florida, 1994.

Roychowdhury, D.G, Das, S.K. and Sundararajan, T.S., "Numerical simulation of natural convection heat transfer and fluid flow around a heated cylinder inside an enclosure", Heat and Mass Transfer, Vol. 38, pp. 565-576, 2002.

Rudraiah, N., Barron, R. M., Venkatachalappa, M., and Subbaraya, C. K., "Effect of magnetic field on free convection in a rectangular enclosure", Int. J. Engng. Sci., Vol. 33, pp. 1075-1084, 1995.

Saeidi, S. M., and Khodadadi, J. M., "Forced convection in a square cavity with inlet and outlet ports", Int. J. of Heat and Mass Transfer, Vol. 49, pp. 1896-1906, 2006.

Sasaguchi, K., Kuwabara, K., Kusano, K., and Kitagawa, H., "Transient cooling of water around a cylinder in a rectangular cavity- a numerical analysis of the effect of the position of the cylinder", Int. J. of Heat and Mass Transfer, Vol. 41, pp. 3149-3156, 1998.

Shuja, S.Z., Yilbas, B.S. and Budair, M.O., "Natural convection in a square cavity with heat generating body: Entropy consideration", Heat and Mass Transfer, Vol. 36, pp. 343-350, 2000.

Shuja, S.Z., Yilbas, B.S. and Iqbal, M.O., "Mixed convection in a square cavity due to heat generating rectangular body", Int. J. of Numer. Methods for Heat & Fluid Flow, Vol. 10, No. 8, pp. 824-841, 2000.

Shuja, S.Z., Yilbas, B.S., Khan, S.M.A., "Flow over solid blocks in open ended cavity: Effects of blocks' orientations and aspect ratios on the heat transfer rates," International Journal of Numerical Methods for Heat & Fluid Flow, vol. 19, no. 5, pp. 633 – 649, 2009.

Shercliff, J. A., A Textbook of Magnetohydrodynamics, First Ed., Pergamon Press, UK, 1965.

Singh, S., and Sharif, M. A. R., "Mixed convective cooling of a rectangular cavity with inlet and exit openings on differentially heated side walls", Numer. Heat Transfer, Part A Vol. 44, pp. 233–253, 2003.

Sudipta Ray, Dipankar Chatterjee, "MHD mixed convection in a lid-driven cavity including heat conducting circular solid object and corner heaters with Joule heating", International Communications in Heat and Mass Transfer, Vol. 57, pp. 200-207, 2014.

Tahseen Ahmad Tahseen, "An experimental study for mixed convection through a circular tube filled with porous media and fixed horizontally and inclined", Modern Applied Science, Vol. 5, No. 2, 2011.

Tasnim, S. H., and Collins, M. R., "Numerical analysis of heat transfer in a square cavity with a baffle on the hot wall", Int. Commun. Heat Transfer, Vol. 31, No. 5, pp. 639-650, 2004.

Tasnim, S. H., and Collins, M. R., "Suppressing natural convection in a differentially heated square cavity with an arc shaped baffle", Int. Commun. in Heat and Mass Transfer, Vol. 32, pp. 94-106, 2005.

Turki, S., Abbassi, H. and Nasrallah, S.B., "Two-dimensional laminar fluid flow and heat transfer in a channel with a built-in heated square cylinder", Int. J. of Thermal Sciences, Vol. 42, pp. 1105-1113, 2003.

Xu, F., Patterson, J. C., and Lei, C., "Experimental observations of the thermal flow around a square obstruction on a vertical wall in a differentially heated cavity", Experiments in Fluids, Vol. 40, pp. 364-371, 2006.

Yang, C. S., Jeng, D. Z., Yih, K. A., Gau, C and Aung, Win, "Numerical and analytical study of reversed flow and heat transfer in a heated vertical duct" J. Heat Transfer, Vol. 131, No.7, 072501, 2009.

Yedder, R.B. and Bilgen, E., "Laminar natural convection in inclined enclosures bounded by a solid wall", Heat and Mass Transfer", Vol. 32, pp. 455-462, 1997.

Yucel, N. and Turkoglu, H., "Numerical analysis of laminar natural convection in enclosures with fins attached to an active wall", Heat and Mass Transfer, Vol. 33, pp. 307-314, 1998.

Zienkiewicz, O. C. and Taylor, R. L., "The finite element method", Fourth Ed., McGraw-Hill, 1991.